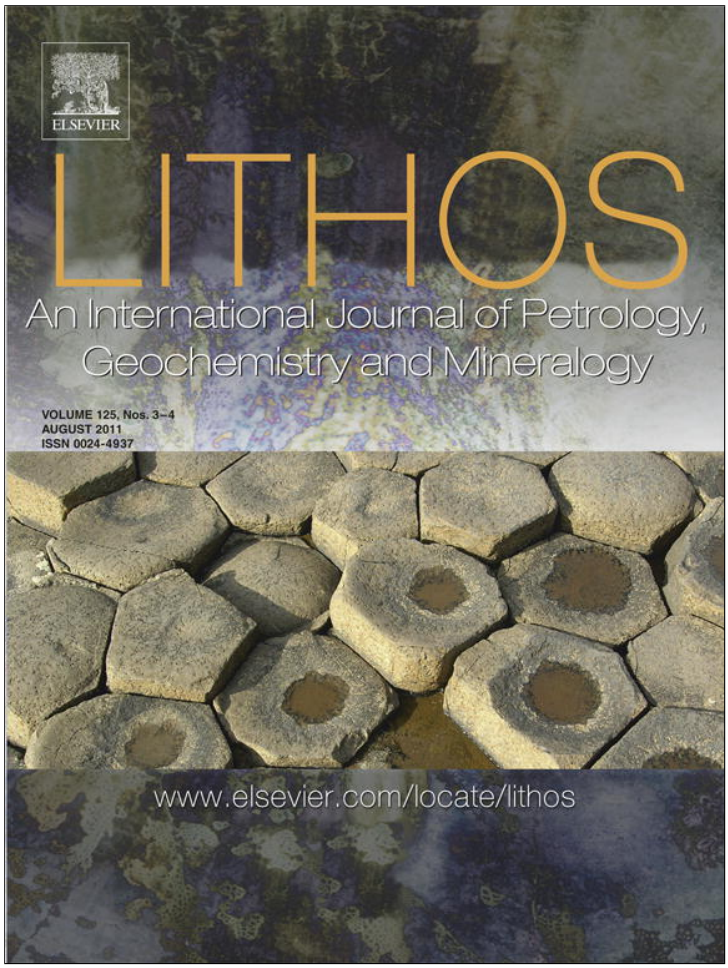

Lithos 125 (2011) 845–874

Contents lists available at ScienceDirect

Lithos

journal homepage: www.elsevier.com/locate/lithos

Origin and evolution of overlapping calc-alkaline and alkaline magmas: The Late Palaeozoic post-collisional igneous province of Transbaikalia (Russia)

B.A. Litvinovsky [a,*], A.A. Tsygankov [b], B.M. Jahn [c], Y. Katzir [a], Y. Be'eri-Shlevin [d]

[a] Dept. of Geological and Environmental Sciences, Ben Gurion University of the Negev, Beer Sheva 84105, Israel
[b] Geological Institute, Siberian Division of the Russian Academy of Sciences, Ulan-Ude 670047, Russia
[c] Institute of Earth Sciences, Academia Sinica, Taipei 11529, Taiwan
[d] Nordsim, Laboratory for Isotope Geology, Swedish Museum of Natural History, Stockholm SE-10405 Sweden

ARTICLE INFO

Article history:
Received 25 October 2010
Accepted 23 April 2011
Available online 1 May 2011

Keywords:
Calc-alkaline granite
Alkaline and peralkaline granite
Nd–Sr–O isotopes
Post-collisional magmatism
Transbaikalia
Russia

ABSTRACT

The Late Palaeozoic voluminous magmatism in Transbaikalia, Russia (a territory of >600,000 km^2 to the east of Lake Baikal) is highly diverse and complex. Of special interest are (1) the significant overlap in time between magmatic suites commonly ascribed to post-collisional and within-plate settings and (2) the provenance of the coeval, but distinct, granitoid magmas that are closely spaced within a large region. Magmatic activity lasted almost continuously from ~330 Ma to ~275 Ma and included five igneous suites occupying a total area of ~200,000 km^2: (1) the Barguzin suite of high-K calc-alkaline granite (330–310 Ma); (2 and 3) the coeval Chivyrkui suite of low-silica calc-alkaline granitoids and the Zaza suite of high-K calc-alkaline to alkaline granite and quartz syenite which were emplaced between 305 and 285 Ma; and (4 and 5) the partially overlapped in time Lower-Selenga monzonite–syenite suite (285–278 Ma) and the Early-Kunalei suite of alkali-feldspar and peralkaline quartz syenite and granite (281–275 Ma). The overall increase in alkalinity of the granitoids with time reflects the progress from post-collisional to within-plate settings. However, a ~20 m.y. long transitional period during which both calc-alkaline and alkaline granitoids were emplaced indicates the coexistence of thickened (batholiths) and thinned (rift) crustal tracts.

Sr–Nd–O isotope and elemental geochemical data suggest that the relative contribution of mantle-derived components to the generation of silicic magmas progressively increased with time. The high-K calc-alkaline granite magmas that formed the Angara–Vitim batholith were generated by high degree melting of supracrustal metamorphic rocks [$\varepsilon Nd(t) = -5.7$ to -7.7; $\delta^{18}O(Qtz) = 12‰$], with minor contribution of H_2O and K from the underplated mafic magma (the convective diffusion model). The coeval calc-alkaline Chivyrkui suite and the transitional to alkaline Zaza suite formed as a result of mixing of crustal silicic and mantle-derived basic melts in roughly equal proportions. In so doing, the former crystallized immediately from the hybrid magmas, whereas the latter (Zaza suite) formed by fractional crystallization of the hybrid melts following magma mixing. Finally the partly overlapping in time monzonite–syenite (Lower-Selenga) suite and highly alkaline syenite–granite (Early-Kunalei) suite were produced from the similar K-rich basalt source. For the former suite, the magma generation process was dominated by fractional crystallization of K-rich basalt magma. In contrast, the highly alkaline granitoid magmas were likely generated by partial melting (~20%) of K-rich mafic rocks in the lower crust.

1. Introduction

Post-collisional settings are characterized by voluminous, mostly granitoid magmatism. Whereas the collision, the time of maximum convergence, is not favorable for the ascent of magma, the post-collisional period may involve large-scale tectonic movements with an extensional component, giving rise to magma generation and emplacement (Liégeois, 1998). Typical well-studied examples of vast post-collisional magmatism include the Variscan Belt of Europe (Bonin, 2004, 2007) and the Neoproterozoic Tuareg shield of northwestern Africa (Liégeois et al., 1998). The main characteristics of post-collisional settings, including the large scale of the magmatism, its diverse composition and the temporal sequence of igneous suites, are similar in both regions. Post-collisional magmatic activity began with the emplacement of large volumes of high-K calc-alkaline granitoids forming a series of large batholiths (in the Tuareg shield they occupy 40% of the whole territory of 500,000 km^2). Calc-alkaline granitoids were followed by felsic and mafic rocks with progressively increasing alkalinity, including a shoshonitic series. Alkaline–peralkaline granites completed the magmatic cycle. However, in the Tuareg

* Corresponding author. Tel.: +972 8 6461366; fax: +972 08 64 77655.
E-mail addresses: borisl@bgu.ac.il, borislit@mishmarhanegev.org.il (B.A. Litvinovsky).

0024-4937/$ – see front matter © 2011 Elsevier B.V. All rights reserved.
doi:10.1016/j.lithos.2011.04.007

shield and in the Variscan Belt of Europe, alkaline and peralkaline granites intruded after a short or protracted hiatus in magmatism and are thus classified as younger within-plate or post-orogenic suites (Bonin, 1998, 2004; Bonin et al., 1998; Liégeois et al., 1998). Thus, two intercontinental magmatic settings, post-collisional and within-plate, are commonly recognized in mobile belts after completion of collision.

Our study focuses on a vast (≥600,000 km^2) post-collisional igneous province in Transbaikalia, Russia. Recent geochronological studies showed that the majority of the magmas in the Transbaikalian province were emplaced during a ~60 m.y. long time interval in the Late Palaeozoic (Tsygankov et al., 2007, 2010). Most plutons are weakly to non-deformed indicating the attenuation of orogenic deformation and its final cessation during Late Carboniferous times. Like the large post-collisional Tuareg and Variscan European provinces, magmatism in Transbaikalia began with the formation of a large high-K calc-alkaline batholith, the Angara–Vitim batholith (330–310 Ma). However, in Transbaikalia the magmatism continued without interruption for an additional tens of million of years and included the emplacement of highly diverse calc-alkaline, alkaline and peralkaline low-silica to felsic magmas. Thus the rigorous division into two distinct, post-collisional calc-alkaline and within-plate alkaline, tectono-magmatic settings does not hold for Transbaikakia.

Here we use an extensive field, mineralogical and geochemical database for the Late Palaeozoic Transbakalian igneous rocks to define distinct magmatic suites and to give a detailed view of the complicated post-collisional magmatic cycle in the province. These data are combined with a radiogenic and stable isotope database to shed light on the variable sources of the diverse suites. Special emphasis is put on unveiling the sources of coeval, but geochemically distinct, granitoid magmas produced on a substantial scale within a single region. Likewise the setting that gave rise to the emplacement of geochemically non-distinct igneous suites at different times is sought out.

2. Geological setting and overview of geochronological data

Late Palaeozoic granitoids are widespread in Transbaikalia that is disposed near the southern edge of the Siberian Craton (Fig. 1 and Inset). This territory incorporates several terranes, in particular, the Barguzin megablock and adjacent smaller Precambrian terranes (Belichenko et al., 2006 and references therein). The Barguzin megablock is located between the Siberian Craton and the Aldan-Stanovoy shield. To the south it borders the Caledonides that occupy vast territories in southern Siberia and Mongolia (Jahn et al., 2009; Kovalenko et al., 2004). Large Precambrian megablocks, Tuva-Mongolian, Sangilen and Khangay, are disposed to the southeast from the Baikal Lake. The regional long-lived Dzhida suture formed in the late Caledonian stage (Kovalenko et al., 2004) extends through the whole region and intersects Precambrian and Caledonian structures.

A good consensus exists among geologists that accretion of terranes with the Siberian continent occurred during Early Paleozoic times after the closure of the Paleo-Asian ocean at about 450–500 Ma. Until recently the territory under discussion was considered part of a continental margin which was active up to the Triassic–Early Jurassic (240–180 Ma) collision of the North-Asian and Sino-Korean cratons after closure of the northwestern section of the Mongolo-Okhotsk trough; the trough is marked by a chain of Indosinian deposits in the eastern part of the Inset in Fig. 1 (Kovalenko et al., 2004; Windley et al., 2007; Yarmolyuk et al., 2005). The Late Paleozoic magmatism in Transbaikalia was interpreted as a within-plate magmatism defined by a mantle hot spot in the active continental margin (Kovalenko et al., 2004). After compilation and revision of all available data another interpretation was proposed by Tsygankov et al. (2010). Based on the unique abundance of K-rich calc-alkaline granitoids that are not characteristic of within-plate magmatism, and the recent findings of highly deformed Devonian-Carboniferous sea basin deposits (terrigenous and carbonate rocks, with subordinate volcaniclastic material), Tsygankov et al. (2010) suggested that Hercynian orogenesis occurred in Transbaikalia. It is likely that the border between the two plates that collided during Devonian–Carboniferous times is located within the Dzida suture (Fig. 1, Inset). We believe that the characteristics of the igneous suites given later are consistent with this interpretation of tectonic setting.

Systematic study of the granitoids began in the middle of the XXth century in the course of an extensive regional geological mapping at a scale of 1:200,000 and 1: 50,000 carried out by the Geological Survey of the USSR. The results were supplemented by detailed investigations in key areas (e.g., Dvorkin-Samarsky, 1965; Gordienko, 1987; Leontyev et al., 1981; Litvinovsky and Zanvilevich, 1976, 1998; Litvinovsky et al., 1993, 1999a, 1999b; Reyf, 1976; Wickham et al., 1995; Zanvilevich et al., 1985). A vast batholith comprising diverse granitoids of different ages, from Proterozoic to Jurassic, occupies about 50% of the territory of Transbaikalia [e.g., Wickham et al., 1995 and the Map of Magmatic Formations of south Eastern Siberia and northern Mongolia, 1:1,500,000, by Abramovich et al., 1989; Polyakov (1989)]. In most cases older granites are country rocks for younger granites, whereas metamorphic and sedimentary country rocks with clear stratigraphic position are rare.

Extensive U–Pb zircon and Rb–Sr whole rock dating performed during the last two decades led to a new perspective on the evolution of the Late Palaeozoic granitoid magmatism in Transbaikalia (Budnikov et al., 1995; Jahn et al., 2009; Litvinovsky et al., 1995c, 1999a; Reichow et al., 2010; Tsygankov et al., 2007, 2010; Yarmolyuk et al., 1997a, 1997b). Based on the new geochronology and key field observations, a modified evolution for the Late Palaeozoic granitoid magmatism in Transbaikalia was proposed (Tsygankov et al., 2010). The study areas shown in Figs. 2 and 3 represent the distribution of the most characteristic rock types from all of the Late Palaeozoic igneous suites of Transbaikalia. The majority of the samples for the U–Pb zircon dating, Sr–Nd isotope tracer study, and chemical characterization were collected in these areas and are discussed in the following sections. Brief descriptions of the plutons from the study areas are given in Table 1.

Figs. 1 to 4 and Table 1 show that the Late Palaeozoic plutonic cycle occurred almost continuously for 55–60 m.y. Three main stages of magmatic activity can be recognized within this period.

(1) *The Carboniferous stage* (330–310 Ma) comprises the emplacement of very large volumes of calc-alkaline granites of the *Barguzin suite* to form the Angara–Vitim batholith (AVB) and closely associated smaller plutons, occupying a total area of about 150,000 km^2 (Litvinovsky et al., 1993, 1994; Wickham et al., 1995). The AVB is located in the central and northern parts of the region and is confined to the Barguzin megablock. The dominant rock type is granite, mostly coarse-grained, in places porphyritic with microcline phenocrysts. Granites are massive, but linear texture and even gneissosity are not uncommon. The main rock-forming minerals are: microcline ($Or_{86–90}$ $Ab_{10–13}$) making up 40–50% of the rock volume, oligoclase $An_{18–22}$ (18–40%), quartz (25–35%) and variable amount, from 2 to 10%, of iron-rich biotite, with rare hornblende. In places the proportion of plagioclase increases, and the composition shifts to granodiorite. In the upper zones of the granite plutons numerous pegmatite and aplite veins occur. Mafic rocks and low-silica granitoids have not yet been found in the Barguzine suite. These low silica granitoids and gabbro initially were considered to belong to the early stage of the AVB formation (Litvinovsky et al., 1993) but were later proven by U–Pb zircon dating to be much younger, 285–305 Ma (Tsygankov et al., 2010; Table 1 in this paper). They constitute the younger Chivyrkui intrusive suite (see following discussion).

U–Pb ages from central Transbaikalia show that the AVB formed within the time span of 330–310 Ma (Table 1; Fig. 4). In the northern half of the batholith the time interval of granite emplacement was argued to be longer, from 339 to 282 Ma (Bukharov et al., 1992; Rytsk

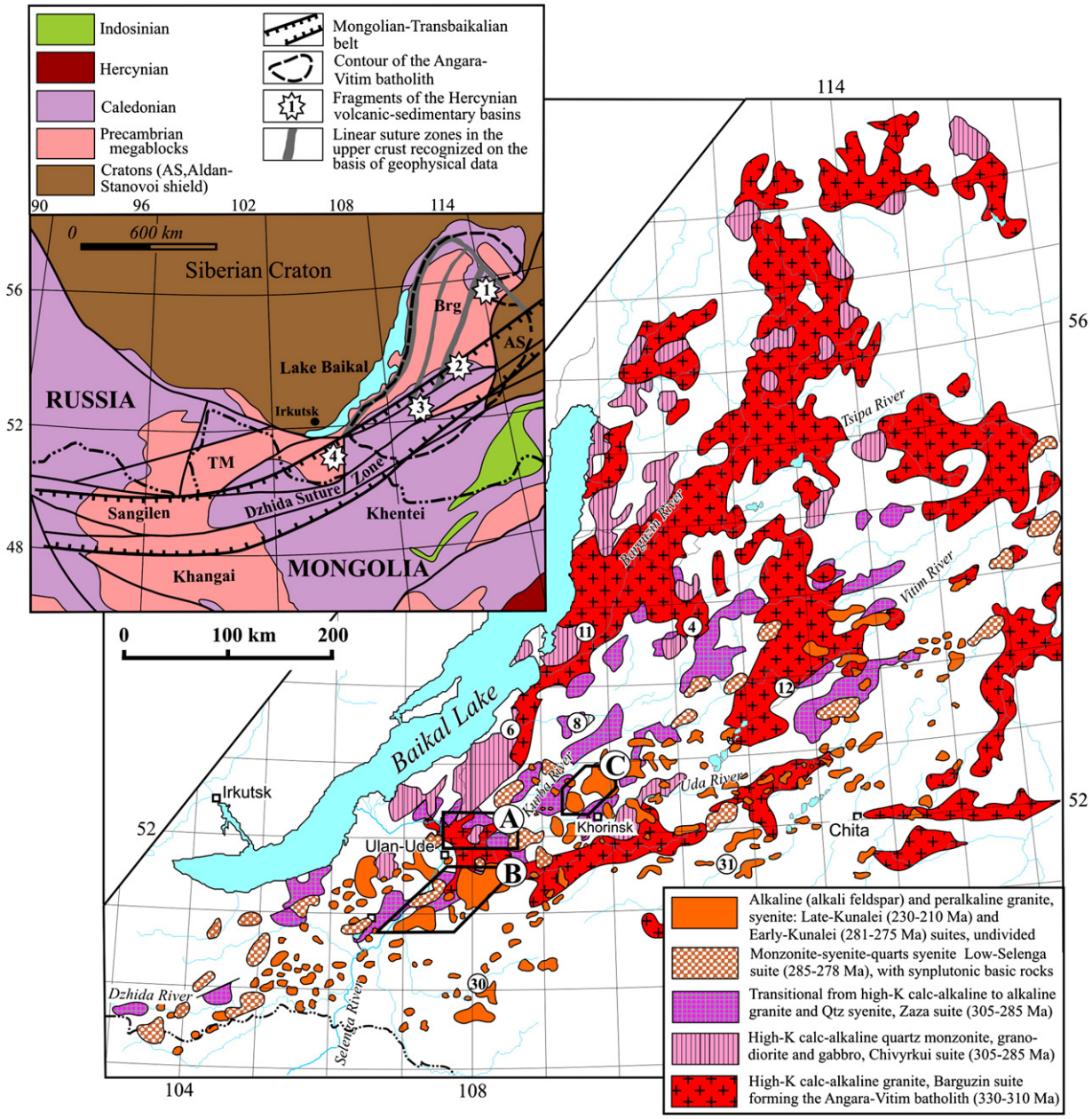

Fig. 1. Late Palaeozoic plutonic suites in Transbaikalia. A, B and C, study areas (see Figs. 2 and 3). In circles are numbers and localities of samples collected for the U–Pb zircon dating outside the study areas; sample numbers as in Table 1. Inset shows the *Tectonic scheme of Transbaikalia and adjacent regions in Late Paleozoic and Triassic*. Abbreviations Brg and TM designate the Barguzin and Tuva-Mongolian Precambrian megablocks respectively. Numbers from 1 to 4 show localities of fragments of the Devonian-Carboniferous volcanic-sedimentary sea basins (1, Uakit; 2, Bagdarin; 3, Ulzutui-Khimgilda; 4, Urma). The scheme was compiled based on data of Kovalenko et al. (2004); Windley et al. (2007); Jahn et al. (2009); Tsygankov et al. (2010).

et al., 2002). Unfortunately, the reliability of these U–Pb ages cannot be tested, since the original data were never published. However, the new unpublished U–Pb zircon ages obtained for typical granites of the Barguzin suite in the central part of the AVB, in the upper and middle reaches of the River Barguzin, support the data on later completion of the batholith emplacement, about 289 ± 1 and 290 ± 3 Ma (V. Yarmolyuk, personal communication, TIMS dating).

(2) *The Late Carboniferous stage* (305–285 Ma). During this stage two intrusive suites were emplaced concurrently, the *Chivyrkui suite* of mainly low-silica granitoids and the *Zaza suite* of leucocratic granite with subordinate quartz syenite. There is a partial overlap in the spatial distribution of the two suites. Granitoids of both suites are abundant in the eastern part of a large linear granite belt extending for a distance of 3000 km throughout southern Siberia and northern Mongolia (Leontyev et al., 1981; Wickham et al., 1995). In Transbaikalia this belt is controlled by the Dzhida suture. However, the plutons of the Chivyrkui suite are abundant also in the northern half of the AVB (Fig. 1). Though the U–Pb zircon ages of the two intrusive suites completely overlap, field relations indicate that in each separate area emplacement of the Chivyrkui granitoids preceded those of the Zaza suite.

The *Chivyrkui suite* comprises plutons formed by several phases of intrusion, each pluton covers a total area of several hundreds to 2000 km^2. The dominant rock type is quartz monzonite. Granodiorite, monzonite, rare quartz syenite and aplitic granite make up the remainder. The occurrence of synplutonic gabbro, synplutonic mafic dykes, microgranular mafic enclaves (MME) and composite microgabbro-aplitic dykes is characteristic of the suite (Litvinovsky

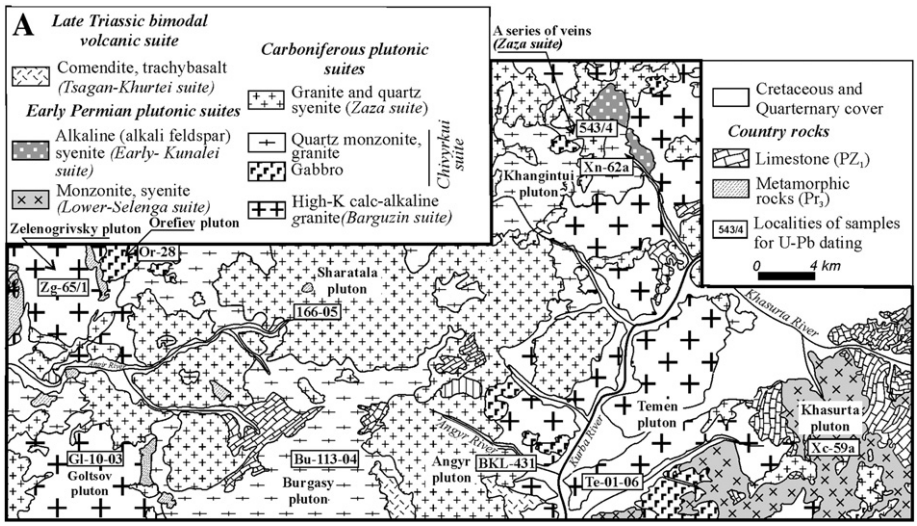

Fig. 2. Sketch map of study area A (see Fig. 1), southern part of the Kurba River basin. Localities and numbers of samples collected for the U–Pb zircon dating are shown (see Table 1). The map is compiled after Reyf (1976) with the authors' supplements.

et al., 1993; Tsygankov et al., 2007). Small gabbroic plutons are also known (Fig. 2). Quartz monzonite is commonly porphyritic with microcline phenocrysts of 3–5 cm, in places up to 10 cm in size. The rock consists of plagioclase An_{25-29} (40 to 50%), latticed microcline $Or_{80-92}Ab_{8-16}$ (25–30%), moderate-magnesium hornblende and biotite (6–13%), quartz (8–15%) and 2 to 3 vol.% of titanite, apatite, magnetite, zircon.

The granitoids of the *Zaza suite* form plutons or batholiths of variable dimensions, the largest being over 3000 km^2. They occupy a total territory of 39,000 km^2 (Leontyev et al., 1981; Litvinovsky et al., 1999b; Wickham et al., 1995) and show a regular pattern of emplacement starting with quartz syenite, followed by granite and late aplite and leucogranite dykes. Granite is the dominant rock type in the suite. Gabbroic rocks with evidence for intrusion into incompletely crystallized quartz syenite (Litvinovsky et al., 1995b) are found so far only in the Shaluta pluton (Fig. 3B).

The quartz syenites and granites are massive pink-colored rocks, the granites containing up to 30–35% modal quartz, the syenites only 10–15%. Perthitic microcline (Or_{80-90} Ab_{10-20}) forms more than half of the rock volume both in granites and in quartz syenites, with plagioclase (An_{10-17} in granites and An_{19-21} in quartz syenites) making up as much as 15–20% modally. In granite, the mafic mineral is biotite; quartz syenite contains small quantities of hornblende in addition to biotite.

(3) *The Early Permian stage* (285–275 Ma). In this final stage of the Late Palaeozoic magmatic cycle magmas with enhanced alkalinity intruded, and again significant overlap in ages of distinct igneous suites is observed. Zircon U–Pb ages of rocks of the *Lower-Selenga suite* of mainly syenite with subordinate monzonite, quartz syenite and granite range from 285 Ma to 278 Ma. Emplacement of the highly alkaline syenites and granites of the *Early-Kunalei suite* started slightly later, at 281 Ma and lasted till 275 Ma (Table 1). Both suites are closely associated not only in time, but also in space (Fig. 1). They are confined to the large Mongolian–Transbaikalian granite belt (MTB). The MTB, earlier recognized as the Mongolian–Transbaikalian Rift Province by Zanvilevich et al. (1985, 1995), extends from northern Mongolia to Transbaikalia (Russia) and further to the Aldan shield (Fig. 1, Inset). The MTB runs along the southern border of the Siberian Craton, and crosscuts Precambrian micro-continental blocks (Khangai, Dzhida, Barguzin) along the Dzhida suture (Jahn et al., 2009; Kovalenko et al., 2004). The MTB extends along a distance of >2500 km, and varies in width from 150 to 250 km (Jahn et al., 2009). The northeastern boundary of the belt is currently undefined. Within the Transbaikalia more than 30 plutons of the Lower-Selenga suite and numerous plutons of the Early-Kunalei highly alkaline (alkali-feldspar and peralkaline) granitoids were recognized. The Lower-Selenga suite is still poorly studied, although the typical Ust-Khilok pluton occupying an area of about 700 km^2 was described in detail (Litvinovsky et al., 1995a) and some new data on the Khasurta pluton have been obtained recently (Table 1; Figs. 2 and 3). The most abundant rock type is coarse- and medium-grained syenite that consists of up to 85–90% perthitic alkali feldspar (Or_{84-92} Ab_{16-21} An_{0-4}) and 5 to 40% oligoclase An_{10-12}, 5–8% biotite, hornblende, and 2.5 – 4% quartz. Monzonite is a heterogeneous rock that consists of irregularly alternating patches of variable (10 to 20%) amounts of mafic minerals (hornblende, biotite and salite). The main part of the rock volume is made up of 48–55% plagioclase (An_{12-22}) and 25–40% alkali feldspar (Or_{80-95} Ab_{20-22}). Rare phenocrysts include resorbed tabular andesine (An_{30-40}) with oligoclase rims. Minor quartz makes up 1.5–2% of the rock volume. One more characteristic feature of the monzonite is the abundance of small melanocratic schlieren and rounded, oval microgranular mafic enclaves (MME) ranging from 3 to 40 cm in size and with diffusive margins. The MME's consist of the same minerals as the host monzonite, but the proportion of mafic minerals is about 50% and plagioclase significantly dominates over alkali feldspar. In rare large MME (>1 m in diameter), relict crystals of clinopyroxene and Ca-plagioclase (An_{48-61}) are common. In both monzonite and syenite, typical synplutonic dykes are made up of K-rich gabbro. Up to 10–15 m thick composite microgabbro–syenitic and microgabbro–monzonitic dykes also occur.

In the *Early-Kunalei suite* the granitoid plutons of alkaline (alkali-feldspar) and peralkaline granites and syenites range in size from 10–15 km^2 to 200 km^2, with a few large plutons of up to 1600 km^2 (e.g., the Bryansky complex in Fig. 3, area B, described in Litvinovsky et al., 2002a). The total area occupied by the exposed plutons is more than 9000 km^2 in Transbaikalia alone (Litvinovsky et al., 1999b). The term 'peralkaline granitoids' is used for granite and quartz syenite with agpaitic index NK/A>1, containing Na-rich amphibole and pyroxene. The 'alkaline (alkali-feldspar) granitoids' include granite and quartz syenite with NK/A ranging from 0.9 to 1. They consist mainly of perthitic alkali feldspar, quartz, Fe-rich biotite and Ca–Na amphibole (the latter mostly in syenite). Below the abbreviations PA and AFS for peralkaline and alkali-feldspar granitoids, respectively, are used. The order of emplacement generally starts with AFS syenite, followed by

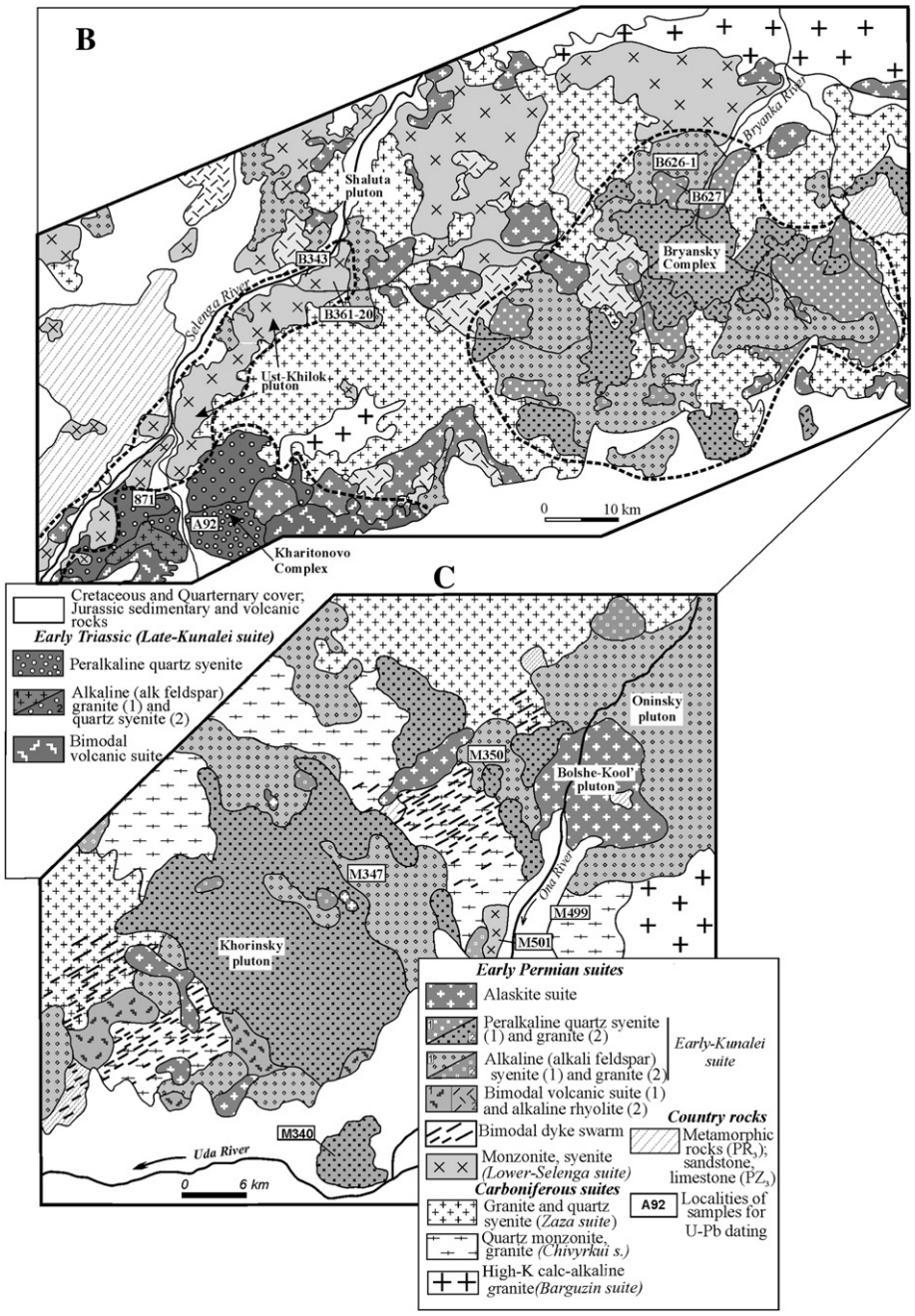

Fig. 3. Sketch maps of study areas B (lower reaches of the Selenga River) and C (lower reaches of the Ona River, see Fig. 1). Localities and numbers of samples collected for the U–Pb zircon dating are shown (see Table 1).

AFS granite to PA syenite, and finally PA granite. Intrusions of syenite and granite magmas occurred in several successive phases, and the proportion of quartz in syenites increases from 3–6 vol.% in the earlier to 10–15 vol.% in the latest phases. Coeval mafic rocks are rare in the granitoid suites, but they occur as MME and as members of composite dykes in the AFS syenites and PA granite of the Khorinsk and Kharitonovo Complexes (Table 1; see also Zanvilevich et al., 1995).

Generally, the highly alkaline plutonic rocks of the MTB are closely associated in space and time with bimodal volcanic series (K-rich basalt, rhyolite, comendite, subordinate trachyte) and bimodal dyke swarms (e.g., Fig. 3, areas B and C). All these rocks are confined to a system of SW-NE grabens (Yarmolyuk et al., 2001). Peralkaline and alkaline granitoids were emplaced into volcanic roofs of similar ages, suggesting shallow depths of crystallization.

It was previously thought that the AFS and PA granitoids were emplaced during a comparatively short span of time at the end of the Permian (see reviews in Yarmolyuk et al., 2001; Zanvilevich et al., 1985). However, recent Rb–Sr and U–Pb dating indicated that the emplacement of highly alkaline granitoids, along with related volcanic rocks, occurred in two distinct episodes: Early Permian, 281–275 Ma, and Late Triassic, 230–210 Ma (Jahn et al., 2009; Litvinovsky et al., 2001; Reichow et al., 2010; Yarmolyuk et al., 2001). The Rb–Sr ages generally agree with the U–Pb dates, but the latter give a better precision. Based on the geochronological data, two highly alkaline syenite-granite suites, Early-Kunalei and Late-Kunalei, were recognized (Jahn et al., 2009; Tsygankov et al. 2010; see also Table 1). So far reliable age data have only been obtained for the central part of the Mongolian–Transbaikalian Belt, within a 350 km-long zone extending from the southwestern angle of Area B (The Kharitonovo complex) to

Table 1
Isotopic ages and brief characteristics of studied plutons.

#	Pluton	Location	Area, km^2	U–Pb age, Ma	Source	Main rock types (mafic minerals)	Color index, vol%	n	Geological and structural characteristics
High-K calc-alkaline granite, Barguzin suite (Angara–Vitim batholith), 330–310 Ma									
1	Zeleno-grivsky	Angyr (Itantsinsky) River basin, Fig. 2	≈80	325 ± 2.8[a] (Zg-66/1)*	Tsygankov et al. (2007)	Gneissic granite (Bt)	1–6	38	Gneissic texture of granite is observed throughout the pluton; it is comformable with metamorphic banded structure of country rocks (crystal schists). Comformable xenoliths and restites of crystal schists are abundant. Stromatite and venite migmatites are common in outer zones. Kfs phenocrysts in granite are about 8 mm (Reyf, 1976).
						Adamellite (Bt, Hb)	1–8		
2	Temen	Kurba River Basin, Fig. 2	450	318 ± 4[a] (Te-10-01-06)*	Tsygankov et al. (2010)	Porphyritic granite (Bt)	1–6	14	Dominant part of the pluton is made up of porphyritic Bt granite (Kfs phenocrysts are up to 12 cm, 3 to 4 cm in average). Even-grained varieties and gneissic granite are rare. Minor thermal effect of intrusion on the host crystal schist and metaconglomerate is recognized.
3	Goltsov	Ulan-Burgasy Range, Fig. 2	120	313.3 ± 3[a] (Gl-10-03)*	Tsygankov et al. (2010)	Granite (Bt)	1–4	27	The pluton is made up of homogeneous isotropic or weakly gneissic porphyritic Bt granite with Qtz phenocrysts. Steeply dipping contacts, abundant vein-like apophyses in the country rocks, xenoliths in marginal zones are characteristic of the pluton.
4	Western Vitim plateau	Upper reaches of the Kidzhimite River, Fig. 1	n.d.	316 ± 2.5 (09–41)*	Tsygankov A.A., unpublished data	Gneissic granite (Bt)	1–3	3	Part of a large pluton made up of medium-grained mildly gneissic Bt granite with rare enclaves of metamorphic rocks
High-K calc-alkalin,e low-silica granitoids (quartz monzonite, granodiorite, quartz syenite) with subordinate gabbro (Chivyrkui suite), 305–285 Ma									
5	Khangintui	Western riverside of the Kurba River, Fig. 2	96	302.3 ± 3.7[a] (Xn-62a)*	Tsygankov et al. (2007)	Qtz syenite (Hb, Bt)	2–8	25	The main rock type is porphyritic quartz syenite with Kfs phenocrysts. Hybrid rocks, mostly granodiorite, are characteristic of marginal zones of the pluton and contact zones around the crystal schist and gabbro xenoliths.
6	Area "Turka"	Southern riverside of the Turka River, Fig. 1	n.d.	290 ± 3	Budnikov et al. (1995)	Granodiorite (Hb, Bt)	9	1	Moderate- to coarse-grained gneissic granodiorite with microcline phenocrysts (Budnikov et al., 1995).
7	Orefiev	Ulan-Burgasy Range, northern riverside of the Angyr (Itantsinsky) River, Fig. 2	≈20-25	290 ± 5[a] (Or-28)*	Tsygankov A.A., unpublished data	Ol-gabbronorite (Ol, Cpx, Opx, Hb, Bt)	20–25	8	Amphibolized gabbro is dominant in the pluton, but small areas of mildly altered gabbro and Ol gabbronorite are found. Marginal zones are made up of Amph-Bt monzonite
						Gabbro (Cpx, Hb, Bt)	18–23		
8	Area "Turka-1"	Southern riverside of the Turka River, Fig. 1	n.d.	289.2 ± 1	Yarmolyuk et al. (1997a)	Granodiorite (Hb, Bt)	10	1	Large pluton made up of porphyritic Bt and Bt-Hbl granodiorite and granite.
9	Burgasy	Ulan-Burgasy Range, Fig. 2	100	287.3 ± 4.1[b]	Tsygankov et al. (2010)	Qtz syenite (Hb, Bt)	3–6	8	The pluton is made up of rocks emplaced in two phases: 1) evolved gabbro – monzonite – syenite association; 2) porphyritic (Afs) quartz syenite (≈90% of the total pluton volume).
						Monzonite (Cpx, Hb, Bt)	12–20	12	MME are abundant in later quartz syenite.
						Syenite (Hb, Bt)	11–15	4	
						Gabbro (Cpx, Hb, Bt)	16–32	2	
10	Khorinsk volcano–plutonic structure	Lower reaches of the Ona River, Fig. 3C		286.3 ± 1.3[c] (M499)*	Reichow et al. (2010)	Quartz monzonite (Hb, Bt)	11	1	Quartz monzonite is country rock for the Khorinsk highly alkaline syenite-granite complex.
11	Nesteriha (Chivyr-kui)	Southern end of the Barguzin Range, Fig. 1	600	298 ± 8	Kozubova et al. (1980)	Quartz monzonite (Hb, Bt)	6–13	12	The pluton consists of quartz monzonite and granodiorite with granitic lenses. Synplutonic mafic dykes and MME are common (Litvinovsky et al., 1993).
12	Romanov-ka	Upper reaches of the Vitim River, village Roman-ovka, Fig. 1	≈150	278.5 ± 2.4[a] (050–04)*	Tsygankov et al. (2007)	Monzonite (Hb, Bt)	5-9	9	The pluton is made up of hybrid Qtz-bearing monzonite and younger quartz monzonite. Xenoliths of gneiss, crystal schist, quartzite, gabbro are abundant. Also abundant are MME and aggregates of Hb, Bt and Pl. Synplutonic mafic dykes are common (Litvinovsky et al., 1993).
						Quartz monzonite (Hb, Bt)	4	1	
Transitional from High-K calc-alkaline to alkaline granite and quartz syenite (Zaza suite), 305–285 Ma									
13	Angyr	Southern riverside of the Angyr (Kurbinsky) River, Fig. 2	≈100	303.4 ± 7.3	Yarmolyuk et al. (1997a)	Leucogranite (Bt)	0.5–1.5	41	Dominant part of the pluton is made up of homogeneous coarse- and medium-grained Bt leucogranite. Subordinate quartz syenite (Hbl, Bt) with rare MME is confined to marginal zones. Contacts between granite and quartz syenite are gradational (Reyf, 1976).
14	Sharatala	Ulan-Burgasy Range, river-head of the Angyr (Itantsinsky) River, Fig. 2	330	286 ± 4.5[a] (166–05)*	Tsygankov et al. (2010)	Granite (Bt)	1–4	31	The pluton consists of fine-grained Bt granite with abundant hybridized xenoliths of crystal schists, gabbro and with MMEs.
15	Shaluta	Lower reaches of the Selenga River, near the Shaluta village, Fig. 3B	120	288 ± 8 (Rb–Sr)	Litvinovsky et al. (1999a)	Quartz syenite (Bt, Hbl)	1–7	10	The pluton is made up of quartz syenite and later leucogranite (second phase of emplacement). In quartz syenite several synplutonic gabbro bodies accompanied by composite dykes are found (Litvinovsky et al., 1995b).

16	A series of veins	Upper reaches of the Birhe-Shibir River (tributary of the Kurba River), Fig. 2		294.4 ± 1[a] (543/4)*	Tsygankov et al. (2007)	Leucogranite (Bt)	1	1	Vein- and dyke-like bodies of leucogranite (thickness up to 20 m) intersecting porphyritic quartz syenite in the northern Khangintui pluton.
17	Unegetei	Eastern part of the Kurba River basin, Fig. 1	≤40	289.2 ± 3.7[b] (023a-04)*	Tsygankov et al. (2010)	Leucogranite (Bt)	0.5	1	The pluton is made up of fine- and medium-grained leucogranite with large blocks of older gneissic granite, gabbro, limestones. Real dimension of the pluton is unknown since its southern part is overlain by Mesozoic deposits of the Uda depression.
Shoshonitic monzonite – syenite – Qtz syenite series (Low-Selenga suite), 285–278 Ma.									
18	Khasurta	Area between the Uda and Kurba Rivers, Fig. 2	900	283.7 ± 4.1[a] (Xc-59a)*	Tsygankov et al. (2007)	Monzonite (Cpx,Hb, Bt)	10–22	29	The pluton consists of fine- and moderate-grained monzonite, Qtz syenite and alkaline granite. Contacts between different rock types are gradational. Rarely banded structure
						Syenite (Hb, Bt)	1–8	26	exhibited in alternating of Qtz syenite and monzonite bands can be seen. Along the
						Alkaline granite (Bt)	1–5	9	contact with Cambrian dolomite, monzonite grades into Cpx syenite.
19	Ust-Khilok	Low reaches of the Selenga River south off Ulan-Ude, Fig. 3B	600	279.5 ± 1.4[c] (B361-20)*	Reichow et al. (2010)	Syenite (Hb, Bt, Px)	2–8	10	The pluton is made up of monzonite and syenite with abundant MME, synplutonic basic dykes and composite dykes (Litvinovsky et al., 1995a).
20				280.3 ± 1.4[c] (B343)*		Syenite (Hb, Bt, Px)			
21	Khorinsk volcanoplutonic structure	Country between the Ona and Kurba Rivers, Fig. 3C		280.4 ± 0.3[c] (M501)*	Reichow et al. (2010)	Syenite from the shoshonitic series	2	1	Country rocks for the Khorinsk highly alkaline syeniite-granite complex.
Peralkaline and alkali feldspar syenite and granite (Early-Kunalei sute), 281–273 Ma									
22	Bryansky	Tsagan-Daban Range (country between the Uda and Khilok Rivers), Fig. 3B	1600	278 ± 1.6[c] (B626-1)*	Litvinovsky et al. (2002a)	Alkali feldspar syenite, granite (Hb, Bt)	2-6	20	The complex intrusive body is made up of two successive plutonic suites, alkali-feldspar and peralkaline. Each suite comprises syenite and granite intrusive stages. In the early suite syenites dominate over granites (proportion 9:1). In the peralkaline suite the proportion is ~1:1. Emplacement of plutonic rocks was preceded by trachydacite – trachyrhyolite and trachybasalt-comendite volcanic suites respectively.
23				277 ± 1.3[c] (B627)*		Peralkaline syenite, granite (Rbk, Aeg)	3-6	21	
24	Khorinsk complex	Country between the Ona and Kurba Rivers, Fig. 3C	~2000	279.8 ± 1.9[c] (M347)*	Reichow et al. (2010)	Alkali feldspar syenite	1–5	18	A cluster of closely spaced plutons of various dimensions occupying a total area of ~2000 km^2. Plutons are mostly made up of alkali feldspar syenite and peralkaline granite. The plutonic stage was preceded by the bimodal volcanic suite and injection of a dyke swarm.
25				278.4 ± 0.9[c] (M340)*		Peralkaline granite	1–4	20	
26				273.6 ± 0.4[c] (M350)*			1–5	8	
27				280 ± 5.3 (Rb–Sr)		Syenite porphyry (dyke swarm)			
Mesozoic highly alkaline granite, syenite, comendite, trachybasalt (Late-Kunalei granitoid and Tsagan-Khurtei volcanic suites), 230–210 Ma.									
28	Kharitonovo	Lower reaches of the Khilok River, Fig. 3B	230	230.1 ± 0.7[c] (871)*	Reichow et al. (2010)	Alkali feldspar syenite (Hb, Bt)	1–5		The pluton consists of peralkaline and alkali feldspar syenite and granite suites. Each suite incorporates several intrusive phases. Plutonic rocks are crosscut by composite microgabbro-syenite dykes (Zanvilevich et al., 1995).
29				229.1 ± 0.6[c] (A92)*		Peralkaline syenite (Na-rich Hb, Px)	2–8		
30	Malo-Kunalei	NE spurs of the Malkhan Range, Fig. 1	120	219.1 ± 0.6[c]	Reichow et al. (2010)	Peralkaline quartz syenite (Na-rich Amphl and Px, annite)	tr.-4	19	The pluton is made up of coarse-grained peralkaline syenite and Qtz syenite with dykes of peralkaline granite (Zanvilevich et al., 1985).
31	Tsagan-Khurtei suite	Tsagan-Khurtei Range, Fig. 1	≈1800	212 ± 5 (Rb–Sr)	Litvinovsky et al. (2001)	Comendite (Cpx, Amph)	tr.-3	9	Bimodal trachybasalt-comendite volcanic suite with secondary trachyandesite and trachyte, thickness >2500 m. Volcanic rocks are intruded by peralkaline granite and nordmarkite plutons, supposedly related to comendite.
						Trachybasalt (Cpx, Ol)	12–19	6	

([a])Sanct-Petersburg, Center of Isotope Researches, All-Russian Geological Institute, SHRIMP-II.
([b])Beiging, Institute of Geological Analysis of the Academy of Geologic Sciences, China, SHRIMP-II.
([c])NERC Isotope Geosciences Laboratory (NIGL), Keyworth, UK.
(Zg-66/1)* — here and below are sample numbers shown in Figs. 2 and 3.
MME, microgranular melanocratic enclaves.
n.d., no data.

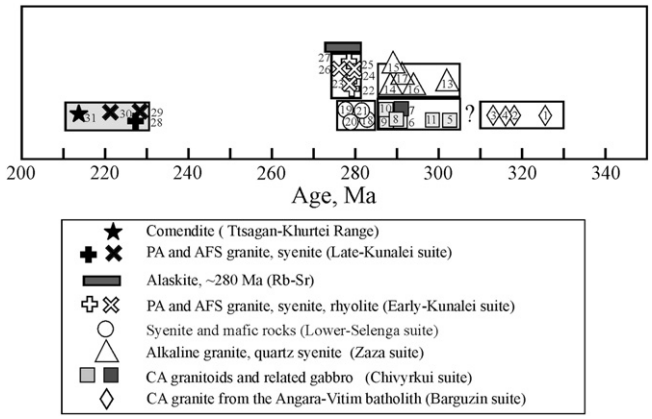

Fig. 4. Sequence of emplacement of Late Palaeozoic and Early Mesozoic igneous suites in Transbaikalia (sample numbers and ages (Ma) are from Table 1).

point 31 (Tsagan-Khurtei) in Fig. 1 (see Fig. 2-SD in the Online supplementary data and Jahn et al., 2009 for more detail). It was found that in some areas Early Permian and Late Triassic highly alkaline granite–syenite complexes are closely spaced (e.g., Bryansky and Kharitonovo Complexes in Fig. 3, area B). A comparative study of the geology, mineralogy and chemistry of the Early Permian and Late Triassic plutons revealed the same order of emplacement and a close similarity of mineral and chemical compositions (Yarmolyuk et al., 2001;). This means that the two highly alkaline syenite–granite suites cannot be distinguished by conventional methods, e.g., by field investigation and petrographic and chemical study. The only way to discriminate them is by isotope age dating. This is the reason that they are shown in Fig. 1 as undivided.

Fig. 4 shows that at the very end of the Late Palaeozoic magmatic cycle, after crystallization of peralkaline granite, emplacement of subsolvus AFS granite occurred. The key observation was made in the Khorinsk volcano–plutonic structure, in which more than a dozen two-feldspar granite plutons intruding peralkaline granite have been mapped (Fig. 3, area C). The largest, the Bolshekool pluton, is about 80 km^2 in area. The granites are alaskitic moderate- to coarse-grained rocks consisting of perthitic alkali feldspar (55–58%), quartz (30–40%), Na-rich plagioclase An_{6-14} (10–15%) and only 2–4% biotite and Fe–Ti oxides. A whole rock Rb–Sr isochron for the Bolshekool pluton yielded an age of 282 ± 5 Ma (Posokhov et al., 2005). This result is consistent with geological observations and, within the error limits, with the U–Pb isotope age of the peralkaline granite (274–280 Ma, Table 1). Similar alaskitic granites are also abundant in the lower reaches of the Selenga River (Fig. 3, area B) and in the Dzhida River basin, about 100–150 km to the west (Litvinovsky et al., 1995c). These age data suggest a significant overlap in the emplacement of the three Early Permian intrusive suites: the Lower-Selenga monzonite–syenite, the Early-Kunalei PA and AFS syenite–granite, and the unnamed two-feldspar alaskite suite.

3. Analytical procedures

3.1. Whole-rock chemical analysis

Major element contents were measured using a combination of wet chemical analysis, atomic absorption spectrometry and titration. Some trace elements (Rb, Sr, Ba, Y, Zr and Nb) were determined by XRF at the Geological Institute, Siberian Division of the Russian Academy of Sciences, Ulan-Ude. The data for rare earth and other trace elements (Hf, Ta, Th, U, Ga, V, Cu, Pb, Zn, Sc and Cs) were obtained using an ICP-MS (Agilent 7500s) at the Department of Geological Sciences, National Taiwan University (NTU) in Taipei. The analytical uncertainties are about 2% for major elements, 5–10% for most trace elements, and 1–5% for all REE except Lu (about 10%). At NTU, a rock powder was first fused to make a glass bead for XRF major element determination. A portion of the used glass bead was then pulverized and dissolved in HF/HNO_3 (1:1) mixture in capped Savilex beakers for >2 h at ca. 100 °C, followed by evaporation to dryness, refluxing in 7 N HNO_3 for >12 h at ca. 100 °C, and finally, diluting the sample solution with 2% HNO_3. An internal standard solution of 5 ppb Rh and Bi was added and the spiked solution was diluted with 2% HNO_3 to a sample/acid weight ratio of 1:2000. An internal Rh standard was used for monitoring the signal shift during ICP-MS measurements. The analytical precision for trace elements was <5% (2-sigma). For more details, see Yang et al. (2005).

3.2. Sr and Nd isotope analyses

Sr and Nd isotope ratios were determined at the Institute of Earth Sciences (IES), Academia Sinica, Taipei. Powdered samples were dissolved in Savilex bombs following a series of standard procedures until samples were completely dissolved. Isolation and purification of Sr and Nd were achieved using a 2-column technique. The Sr fractions were occasionally further purified using a third column. The first column was packed with 2.5 ml cation exchange resin (Bio-Rad AG50W-X8, 100–200 mesh) and was used to collect Sr and REE fractions. The second column used for Sr purification was packed with 1 ml cation exchange resin, identical to the aforementioned. The second column used for Nd isolation was packed with 1 ml Ln-B25-A (Eichron) resin, which was covered on top by a thin layer of anion exchange resin (Bio-Rad AG1-X8, 200–400 mesh).

Mass analyses were performed using a 7-collector Finnigan MAT-262 mass spectrometer in dynamic mode. $^{143}Nd/^{144}Nd$ ratios were normalized against the value of $^{146}Nd/^{144}Nd = 0.7219$, whereas $^{87}Sr/^{86}Sr$ ratios were normalized against $^{86}Sr/^{88}Sr = 0.1194$. During the course of analysis, the measurements on NBS-987 Sr standard yielded $^{87}Sr/^{86}Sr = 0.710320 \pm 0.000036$ (n = 50) using the static mode and $= 0.710237 \pm 0.000020$ (n = 8) using the dynamic mode. All $^{87}Sr/^{86}Sr$ ratios reported herein have been adjusted to NBS-987 = 0.710250. Our measurements on the La Jolla Nd standard yielded 0.511864 ± 0.000006 (n = 4), and on the JMC Nd standard, 0.511821 ± 0.000016 (n = 6). No further adjustment to Nd isotopic ratios was made.

4. Chemical compositions of granitoids and associated mafic rocks

The full dataset of major and trace element compositions for Late Palaeozoic igneous rocks from Transbaikalia includes 579 whole-rock analyses (Online Supplementary Data, Tables 1-SD and 2-SD). The most representative chemical data for granitoids and related mafic rocks are given in Tables 2 and 3, respectively. Since mafic rocks commonly occur as synplutonic bodies and MME of various dimensions, sampling was performed in the central parts of larger bodies and the largest, >2 m in diameter, MMEs. The least hybridized mafic rocks with $SiO_2 \leq 53$ wt.% and the lowest K_2O contents have been chosen for discussion. Analyses of cumulus enriched rocks (anomalously high CaO, Al_2O_3, FeO^t, MgO, and Sr) were excluded from consideration. In the highly alkaline igneous suite, chemical data on plutonic mafic rocks were complemented by data on related high-K basalt from the bimodal volcanic and dyke suites. Comparison of plutonic, volcanic and dyke rocks reveals that their chemical compositions are similar, which supports the assumption that the compositions of samples from the synplutonic bodies characterize typical basalt magmas. The chemical data are plotted in Figs. 5–9.

In MALI vs. SiO_2 diagrams, modified after B. Bonin (personal communication) to take into account highly silicic rocks of up to 80 wt.% SiO_2 (Fig. 5, A1 and A2), all Late Paleozoic igneous rocks fall in two fields, alkali-calcic and alkalic. The Carboniferous suites (Barguzin, Chivyrkui, Zaza) are akali-calcic, and the Early Permian

granitoids (Lower-Selenga, Early-Kunalei and alaskite suites) are mostly alkalic (except some silica-rich PA and AFS granites and alaskites), whereas Early Permian mafic rocks are alkali-calcic, similar to the Carboniferous gabbroids. As a whole, all rocks under consideration are enriched in alkalis. Therefore for further discrimination other classification diagrams are used (Fig. 5).

4.1. Granitoids

4.1.1. The Barguzin suite (330–310 Ma)

The most voluminous granites of this suite are typically high-K calc-alkaline with K_2O ranging from 4 to 6 wt.%, agpaitic index ≤0.85 and A/CNK that varies between 0.97 and 1.08 (Fig. 5B1, C1; Table 2). Granites of the Barguzin suite partially overlap the younger Zaza granites on the major element classification diagrams (Fig. 5, A1, B1, C1), but they contain less K_2O (Fig. 5, B1, B2) and are richer in Sr, Ba, Pb, and P (Figs. 6 and 7, A and C). REE patterns of the Barguzin granites show LREE enrichment [$(La/Yb)_n$ ratio ranges from 18 to 40] and distinct negative Eu anomalies in most samples except two porphyritic granites (Fig. 8A). Almost horizontal patterns for HREE and Eu/Eu* values ≤0.45 suggest a minor role for garnet and an abundance of plagioclase in the residual source.

4.1.2. Chivyrkui and Zaza suites (305–285 Ma)

Igneous rocks of these two coeval suites are fairly distinct in chemical traits, which is consistent with distinctions in their petrographical characteristics and mineral composition. The low-silica Chivyrkui suite granitoids are high-K calc-alkaline (Fig. 5, B1 and C1). Granites and quartz syenites forming the Zaza suite fall in the same field of the SiO_2 vs. K_2O diagram, although some of the quartz syenite samples are confined to the shoshonitic series field (Fig. 5, B2). Granitoids of the Zaza suite have agpaitic index ranging from 0.73 to 0.95 and plot in two fields, calc-alkaline and alkaline; therefore they are regarded as transitional from high-K calc-alkaline to alkaline (Fig. 5, C2). Silica-variation diagrams (Fig. 6) and bulk crust-normalized multi-element spidergrams (Fig. 7, B, C) show that elevated alkalis content in the Zaza granitoids is accompanied by enhanced Rb, Th and Nb, whereas Sr, Ba, Pb, Eu concentration is lower compared to granitoids of the Chivyrkui suite. The REE patterns of both suites show similar LREE enrichment, with $(La/Yb)_n = 9–34$ for the Chivyrkui and 14–34 for the Zaza suites. Despite almost total overlap of REE patterns, two differences are clearly seen (Fig. 8C): (1) pronounced negative Eu anomalies in granitoids of the Zaza suite ($Eu/Eu^* = 0.35–0.57$) and insignificant Eu anomalies in the Chivyrkui suite (Eu/Eu* close to unity); (2) the HREE segments are almost horizontal in the Zaza suite but in coeval granitoids of the Chivyrkui suite the average $(Gd/Yb)_n$ is ~3.

4.1.3. Lower-Selenga and Early-Kunalei suites (285–275 Ma)

The granitoids of both suites are characterized by high K and total alkalinity (Fig. 5A2, B2 and Table 2). The compositions of the Lower-Selenga monzonites and syenites plot in the field of the shoshonitic series (Fig. 5B). Despite their enhanced alkalis content (12–13 wt.% $Na_2O + K_2O$), these rocks are alumina rich and, owing to this, the agpaitic index for almost all samples is <0.85 (Fig. 5, B2). This fact indicates that the rocks are calc-alkaline rather than alkaline. The syenites of the Lower-Selenga suite are enriched in Sr and Ba (about 500–1500 ppm, Tables 2 and 1-SD) and Zr (300–600 ppm, Fig. 6). The REE patterns are fairly similar to those of the granitoids from the Chivyrkui suite (Fig. 8, B and D); they have $(La/Yb)_N$ ratios from 10 to 27 and display small or no negative Eu anomalies.

The granitoids of the Early-Kunalei suite are typical alkaline and peralkaline rocks (Fig. 5, B2 and C2). Their geochemical features are characteristic of A-type granite: very low Sr and Ba and high Rb, Nb and Zr (Table 2; Fig. 6). This is clearly exhibited in troughs and peaks in the bulk crust-normalized multi-element spidergrams (Fig. 7, E and F). The spidergrams of quartz syenites and granites are similar, but the variability in granites is more pronounced. The REE patterns show distinct negative Eu anomalies that are larger in granitic rocks: the Eu/Eu* values vary in quartz syenite from 0.42 to 0.56 and in granite this value decreases to 0.14–0.36. $(La/Yb)_N$ ratios range from 9 to 24. HREE segments in granite are almost horizontal, whereas in quartz syenites they are gently dipping (Fig. 8, E and F).

The syenites of the Lower-Selenga and quartz syenites of the Early-Kunalei suites are fairly similar in mineralogy (although the former is plagioclase-bearing and impoverished in quartz), but they show a number of distinct chemical characteristics. The Lower-Selenga syenites have higher Sr (Fig. 6), Ba, Th and Pb (Fig. 7, D and E, Tables 2 and 1-SD, Supplementary data) than the Early-Kunalei syenites. Furthermore, the Lower-Selenga syenites display weak negative Eu anomalies, whereas in the Early-Kunalei syenites there are significant negative Eu anomalies (Fig. 8, D and E). On the other hand, abundances of Nb and Zr as well as Rb overlap almost completely (Fig. 6 and Fig. 3-SD, Online supplementary data), despite noticeable differences in silica content.

The chemical composition of the *alaskite* that intrudes peralkaline granite (see Section 2) corresponds to a high silica alkaline granite with SiO_2 up to 78 wt.% (Fig. 5D). Compared with the peralkaline granite, the alaskite contains less Zr, Nb and Hf (Figs. 6 and 7F). The alaskite is characterized by the concave distribution and low abundances of all rare earth elements (Fig. 8F). This feature also distinguishes the alaskite from the Zaza granite (Fig. 8C) that is similar to the alaskite in mineral composition.

The most prominent chemical trend manifested in the Late Paleozic igneous province of Transbaikalia is increase in alkalinity of granitoids with time: from high-potassium calc-alkaline (Barguzin and Chivyrkui suites) to transitional Zaza suite, then to shoshonitic Lower-Selenga and highly alkaline (AFS and PA) Early-Kunalei suites. However, overlap in time between the different types of granitoids complicates this trend.

4.2. Mafic rocks

Mafic rocks, most of them synplutonic, are found in all the granitoid suites except for the earliest Barguzin suite. In the Early-Kunalei suite, trachybasalt from the pre-granitic bimodal volcanic suite and bimodal dyke suite are similar to the synplutonic microgabbro (Tables 3 and 2-SD). The chemical compositions are plotted in Figs. 5, 6, and 9. Mafic rocks from all suites are rather similar and can be referred to as high-K calc-alkaline to shoshonitic (Fig. 5, B1 and B2); the latter are characterized by potassium enrichment: $K_2O > Na_2O–2$ (Le Maitre, 1989). Samples with lower K_2O content were collected in the Orefyev gabbro–monzodiorite pluton (Fig. 2, Table 1), but it is likely that the low-silica rocks in the pluton are enriched in cumulus mafic minerals (Tsygankov et al., 2010). Therefore these chemical data are not used in the discussion later and are not shown in the geochemical plots. In the TAS (total alkalis vs. SiO_2) classification of Middlemost (1997) (not shown) almost all the samples plot in the monzogabbro and monzodiorite fields, and samples from different suites show significant compositional overlap. All mafic rocks are highly-aluminous (16.5–19.5 wt.% Al_2O_3), rich in K_2O (2.1–2.7 wt.%), Zr (120–190 ppm) and moderately depleted in MgO and CaO (4–5 and 6–8 wt.%, respectively). A few mafic rocks from the Chivyrkui suite have lower Rb, Zr, but higher Ba, Sr and Pb concentrations (Figs. 6 and 9). The REE patterns of the mafic rocks from the four suites are quite uniform. They are LREE-enriched, with $La_N = 100–200\times$ chondrites and $(La/Yb)_N = 8–23$, and the Eu anomaly is generally weak to absent (Fig. 9, A, C, E, F). Overall, all the mafic rocks under consideration are distinguished from OIB by clear Th, U, Nb, Ti troughs, and K, Ba, Pb peaks (Fig. 9, B, D, F, and H) indicating that these rocks are similar to continental basalts commonly found in interiors of cratons. It should be noted that one type of mafic rock, the microgabbro that makes up large (tens of metres) bodies within

Table 2
Chemical composition (wt.%, ppm) of representative rock types from the Late Palaeozoic granitoid suites in Transbaikalia, Russia.

Suite	High-K calc-alkaline granite, Barguzin suite (Angara-Vitim batholith), 330–310 Ma								High-K calc-alkaline quartz monzonite, granodiorite, quartz syenite with subordinate gabbro (Chivyrkui suite), 305–285 Ma						
Pluton/ Complex	Goltsov		Temen			Zelenogrivsky			Burgasy		Khangintui		Nesterikha	Turka pluton	
Sample no.	Gl-8/ 3-03*	Gl-1/ 2-03*	Hk-10/ 2-06*	Hk-12-06*	Hk-15-06*	Zg-51/ 2-03	Zg-51-03*	Zg-64/ 3-03*	Bu-07-68/4*	Bu-113/ 5-06*	Xn-6-02*	Xn-62-02	BKL549	BKL267	BKL290
Rock type	Bt-Gr	Bt-Gr	Porph Q-Sy	Porph Gr	Porph Gr	Bt-Gr	Bt-Gr	Bt-Gr	Mnz	Q-Sy	Q-Sy	Q-Sy	Q-Mnz	Q-Mnz	Q-Mnz
SiO_2	71.50	71.80	68.40	70.80	71.40	72.40	72.50	73.60	57.20	62.90	62.20	68.30	66.83	62.95	66.27
TiO_2	0.26	0.25	0.48	0.34	0.37	0.26	0.28	0.15	1.31	0.64	0.78	0.48	0.39	0.54	0.56
Al_2O_3	14.70	14.70	16.20	14.60	14.10	14.60	14.60	14.20	17.05	17.20	16.75	15.50	16.87	16.25	16.20
Fe_2O_3	0.87	0.73	1.35	1.33	1.18	0.74	0.78	0.64	2.59	2.13	2.47	2.03	1.42	2.43	1.73
FeO	0.95	1.14	0.96	0.60	1.12	0.72	0.76	0.57	4.72	2.19	2.92	1.38	1.79	2.86	2.05
MnO	0.03	0.03	0.05	0.04	0.05	0.02	0.02	0.01	0.10	0.11	0.09	0.07	0.07	0.12	0.08
MgO	0.40	0.37	0.53	0.45	0.54	0.34	0.38	0.25	3.00	1.46	2.20	0.94	0.90	1.90	1.30
CaO	1.37	1.50	1.93	1.62	1.70	1.26	1.48	0.82	5.33	3.35	4.14	2.65	3.20	3.90	3.20
Na_2O	4.27	4.20	4.19	4.00	4.13	3.77	3.77	2.99	4.48	4.51	4.00	3.96	4.38	3.81	4.18
K_2O	4.32	4.39	4.74	4.95	4.22	5.00	4.47	6.23	2.85	4.32	3.35	4.54	3.36	3.79	3.74
P_2O_5	0.09	0.07	0.10	0.13	0.13	0.07	0.11	0.03	0.48	0.22	0.35	0.15	0.17	0.24	0.22
LOI	0.51	0.35	0.37	0.39	0.48	0.34	0.60	0.40	1.24	0.98	0.80	0.41	0.64	0.84	0.20
Total	99.27	99.53	99.30	99.25	99.42	99.52	99.75	99.86	100.35	100.01	100.05	100.41	100.02	99.63	99.75
Ba	827	1104	771	984	1007	711	751	1482	1256	1240	1354	804	1700	1300	970
Rb	183	144	208	222	234	234	218	258	94	134	80	207	74	130	120
Sr	373	551	416	494	521	341	403	313	1213	577	883	594	810	890	1000
Cs	4.86	3.60	2.95	5.54	6.22	5.83	4.64	4.34	n.d.	5.43	n.d.	n.d.	n.d.	n.d.	n.d.
Ga	17.1	20.5	22.0	21.0	21.1	18.4	20.7	14.3	21.9	18.2	17.5	18.4	n.d.	n.d.	n.d.
Ta	0.90	1.56	0.86	0.84	0.92	1.05	0.47	0.29	0.91	0.96	n.d.	n.d.	n.d.	0.50	0.30
Nb	18.8	15.5	12.5	12.7	11.7	17.0	13.1	10.2	14.7	14.8	6.7	12.7	n.d.	5.5	1.0
Hf	3.78	4.67	5.60	5.04	5.25	3.18	5.94	2.79	5.09	7.45	6.55	5.72	n.d.	4.00	2.70
Zr	163	212	202	166	165	126	215	142	249	296	228	194	n.d.	160	105
Y	14	14	13	11	10	8	7	6	19	27	15	17	n.d.	n.d.	n.d.
Th	15.7	10.8	18.5	24.9	17.7	12.9	14.6	15.5	8.9	14.1	10.1	43.3	n.d.	n.d.	n.d.
U	5.02	1.23	2.83	4.85	3.75	2.48	2.41	1.92	1.99	2.87	1.85	6.78	n.d.	n.d.	n.d.
Cr	0.5	7.2	n.d.	n.d.	n.d.	5.6	10.0	4.2	56.0	n.d.	19.3	n.d.	11.0	9.1	10.0
Ni	12.2	6.1	n.d.	n.d.	n.d.	3.0	13.8	0.8	n.d.	n.d.	18.0	n.d.	3.0	10.0	6.8
Co	3.0	1.8	2.9	2.0	2.8	1.9	1.8	0.8	19.0	9.6	10.8	3.9	4.5	9.7	6.2
Sc	3.5	2.7	3.1	2.5	2.1	1.4	2.9	1.0	8.5	10.5	n.d.	n.d.	4.2	17.0	9.3
V	24.5	16.3	28.0	21.4	18.7	9.9	16.5	6.8	130.4	90.4	67.6	22.2	43.0	100.0	41.0
Cu	5.1	3.3	0.7	0.5	3.1	2.9	2.9	1.3	57.3	7.2	16.3	3.9	6.7	40.0	14.0
Pb	171	18	23	24	26	24	22	37	179	29	18	27	26	30	20
Zn	45	34	52	46	54	31	59	18	n.d.	77	64	65	45	110	12
La	41	40	38	41	36	33	37	23	66	56	41	60	30	38	35
Ce	78	83	71	64	64	54	53	52	112	98	88	106	57	110	70
Pr	7.3	7.0	6.8	6.9	6.6	5.1	5.5	3.8	13.5	10.6	9.6	11.1	8.4	13.0	10.0
Nd	23	23	23	22	23	16	18	12	50	39	36	38	27	32	26
Sm	3.77	3.75	3.39	3.61	3.25	2.54	2.65	1.87	8.29	6.95	5.84	6.01	3.70	6.20	6.00
Eu	0.65	0.68	0.90	0.84	0.89	0.58	0.70	0.42	2.35	1.59	1.65	1.30	0.64	1.50	1.30
Gd	4.62	3.99	2.91	2.65	2.74	3.11	2.98	2.11	5.51	6.32	4.97	5.07	2.30	5.90	5.10
Tb	0.62	0.55	0.41	0.36	0.46	0.45	0.40	0.30	0.76	0.84	0.64	0.65	n.d.	n.d.	n.d.
Dy	2.42	2.40	1.88	1.83	2.03	1.44	1.30	1.20	3.63	4.87	3.44	3.61	2.20	3.20	2.30
Ho	0.49	0.47	0.42	0.39	0.33	0.27	0.24	0.23	0.75	0.89	0.66	0.70	n.d.	0.65	n.d.
Er	1.52	1.49	0.92	1.07	0.89	0.90	0.78	0.70	1.53	2.43	1.85	2.04	n.d.	n.d.	n.d.
Tm	0.22	0.21	0.18	0.16	0.15	0.10	0.09	0.10	0.23	0.41	0.24	0.27	n.d.	n.d.	n.d.
Yb	1.56	1.43	1.06	1.05	1.01	0.79	0.67	0.71	1.40	2.93	1.65	2.06	1.00	1.80	1.10
Lu	0.25	0.22	0.17	0.16	0.15	0.12	0.10	0.11	0.20	0.37	0.25	0.32	0.15	0.55	0.15
*Eu/Eu**	0.48	0.53	0.85	0.79	0.89	0.63	0.76	0.64	1.00	0.72	0.91	0.70	0.62	0.75	0.70
$(La/Yb)_n$	18.9	20.0	25.4	27.8	25.8	30.1	39.8	23.2	33.9	13.7	18.0	21.0	21.5	15.1	22.8
NK/A	0.80	0.79	0.74	0.82	0.81	0.80	0.76	0.82	0.61	0.70	0.61	0.74	0.64	0.64	0.68
A/CNK	1.03	1.02	1.04	0.98	0.97	1.05	1.06	1.08	0.85	0.94	0.94	0.95	1.01	0.93	0.97

[(1)]Abbreviations: Bt-gr, biotite granite; Porhp Q-Sy and Gr, porphyritic quartz syenite and granite; Q-Mnz, quartz monzonite; Mnz, monzonite; Sy, syenite; AFS-Sy and AFS-gr, alkali feldspar syenite and granite; PA-sy and PA-gr, peralkaline syenite and granite; Sy-Gr, syenogranite. [(2)]$Eu/Eu^* = Eu_n/(Sm_n{*}Gd_n)^{1/2}$ or $Eu_n/(Sm_n{*}2/3 + Tb_n{*}1/3)$; NK/A = $(Na_2O + K_2O)$ / Al_2O_3 mol.% A/CNK = $(Al_2O_3 /CaO + Na_2O + K_2O)$ mol.%. [(3)]Chemical data are compiled from Litvinovsky et al., 1993, 1995a; 2002a; Antipin et al., 2006; Tsygankov et al., 2007, 2010; Jahn et al., 2009. * original analyses.

the youngest alaskite, is characterized by lower alkalis (1.6 wt.% K_2O, 2.7–3 wt.% Na_2O, 30 ppm Rb), lower SiO_2 and Al_2O_3 (49 wt.% and 16 wt.%, respectively) and enhanced MgO (6.5 wt.%) and CaO (10 wt.%) that is more typical of medium-K basalts (Table 3, samples B76-1 and B79 from the Bolshekool pluton shown by two asterisks in the lower left part of Fig. 5, A2). Interestingly, the enclosing alaskite, though alkaline, has noticeably lower agpaitic index (0.85–0.95) than the preceding peralkaline granite.

As a whole, mafic rocks formed at different stages of the Late Palaeozoic cycle, unlike granitoids of this cycle, do not reveal any systematic trend of compositional change with time.

5. Radiogenic isotope data

The Sm–Nd and Rb–Sr isotope data are presented in Table 4. In this table the original data for the Carboniferous igneous suites are

Transitional from high-K calc-alkaline to alkaline granite and quartz syenite (Zaza suite), 305–285 Ma								Shoshonitic monzonite–syenite –Qtz syenite series, Low-Selenga suite, 285–278 Ma.					
Angyr		Shaluta		Sharatala		Middle-Turka pluton		Khasurta		Ust-Khilok			
002/1-04*	044/1-04*	zz-1	K47	162-05*	166-05*	BKL438	BKL464	Xc-59-02*	Xc-67-03*	A7-7	B111	B341	B361-20
Gr	Gr	Q-Sy	Gr	Gr	Gr	Gr	Gr	Mnz	Sy	Mnz	Mnz	Sy	Sy
71.80	74.00	66.00	73.20	70.60	72.50	71.72	71.33	55.90	60.00	57.00	57.40	61.20	62.00
0.21	0.16	0.67	0.24	0.37	0.20	0.25	0.36	0.96	0.60	1.14	1.09	1.17	0.68
14.20	14.30	16.00	13.80	14.50	14.35	14.38	14.46	19.50	16.80	20.55	19.19	17.40	18.30
1.37	0.66	1.94	2.20	1.10	0.84	0.82	1.12	2.55	3.30	1.65	2.68	2.55	1.79
0.16	0.31	2.13	0.28	1.21	0.61	0.80	0.62	3.59	2.43	3.68	2.92	2.44	1.02
0.05	0.02	0.09	0.04	0.03	0.04	0.11	0.11	0.16	0.09	0.06	0.12	0.11	0.09
0.39	0.13	0.76	0.23	0.59	0.31	0.30	0.40	2.19	1.33	1.33	1.65	1.07	0.50
0.95	0.63	2.04	0.90	1.51	0.83	0.90	1.00	4.24	3.16	3.70	3.36	2.00	1.45
4.20	3.87	4.92	3.50	3.60	3.66	4.38	4.12	4.95	4.00	5.15	4.45	5.34	5.70
5.38	5.75	5.02	4.92	6.30	6.67	5.27	5.71	4.00	7.44	4.41	5.47	5.67	7.68
0.08	0.03	0.23	0.07	0.11	0.05	0.06	0.09	0.39	0.31	0.40	0.42	0.26	0.14
0.46	0.31	0.33	1.13	0.47	0.43	0.44	0.66	0.86	0.61	1.10	0.66	0.37	0.61
99.25	100.14	100.13	100.51	100.39	100.49	99.43	99.98	99.29	100.07	100.17	99.41	99.58	99.96
495	132	760	450	1186	380	471	490	1607	2408	1650	4140	1300	800
225	182	160	180	181	220	271	130	110	165	79	62	105	120
329	73	380	180	367	133	192	160	782	784	1217	1225	380	260
n.d.	n.d.	n.d.	n.d.	3.80	4.18	n.d.	n.d.	2.48	2.14	n.d.	n.d.	n.d.	n.d.
20.0	18.4	n.d.	n.d.	18	19.3	n.d.	n.d.	21.5	19.0	n.d.	n.d.	n.d.	n.d.
1.00	0.81	1.90	1.70	1.54	1.14	1.20	0.90	0.91	0.99	n.d.	n.d.	n.d.	0.55
30.4	22.7	38.0	20.0	21.4	22.5	19.0	12.5	17.3	14.9	13.0	7.0	27.0	9.0
5.87	3.20	7.30	4.70	8.87	6.42	6.50	6.50	0.93	2.55	n.d.	n.d.	n.d.	9.50
209	95	470	170	327	241	190	180	210	120	613	456	620	680
24	18	40	25	25	16	n.d.	n.d.	20	25	21	21	37	16
28.4	22.4	39.0	34.0	16.9	17.7	n.d.	n.d.	13.1	12.0	n.d.	n.d.	n.d.	4.8
2.17	2.35	3.50	2.90	3.42	1.38	n.d.	n.d.	1.59	3.46	n.d.	n.d.	n.d.	n.d.
3.3	6.6	10.0	6.0	n.d.	n.d.	8.3	6.3	2.7	2.6	15.0	n.d.	n.d.	n.d.
5.5	4.5	n.d.	7.0	n.d.	n.d.	5.8	4.4	3.4	2.3	21.0	n.d.	n.d.	n.d.
2.0	0.7	3.0	2.0	4	1.2	3.6	3.3	9.7	4.3	16.0	n.d.	n.d.	n.d.
n.d.	n.d.	4.0	3.0	3	3.3	3.1	4.6	7.7	8.7	n.d.	n.d.	n.d.	n.d.
17.1	n.d.	17.0	10.0	30	9.8	19.0	15	101	66	132	n.d.	n.d.	n.d.
9.5	9.8	n.d.	n.d.	4	2.3	3.0	3	7.1	5.2	n.d.	n.d.	n.d.	n.d.
23	20	n.d.	n.d.	21	36	34	24	49	36	n.d.	n.d.	n.d.	n.d.
30	15	n.d.	n.d.	36	66	27	42	67	70	n.d.	n.d.	n.d.	n.d.
48	48	55	55	78	71	64	73	58	56	37	41	80	38
102	96	100	120	155	127	105	210	109	110	78	82	150	69
10.8	8.8	n.d.	n.d.	13.4	11.1	12.0	17.0	11.7	12.4	n.d.	n.d.	n.d.	n.d.
35	26	31	34	47	34	29	49	41	46	35	36	54	30
5.83	4.12	4.70	5.00	7.07	4.92	4.50	6.00	7.1	8.4	5.2	5.7	9.8	5.2
0.97	0.43	0.85	0.68	1.26	0.82	0.70	0.82	1.73	1.63	1.40	3.00	1.80	1.50
4.54	3.16	n.d.	n.d.	6.48	3.94	5.00	7.00	4.78	6.25	3.60	n.d.	n.d.	4.30
0.71	0.51	0.62	0.66	0.76	0.52	n.d.	n.d.	0.71	0.88	n.d.	0.68	1.30	0.69
3.87	3.31	n.d.	n.d.	4.77	3.02	2.80	5.60	3.92	4.98	n.d.	n.d.	n.d.	n.d.
0.75	0.59	n.d.	n.d.	0.84	0.54	0.56	1.00	0.75	1.01	n.d.	n.d.	n.d.	n.d.
2.51	1.87	n.d.	n.d.	2.27	1.62	n.d.	3.30	2.18	2.76	1.50	n.d.	n.d.	1.77
	0.25	n.d.	n.d.	0.36	0.23	n.d.	n.d.	0.31	0.42	n.d.	n.d.	n.d.	n.d.
2.50	1.86	1.90	2.20	2.32	1.80	2.30	3.60	1.95	2.77	1.20	1.10	3.40	1.77
0.46	0.28	n.d.	n.d.	0.31	0.23	0.25	0.43	0.29	0.42	0.16	0.17	0.50	0.29
0.56	0.35	0.57	0.43	0.56	0.55	0.45	0.39	0.86	0.66	0.94	1.69	0.58	0.94
13.8	18.6	20.8	17.9	24.0	28.5	20.0	14.5	21.2	14.6	22.1	26.7	16.9	15.4
0.90	0.88	0.85	0.80	0.88	0.92	0.90	0.90	0.64	0.87	0.65	0.69	0.86	0.97
0.98	1.04	0.93	1.08	0.93	0.97	0.99	0.98	0.97	0.82	1.03	0.99	0.94	0.90

(continued on next page)

combined with our isotope data for Early Permian and Late Triassic highly alkaline magmatic rocks (Jahn et al. (2009). They are illustrated in Fig. 10 that allows a discussion of the isotopic evolution of the source regions from the Late Palaeozoic to the Early Mesozoic stages. Fig. 10A shows a plot of εNd(T) vs. intrusive age for all types of magmatic rocks of the Late Palaeozoic cycle. Unlike the mostly positive εNd(T) values of granitoids from the Central Asian Orogenic Belt (Jahn, 2004; Kovalenko et al., 2004 and references therein), the Late Palaeozoic plutonic rocks from Transbaikalia are characterized by negative εNd(T) values. This is true for both felsic and mafic rocks (Fig. 10A). The data set also indicates that granitoids and mafic rocks of the same suite show roughly similar isotopic compositions. Generally a trend of increasing εNd(T) values from the older to younger stages is observed. The Early Mesozoic rocks, however, have a range of εNd(T) values from −1.5 to +4, but the majority have positive values (Table 4; Fig. 10A). A trend of increasing εNd(T) values

Table 2 (*continued*)

Suite	Peralkaline and alkali feldspar syenite and granite (Early-Kunalei sute), 280–273 Ma.							
Pluton/Complex	Bryansky				Khorinsk complex			Bolshekool
Sample no.	B406	B627	B378	B371	M347	3070	M340	M351
Rock type	AFS-Sy	PA-Sy	PA-Gr	PA-Gr	AFS-Sy	AFS-Gr	PA-Gr	Sy-Gr
SiO_2	64.60	65.00	69.80	74.00	65.80	72.18	74.00	75.80
TiO_2	0.55	0.62	0.40	0.21	0.51	0.30	0.25	0.19
Al_2O_3	16.20	16.80	13.60	12.00	17.30	13.99	12.89	12.60
Fe_2O_3	1.61	1.64	1.50	0.87	0.93	0.81	1.11	0.91
FeO	3.49	1.01	2.09	1.48	1.27	0.75	0.52	0.53
MnO	0.10	0.12	0.15	0.10	0.12	0.05	0.10	0.06
MgO	0.36	0.40	0.41	0.21	0.17	0.14	0.06	0.01
CaO	0.43	0.46	0.32	0.14	0.38	0.56	0.03	0.27
Na_2O	5.89	6.42	5.10	4.40	5.31	4.61	4.66	3.94
K_2O	5.85	5.73	5.56	4.66	6.76	5.38	4.95	4.47
P_2O_5	0.08	0.10	0.04	0.02	0.10	0.07	0.02	0.06
LOI	0.88	1.31	1.33	1.36	0.69	0.50	1.06	0.51
Total	100.04	99.61	100.30	99.45	99.34	99.34	99.65	99.35
Ba	390	80	150	66	180	195	53	92
Rb	150	130	260	250	120	210	220	245
Sr	52	34	19	12	28	46	4	27
Cs	n.d.	n.d.	n.d.	n.d.	n.d.	n.d.	1.54	3.10
Ga	19.0	26.0	18.0	27.0	22.0	23.6	22.1	18.1
Ta	1.50	n.d.	4.90	4.20	1.12	3.20	1.54	1.31
Nb	27	38	63	47	25	44	31	26
Hf	15.0	n.d.	14.0	21.0	20.0	12.5	8.9	4.6
Zr	610	930	850	560	970	500	330.0	130
Y	53	64	110	77	42	43	39.0	12
Th	28.0	n.d.	43.0	38.0	16.8	45.2	21.7	23.6
U	3.70	n.d.	6.70	6.20	3.46	7.40	2.77	2.32
Cr	n.d.	n.d.	n.d.	n.d.	n.d.	n.d.	n.d.	n.d.
Ni	n.d.	n.d.	n.d.	n.d.	n.d.	n.d.	n.d.	n.d.
Co	n.d.	n.d.	n.d.	n.d.	n.d.	n.d.	n.d.	n.d.
Sc	n.d.	n.d.	n.d.	n.d.	n.d.	n.d.	n.d.	n.d.
V	n.d.	n.d.	n.d.	n.d.	n.d.	n.d.	7	49
Cu	n.d.	n.d.	n.d.	n.d.	n.d.	n.d.	4	8
Pb	n.d.	n.d.	n.d.	n.d.	n.d.	n.d.	33	26
Zn	n.d.	n.d.	n.d.	n.d.	n.d.	n.d.	67	33
La	120	120	98	66	74	57	50	33
Ce	260	240	220	170	245	141	96	50
Pr	n.d.	n.d.	n.d.	n.d.	17.5	13.0	9.0	3.6
Nd	100	81	84	67	63	43	30	9
Sm	13.00	12.00	13.00	12.00	10.46	7.90	5.08	1.29
Eu	1.40	1.20	1.10	0.77	0.76	0.45	0.32	0.14
Gd	n.d.	n.d.	n.d.	n.d.	7.83	5.96	4.18	1.13
Tb	1.60	1.50	2.20	2.30	1.27	1.04	0.71	0.18
Dy	n.d.	n.d.	n.d.	n.d.	6.75	6.16	4.27	1.32
Ho	n.d.	n.d.	n.d.	n.d.	1.36	1.32	0.94	0.34
Er	n.d.	n.d.	n.d.	n.d.	4.12	4.30	3.03	1.27
Tm	n.d.	n.d.	n.d.	n.d.	0.64	0.75	0.50	0.25
Yb	4.40	3.60	8.50	7.90	4.38	5.43	3.58	2.00
Lu	0.58	0.51	1.30	1.10	0.72	0.83	0.58	0.35
*Eu/Eu**	0.34	0.32	0.25	0.18	0.25	0.19	0.21	0.35
$(La/Yb)_n$	19.6	23.9	8.3	6.0	12.2	7.5	10.0	11.8
NK/A	0.99	1.00	1.06	1.02	0.93	0.96	1.01	0.90
A/CNK	0.97	0.96	0.91	0.96	1.04	0.97	0.99	1.07

with decreasing age is also present in the Mesozoic rocks, but negative εNd(T) are limited to the early Mesozoic granitoids (e.g., the Kharitonovo complex and the Yermakovka pluton).

Depleted-mantle-based Nd model ages (T_{DM}) were calculated for the felsic rocks using a two-stage model (DePaolo et al., 1991; Keto and Jecobsen, 1987). This was done in order to offset the effect of fractional crystallization, which may lead to aberrant model ages. However, a single-stage model was used for the T_{DM} calculation for mafic rocks. Table 4 shows that the variation in model ages roughly mirrors that of the εNd(T) values: ~1.57–1.70 Ga in the Barguzin suite; 1.47–1.67 Ga in the coeval Chivyrkui and Zaza suite, and 1.27–1.40 Ga in the three early Permian suites. The Early Mesozoic felsic and mafic rocks have significantly younger model ages from 0.76 to 1.11 Ga (Table 4). There is little difference in εNd(T) and T_{DM} between the felsic and mafic rocks, between the PA and AFS granitoids and between the syenite and granite from the same suite (Fig. 10; Table 4).

The Sr isotope data are roughly consistent with the Nd isotope data, although trends are less clear owing to the fairly large uncertainty in the calculated I(Sr) values. The uncertainty in I(Sr) calculation for individual samples increases with increasing $^{87}Rb/^{86}Sr$ ratios. When $^{87}Rb/^{86}Sr$ ratios are >5–10, the induced errors in calculated I(Sr) become too large to yield significant I(Sr) values for petrogenetic interpretation (Jahn, 2004; Jahn et al., 2009; Wu et al., 2002). $^{87}Rb/^{86}Sr<5$ ratios are characteristic of the Carboniferous suites and early Permian Lower-Selenga suite (Table 4). However, in the vast majority of samples from the highly alkaline (peralkaline and alkali feldspar) granitoids these ratios range from 20 to 80, so the I(Sr) values are mostly unreasonable (from 0.67465 to 0.76516) and

Table 3
Chemical composition (wt.%, ppm) of representative mafic rocks from the Late Paleozoic igneous suites from Transbaikalia, Russia.

Suite	Gabbro, Chivyrkui suite, 305–285 Ma						Gabbro, Zaza suite, 305–285 Ma		Microgabbro, Low-Selenga suite, 285–278 Ma					Mafic rocks, Early-Kunalei sute, 281–275 Ma					Sisson et al., 2005 (experim.)
Pluton	Orefyev		Burgasy		Nesterikha		Shaluta		Khasurta		Ust-Khilok			Khorinsk complex			Bolshekool		
Sample no.	Or-28/2-02*	Or-35-02*	Bu-19/1-02*	Bu-07-68/6*	M175-1	M175-5	K4-4	K43-8a	Xc-13/3-02*	Xc-13/6-02*	B517-3	B342	368-21	M393	M342	M606	B79	B76-1	AD19-93
Rock type	Gb	Ol-Gb	Gb	Gb	Gb	Gb	Gb	Gb	Gb	Gb	mGb	mGb	MME	*dyke*	*Volcan*	*MME*	*Gbsgr*	*Gbsgr*	High-K bas
SiO_2	47.80	51.50	52.00	51.40	50.00	51.20	50.50	51.20	48.40	50.60	48.70	48.90	49.20	50.79	51.80	50.20	48.74	49.44	50.74
TiO_2	1.46	1.12	1.21	1.49	1.22	0.96	0.86	0.94	1.40	1.15	1.52	1.41	1.47	0.92	1.44	0.93	1.41	1.00	1.25
Al_2O_3	19.75	19.15	19.00	18.1	16.50	17.10	15.90	17.65	17.95	18.65	17.80	17.40	18.95	17.8	18.00	20.1	15.95	16.13	19.71
Fe_2O_3	3.86	1.67	2.89	4.66	2.98	2.92	2.25	2.48	4.80	3.82	3.19	6.06	3.60	3.12	2.22	3.25	3.68	3.70	9.69
FeO	6.62	7.82	4.29	6.61	5.80	5.48	6.41	6.14	6.84	6.02	6.70	4.38	6.94	5.12	6.29	4.23	6.11	4.71	
MnO	0.13	0.14	0.11	0.16	0.14	0.15	0.18	0.17	0.13	0.15	0.14	0.18	0.13	0.14	0.13	0.13	0.12	0.13	0.15
MgO	3.84	4.68	3.92	6.70	5.60	4.72	7.28	5.12	4.75	4.88	5.30	4.34	4.24	5.21	5.23	3.72	6.27	6.56	4.52
CaO	9.33	7.90	8.37	7.56	7.40	6.66	9.45	6.15	8.00	6.93	7.90	8.94	6.12	7.09	6.53	8.36	9.60	10.39	7.39
Na_2O	3.38	3.63	3.85	3.13	3.12	3.94	3.47	4.18	3.48	3.72	3.76	3.81	4.79	3.29	4.30	3.52	2.69	3.00	3.76
K_2O	1.22	1.78	2.69	1.74	2.40	2.48	2.23	2.53	2.12	2.47	2.01	2.01	2.20	2.32	2.12	2.30	1.58	1.54	2.32
P_2O_5	0.38	0.29	0.46	0.50	0.45	0.32	0.34	0.44	0.33	0.38	0.82	0.51	0.59	0.27	0.33	0.28	0.79	0.36	0.46
LOI	1.72	0.66	0.70	2.41	3.64	3.60	1.35	3.41	1.34	1.49	2.30	1.88	1.79	3.76	1.74	2.35	2.26	2.42	
Total	99.49	100.34	99.49	104.46	99.25	99.53	100.22	100.41	99.54	100.26	100.14	99.82	100.02	99.83	100.13	99.37	99.20	99.38	100
Ba	839	1192	961	688	1160	1190	860	990	1600	1400	1100	800	1953	760	590	830	1000	1150	
Rb	16	18	47	39	82	65	65	133	51	50	59	62	80	60	41	55	34	25	
Sr	1357	1352	1481	1088	890	990	920	1049	1430	1350	1500	1260	1415	780	640	920	1360	1150	
Ga	21	21	20	20	n.d.	n.d.	n.d.	n.d.	n.d.	n.d.	n.d.	n.d.	n.d.	18.42	28.90	19.6	n.d.	n.d.	
Ta	0.22	0.34	0.41	0.57	n.d.	n.d.	0.54	0.55	n.d.	n.d.	n.d.	n.d.	n.d.	0.81	1.51	0.81	n.d.	n.d.	
Nb	4.1	4.1	8.0	10.1	n.d.	n.d.	12	9	5	7	11	6	7	7	9	6	6	4	
Hf	3.62	1.55	3.53	3.31	n.d.	n.d.	3.4	4.1	n.d.	n.d.	n.d.	n.d.	n.d.	4.16	6.93	2.26	n.d.	n.d.	
Zr	164	162	170	137	104	174	140	151	140	140	190	120	177	170	230	150	100	84	
Y	21	20	22	22	n.d.	n.d.	35	22	17	17	29	36	34	22	30	20	19	14	
Th	3.18	1.19	3.40	8.25	n.d.	n.d.	4.0	9.6	n.d.	7.00	4.0	2.7	n.d.	4.49	4.40	3.27	n.d.	n.d.	
U	0.90	0.39	0.80	2.13	n.d.	n.d.	n.d.	1.10	n.d.	n.d.	0.46	0.31	n.d.	1.13	1.31	0.96	n.d.	n.d.	
Cr	n.d.	n.d.	n.d.	110	n.d.	n.d.	250	97	n.d.	n.d.	n.d.	n.d.	27	n.d.	n.d.	n.d.	n.d.	n.d.	
Ni	n.d.	n.d.	n.d.	n.d.	n.d.	n.d.	76	36	n.d.	n.d.	n.d.	n.d.	35	n.d.	n.d.	n.d.	n.d.	n.d.	
Co	29.3	31.5	22.2	42.2	n.d.	n.d.	36	31	n.d.	n.d.	34	n.d.	31	n.d.	n.d.	n.d.	n.d.	n.d.	
Sc	24.9	20.9	18.2	19.0	n.d.	n.d.	30	18	n.d.	n.d.	n.d.	n.d.	n.d.	n.d.	n.d.	n.d.	n.d.	n.d.	
V	253	184	148	238	n.d.	n.d.	195	100	n.d.	n.d.	120	n.d.	185	171	231	218	n.d.	n.d.	
Cu	57	15	36	157	n.d.	n.d.	n.d.	n.d.	22	32	n.d.	n.d.	n.d.	44	14	21	n.d.	n.d.	
Pb	68	59	13	621	n.d.	n.d.	n.d.	n.d.	14	12	n.d.	n.d.	n.d.	6	24	8	n.d.	n.d.	
Zn	94	71	100	n.d.	n.d.	n.d.	n.d.	n.d.	88	90	n.d.	n.d.	n.d.	74	812	78	n.d.	n.d.	
La	32	32	44	54	n.d.	n.d.	43	46	n.d.	n.d.	35	50	47	29	42	31	n.d.	n.d.	
Ce	65	60	84	92	n.d.	n.d.	100	93	n.d.	n.d.	77	120	92	60	91	63	n.d.	n.d.	
Pr	7.3	6.4	8.9	12.0	n.d.	n.d.	n.d.	n.d.	n.d.	n.d.	n.d.	n.d.	n.d.	7.1	12.0	7.4	n.d.	n.d.	
Nd	29	25	35	46	n.d.	n.d.	42	34	n.d.	n.d.	36	57	42	27	53	28	n.d.	n.d.	
Sm	5.72	5.50	6.81	8.36	n.d.	n.d.	8.4	6.0	n.d.	n.d.	7.30	8.70	7.60	5.17	11.03	5.36	n.d.	n.d.	
Eu	1.85	1.86	1.97	2.09	n.d.	n.d.	1.9	1.4	n.d.	n.d.	2.00	2.00	2.20	1.36	3.25	1.38	n.d.	n.d.	
Gd	5.15	4.47	5.66	6.35	n.d.	n.d.	n.d.	n.d.	n.d.	n.d.	n.d.	n.d.	n.d.	4.88	10.13	5.58	n.d.	n.d.	
Tb	0.69	0.60	0.89	0.76	n.d.	n.d.	1.1	0.8	n.d.	n.d.	0.93	1.30	0.84	0.58	1.51	0.60	n.d.	n.d.	
Dy	3.82	3.56	4.15	4.13	n.d.	n.d.	n.d.	n.d.	n.d.	n.d.	n.d.	n.d.	n.d.	4.08	7.96	3.95	n.d.	n.d.	
Ho	0.79	0.74	0.85	0.84	n.d.	n.d.	n.d.	n.d.	n.d.	n.d.	n.d.	n.d.	n.d.	0.84	1.55	0.82	n.d.	n.d.	
Er	2.30	1.89	2.53	1.71	n.d.	n.d.	n.d.	n.d.	n.d.	n.d.	2.00	2.70	1.80	2.32	4.17	2.25	n.d.	n.d.	
Tm	0.30	0.28	0.31	0.31	n.d.	n.d.	n.d.	n.d.	n.d.	n.d.	n.d.	n.d.	n.d.	0.32	0.56	0.31	n.d.	n.d.	
Yb	1.77	1.38	1.67	1.81	n.d.	n.d.	2.3	1.8	n.d.	n.d.	n.d.	n.d.	1.50	2.24	3.52	2.12	n.d.	n.d.	
Lu	0.29	0.23	0.28	0.31	n.d.	n.d.	n.d.	n.d.	n.d.	n.d.	0.34	0.38	0.17	0.33	0.51	0.30	n.d.	n.d.	
*Eu/Eu**	1.02	1.11	0.94	0.84	n.d.	n.d.	0.71	0.73	n.d.	n.d.	0.87	0.70	0.94	0.82	0.92	0.77	n.d.	n.d.	
$(La/Yb)_n$	13.10	16.74	18.92	21.21	n.d.	n.d.	13.41	18.33	n.d.	n.d.	n.d.	n.d.	22.48	9.43	8.54	10.59	n.d.	n.d.	
NK/A	0.35	0.41	0.49	0.39	0.47	0.54	0.51	0.55	0.45	0.47	0.47	0.49	0.54	0.45	0.52	0.41	0.38	0.41	
A/CNK	0.83	0.86	0.78	0.87	0.78	0.80	0.63	0.85	0.79	0.87	0.78	0.70	0.88	0.85	0.85	0.85	0.68	0.63	

(1) Abbreviations: Gb, gabbro; Ol-Gb, olivine gabbro; mGb, microgabbro; MME, microgranular mafic enclave; dyke, dykes of basalt; volcan, basaltic volcanics; Gbsgr, microgabbro enclaves in syenogranites.
(2) Chemical data are compiled from Litvinovsky et al., 1993, 1995a; 2002a; Jahn et al., 2009. *original analyses.
(3) In the last column, the composition of high-K basalt used in melting experiments is given after Sisson et al. (2005). Mellting to the degree of ~20% produced partial melt of the alkaline granite composition (see Discussion).

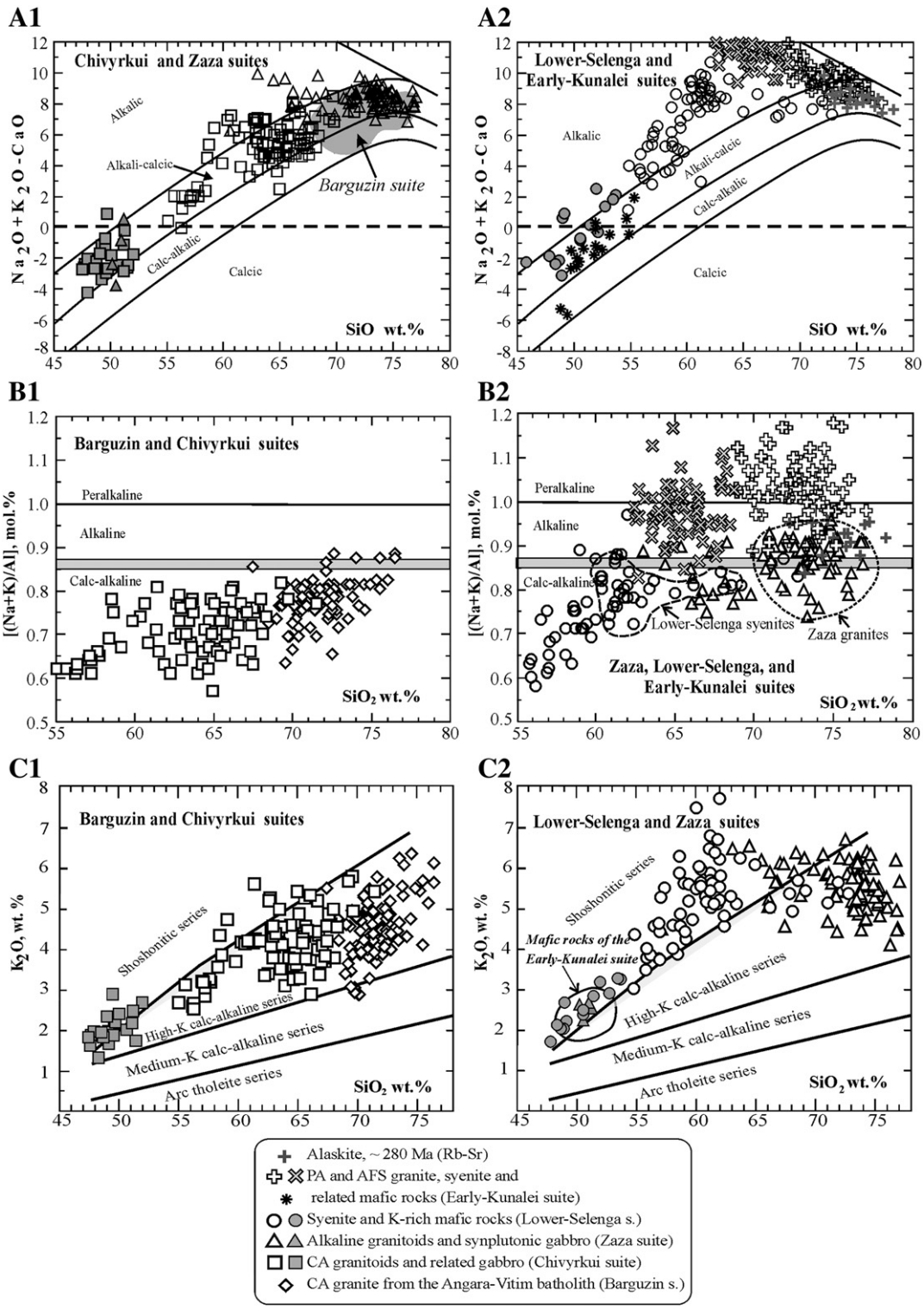

Fig. 5. Compositions of Late Palaeozoic granitoids shown on selected classification diagrams. A1 and A2, SiO_2 vs. MALI (the modified alkali-lime index) diagrams for Late Carboniferous (A1) and Early Permian (A2) igneous suites, after Frost et al. (2001).B1 and B2, SiO_2 vs. $(Na_2O + K_2O)/Al_2O_3$, mol% diagrams (agpaitic index), after Liégeois and Black (1987). C1 and C2, SiO_2 vs. K_2O diagram for calc-alkaline plutonic rocks, with simplified boundary lines, after Rickwood (1989).

geologically meaningless (shown in italics in Table 4). To obtain a more reliable set of initial Sr data for granitoids, we calculated the I (Sr) values from WR isochrons in plutons which yielded Rb–Sr ages comparable to the U–Pb zircon ages (Table 5). These data, along with a few reliable samples, are shown in the $(^{87}Sr/^{86}Sr)_T$ vs. age diagram (Fig. 10B). The diagram demonstrates that, despite significant overlap in I(Sr) values for all Late Palaeozoic granitoids, there is a general trend of decreasing I(Sr) with decreasing age of the granitoid intrusions. As expected, this trend is a mirror image of the trend established from the Nd isotopic variation.

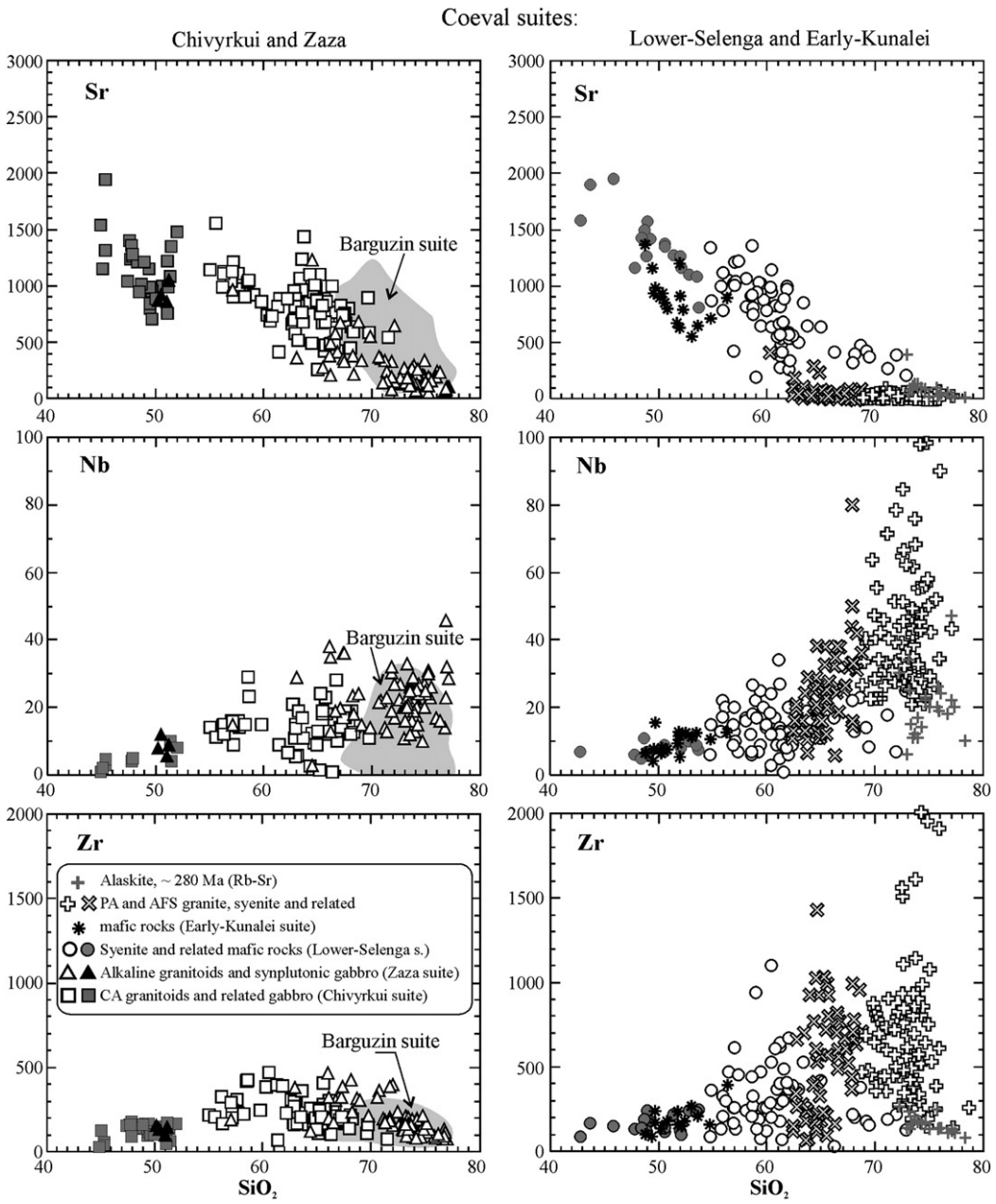

Fig. 6. Silica variation diagrams demonstrating concentrations and compositional trends of selected trace elements in granitoids of coeval Late Palaeozoic igneous suites.

6. Discussion

6.1. Provenance of the Late Palaeozoic felsic magmas based on Sr–Nd–O isotope constraints

Radiogenic and stable isotope ratios are commonly considered as the most reliable tracers of magma sources. The Sr–Nd isotope data given in this paper (Table 4; Fig. 10) are discussed here together with the results of an oxygen isotope study by Wickham et al. (1996). Since most Transbaikalian rocks suffered extensive meteoric-hydrothermal alteration, only $\delta^{18}O$ values of titanite, quartz and whole-rock granite samples with $\Delta^{18}O$(Qtz–Fsp) = 0 to +2‰, $\Delta^{18}O$(Qtz–WR) ~1 and $\Delta^{18}O$ (Ttn–WR)~−4, which are close to the expected equilibrium fractionations at magmatic temperatures (Wickham et al., 1996), were considered as representative of magmatic values. For related gabbro most data were obtained from whole-rock samples. In a few samples $\delta^{18}O$ was measured also in amphibole and plagioclase which showed fairly low, mantle-like values for amphibole (6.10 and 6.88‰) and higher values, 8.33–8.57‰, for plagioclase. The oxygen isotope data ratios considered as magmatic are presented in Table 6 and Fig. 11, along with unpublished authors' data for 11 mineral samples analyzed at the University of Wisconsin, USA in collaboration with Prof. J. Valley.

The radiogenic and stable isotope data demonstrate gradual change of εNd(T), I(Sr) and $\delta^{18}O$ values in felsic and mafic rocks during a protracted period of time, about 120 m.y., from Carboniferous to Late Triassic (Figs. 10, 11). At first glance this can be interpreted as systematic change in the proportion of mantle- and crust-derived components in the silicic magmas. However, petrogenetic interpretation of the Sm–Nd isotope data is complicated by the fact that all Late Palaeozoic mafic rocks have negative εNd(T) values ranging from −5 to −1 (Fig. 10). This concerns both plutonic and

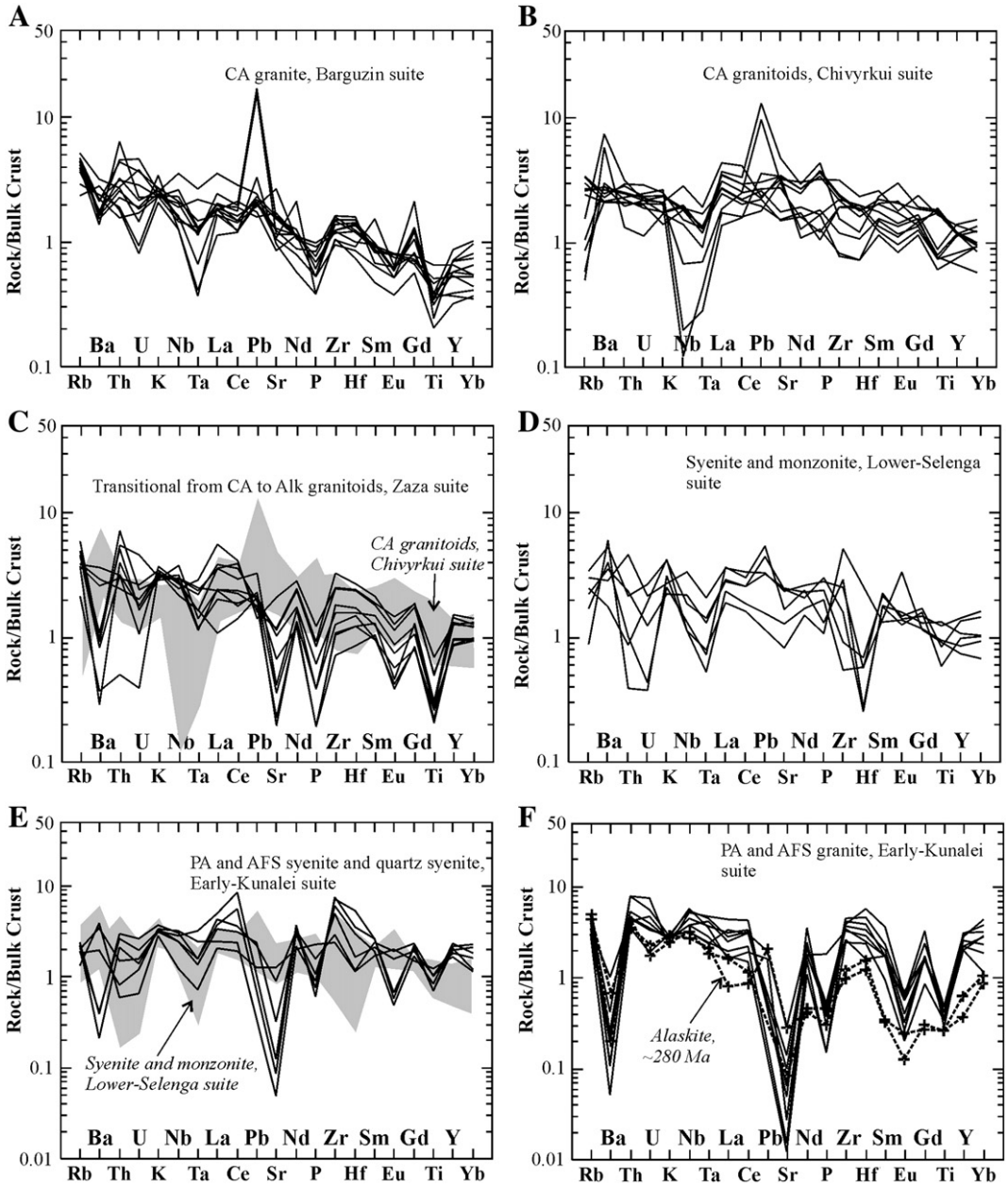

Fig. 7. A–F, Bulk crust-normalized spidergrams for the granitoids of the Late Palaeozoic igneous suites. In C and E, compositions of coeval suites (Chivyrkui and Lower-Selenga suites, respectively) are shown as gray fields. The bulk crust composition after Rudnick and Gao (2003).

volcanic mafic rocks. Yarmolyuk et al. (1998, 2002) have earlier reported that Late Palaeozoic K-rich basalts of the MTB are characterized by slightly negative (−3) to near-zero εNd(T) values. We interpret such an isotopic signature in mafic rocks to be characteristic of the mantle beneath the Transbaikalia region in the Carboniferous – Permian. It is likely that lithospheric mantle was enriched in the ancient acid crust material subducted during accretion and collision of the two continental plates. This inference is supported by mildly enhanced I(Sr) ratios, 0.7050–0.7060 (Fig. 10B), and clear negative Nb anomalies in multi-element spidergrams (Fig. 9).

Another feature of the Sm–Nd isotope data is the significant overlap of εNd(T) values in felsic and related mafic rocks and their similar model ages (Table 4; Fig. 10) This suggests that silicic magmas included a significant mantle-derived component at each stage of magmatic activity. However, the negative εNd(T) values of the mafic rocks cannot be used for a realistic estimate of the proportions of mantle versus ancient continental crust components. A more reliable petrogenetic interpretation should be based on comparative consideration of radiogenic and stable isotope data.

Granites from the *Barguzin igneous suite* (the Angara–Vitim batholith) have the lowest εNd(T) values ranging from −5.7 to −7.7, approaching the values of Proterozoic crust (Fig. 10). The T_{DM} age is the oldest, 1.57–1.70 Ga. Also these rocks have the highest $\delta^{18}O$(WR) values, from 10 to 12‰, which may be considered as magmatic supported by corresponding $\delta^{18}O$ values in titanite (7.2–7.6‰) and quartz (11–14‰). It is worth noting that the $\delta^{18}O$(WR) value for gneiss sampled from a large metamorphic roof pendant (Table 6, sample 604) is 12.2‰, which is similar to that for the granite. Thus it is probable that ancient continental crust rocks were the main source of the granite making up the Angara–Vitim batholith.

In contrast to the calc-alkaline granites of the Barguzin suite, the youngest Late Palaeozoic highly alkaline intrusive rocks (*Lower-Selenga suite* and almost concurrent *Early-Kunalei suite*) demonstrate

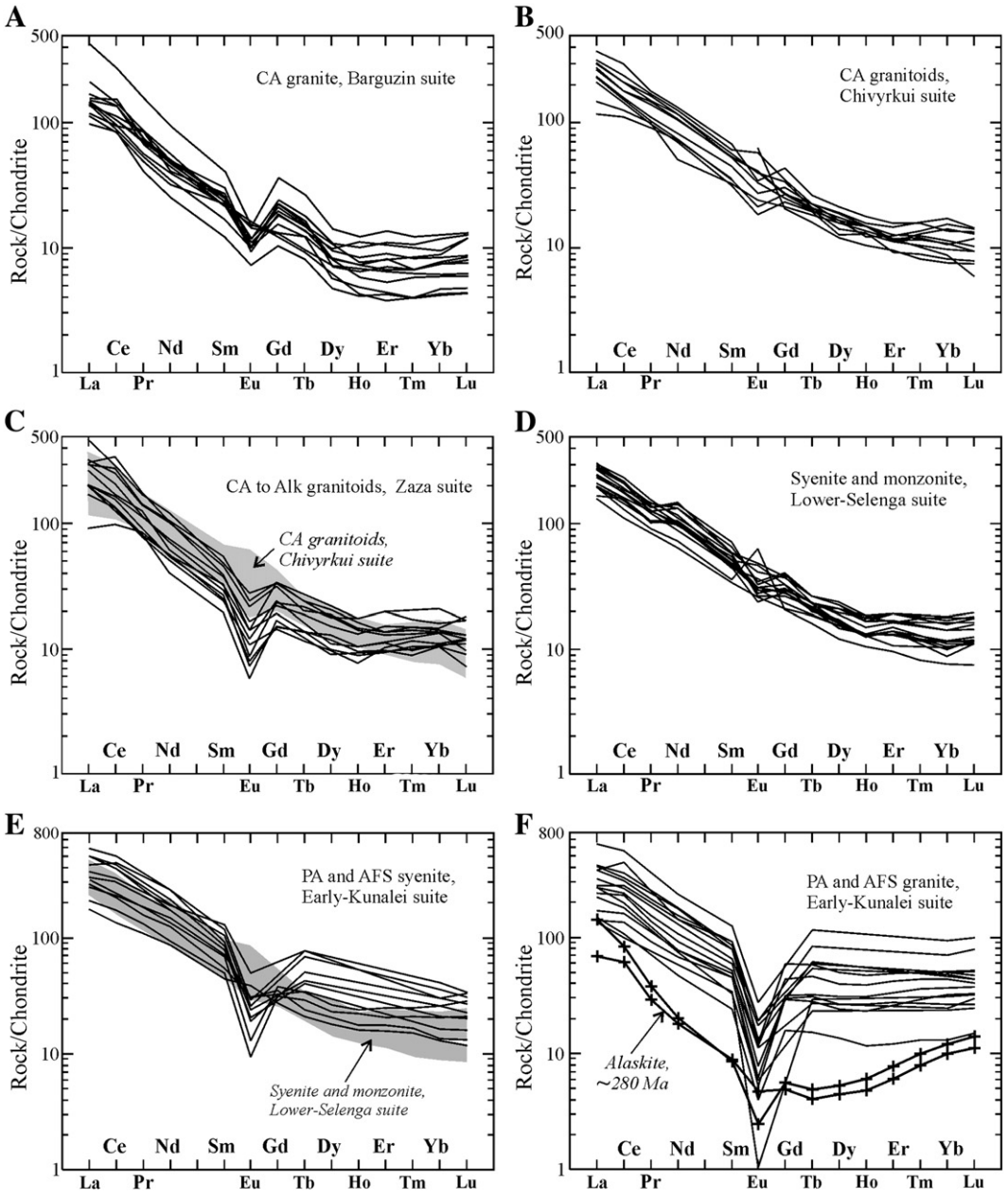

Fig. 8. A–F, REE patterns of granitoids from the Late Palaeozoic igneous suites. In C and E, compositions of coeval Chivyrkui granitoids and Lower-Selenga syenite–monzonite, respectively, are shown as gray fields. Here and in Fig. 9 chondrite values are from Sun and McDonough (1989).

isotopic evidence of a predominance of a mantle-derived component in the felsic rocks. This is exhibited in the overlap of the εNd(T) values and young model ages (T_{DM} = 1.27–1.40 Ga) for mafic and felsic rocks from each suite (Fig. 10A; Table 4). The younger model age suggests increased proportion of the asthenosphere source. The $\delta^{18}O$ values are mantle-like, 6–7‰ in whole-rock samples and 3.4 to 4.99‰ in titanite (Fig. 11; Table 6). Slightly higher $\delta^{18}O$(WR) in selected samples, from 7.17 to 7.5‰, suggests minor admixture of an ancient continental crust component in some of the syenites from the Lower-Selenga suite. At the same time, mild distinctions between the two suites should be noted: εNd(T) values in mafic rocks from the Lower-Selenga suite are −4.1 and −4.5, whereas in the Lower-Kunalei suite they range from −3.5 to almost zero suggesting that some of the mafic rocks are not related to granitoids. In felsic rocks these values range from −3.7 to −4.9 and from −2.0 to −4.1, respectively. These observations also indicate that, despite significant temporal overlap and the predominance of a mantle component, the protoliths of the two suites were not identical.

Alaskite that intruded peralkaline granite in the Khorinsk volcano–plutonic structure (Early-Kunalei suite) is characterized by mildly negative εNd(T), −2.2 and −2.6 and low $\delta^{18}O$(WR) values, 5.9‰ and 6.8‰, which points to the prevalence of a mantle-derived component in the granite magma. However, it is unlikely that the granite magma was produced from the same source as the highly alkaline granitoids. This conclusion follows from the comparison of chemical traits: the alaskite is richer in Sr and Ba (Fig. 7F) and contains less REE and Zr (Figs. 7F and 8F). Likewise related mafic rocks that occur as large MMEs in the syenogranite are significantly enriched in CaO, Sr, Ba, MgO and contain much less Rb, Zr and K_2O as compared with mafic rocks related to AFS and PA granitoids (Table 3).

The radiogenic and oxygen isotopic data for the coeval low-silica granitoids of the *Chivyrkui suite* and quartz syenite–granite *Zaza suite*

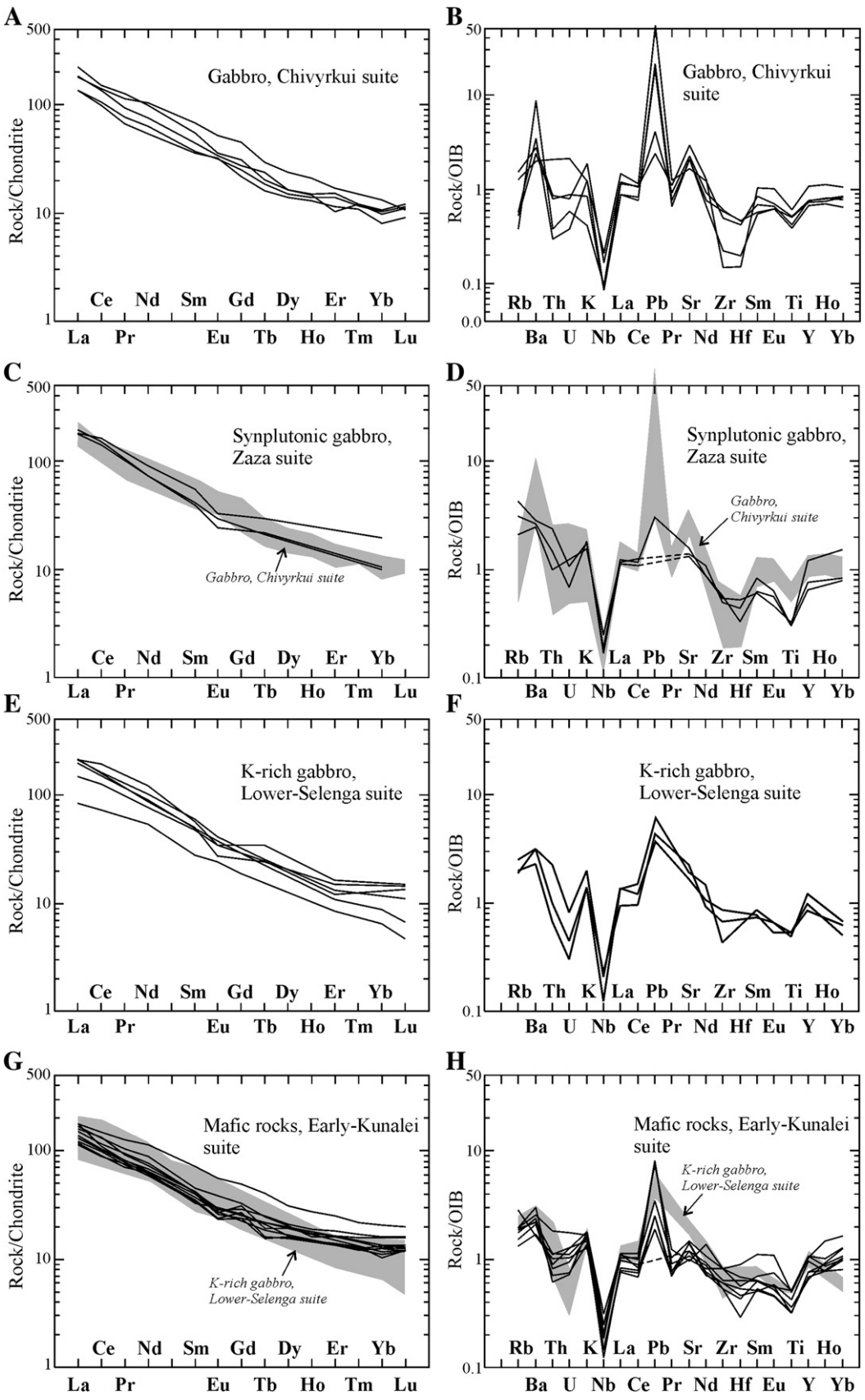

Fig. 9. A–H, chondrite normalized REE patterns and primitive mantle-normalized spidergrams for mafic rocks from Late Palaeozoic igneous suites. In C, D, and G, H compositions of coeval mafic rocks (Chivyrkui and Lower-Selenga, respectively) are shown as gray fields. Primitive mantle values are from Sun and McDonough (1989).

are intermediate between those for the Barguzin and Early-Kunalei suites (Figs. 10 and 11; Tables 4 and 6). The $\delta^{18}O$ values for the whole-rock samples and quartz are 2–3‰ lower than those in the Barguzin suite and 2–3‰ higher than in the Lower-Selenga suite. Similar distinctions are observed for the $\delta^{18}O$ values in titanites from the Zaza, Barguzin and Lower-Selenga suites (Fig. 11). The εNd(T) values for granitoids from the Chivyrkui and Zaza suites overlap, though in the former they vary widely, from −4.6 to −13.1, i.e. to ancient continental crust values, whereas in the Zaza suite variation is minimal, from −5.5 to −5.7, and they are intermediate between the granitoids from the Barguzin and Lower-Selenga suites. Taken together, these observations suggest involvement of crust- and mantle-derived materials in the generation of silicic magmas. If granite from the Barguzin suite is assumed to be a crust-derived end-member, while highly alkaline rocks are mantle-derived, the proportion of crustal component in granitoids from the Chivyrkui and Zaza suites can be estimated at about 50%.

Rocks from the the late Triassic *Late-Kunalei suite* are distinguished from the compositionally similar *Early-Kunalei suite* by their positive εNd(T) values (Table 4; Fig. 10). Both silicic and mafic rocks are characterized by similar εNd(T) and I(Sr) values, +1 to +4 and 0.7040 – 0.7050 respectively, and similar young model age ranging from 0.76 to 1.10 Ga. This suggests cogenetic derivation of mafic and felsic magmas from a mildly depleted mantle source (Jahn et al., 2009). Such interpretation is consistent with the typical mantle-like oxygen isotope data: the $\delta^{18}O$(WR) values range mostly from 5.1 to 7‰; the $\delta^{18}O$(Ttn) values are the lowest, from 2.8 to 3.8‰ (Fig. 11).

6.2. Variable models of felsic magma generation in Transbaikalia

6.2.1. The Angara–Vitim batholith (Barguzin suite)

Geophysical modeling, based upon interpretation of gravitational anomalies and seismic sounding, suggests that the numerous plutons that make up the AVB take the form of a large plate-like granitoid body of about 200,000 km^2 in area. The thickness of the batholith ranges from several km to 30 km with a mean thickness of 10–15 km (geophysical data of A.M. Alackshin in Litvinovsky et al., 1993). The current crust thickness for the territory occupied by the AVB is ca. 40–45 km (Pismenny and Alakshin, 1984). The batholith was emplaced at a depth of 10–15 km (Litvinovsky et al., 1993), and since then the crust in the region has significantly thinned (Kovalenko et al., 2004; Windley et al., 2007; Yarmolyuk et al., 2005). It follows that the batholith had to be emplaced in a thickened crust. Since the AVB is exposed at the surface of a very large territory (Fig. 1), it is assumed that its roof and the uppermost part have been completely eroded. This provides minimal crustal thickness estimates at 60 – 65 km at the time of batholith emplacement.

The Sr–Nd–O isotope data (see earlier discussion) attest that granite magmas were mostly crust-derived. Based on the average chemical composition of the batholith (616 whole-rock analyses of granites) and the average compositions of the potential sources rocks such as Precambrian gneiss and crystalline schist in Transbaikalia and other well-studied regions in the world, mass-balance calculations were performed (Litvinovsky et al., 1993). They demonstrated that granite magma of the given composition could be produced by 60–70% melting of metamorphic lithologies (gneiss and schist in proportion 3:1). Such a high melting percentage provides high extent of magma separation and may account for the formation of a 10–15 km-thick granite body from a metamorphic source layer of a realistic thickness, about 20–25 km. However, in the middle-lower crust (6–10 kbar) melting processes are constrained by temperature and H_2O content in the potential source rocks of quartz diorite–granodiorite composition. Numerous melting experiments demonstrated that crust-derived granite melts were likely produced at temperature of 800 ± 50 °C (Johannes and Holtz, 1996; Vielzeuf and Holloway, 1988 and references therein); further increase in temperature would result in shifting the partial melt composition from granite to low silica granodiorite and quartz monzonite, which are rare in the Angara–Vitim batholith. Another constraint is a fairly low, 1–2 wt.%, H_2O content in the source metamorphic rocks (H_2O is bonded mostly in micas and amphiboles) that can provide only 25–30% of granite at 6–10 kbar and 800–850 °C (Johannes and Holtz, 1996; Shkodzinsky, 1985). Decrease of pressure to ~3 kbar (upper level of the batholith emplacement) does not resolve the problem: experiments showed that the percentage of granite melt would increase to ~35–40%, still two times less than the required values. Only the influx of H_2O in the course of magma production can provide the high extent of melting required by the mass balance calculations at realistic temperatures and pressures. A model of crustal anatexis that was accompanied by a limited influx of H_2O-enriched volatiles from underplating basalt magmas (convective diffusion) was suggested by Litvinovsky and Podladchikov (1993). It is described in detail in the cited paper, with a mathematical formulation of the conditions favoring this type of anatexis. In the following discussion only some main ideas that are relevant to the AVB formation are outlined.

The critical thickness of a melted layer capable of convection is about 100 m (Huppert and Sparks, 1988; Wickham, 1987). Hence the generation of voluminous silicic magma in the crust had to be accompanied by extensive convective flow soon after the onset of wholesale melting. Convection was also vigorous in the underplating mantle-derived mafic melts; it was attenuated when the extent of crystallization reached 60–70%. At that point, the viscosity of the mafic melt exceeded 10^{12}–10^{14} poise, and convection became too weak.

Well-developed convection with $Ra \sim 10^6$ (Raleigh number, a dimensionless parameter characterizing the intensity of convective movements) increases the diffusive mass flux by a factor of 1000 as compared with that which would occur without convective movement. Whereas the result of diffusion may be disregarded in the absence of convection, this mechanism of mass transport may play an important role when convection occurs. Thus the combination of diffusion and convective movement of the magmatic liquid (convective diffusion) can be the key mechanism, which provides a solution to the mass transfer problem in the water-undersaturated system.

The flux of some melt components by diffusion leads to the establishment of “transient two-liquid equilibria” (Watson, 1976, 1982) with some components showing strong preference for silicic over mafic liquid. Experimental data and model calculations for H_2O solubility indicate that in terms of mass contents, the distribution coefficients for H_2O at the contacts between silicic and mafic magmas range from 1.2 to 1.5. It follows that when the subjacent basalt melt with initial 1–2 wt.% H_2O is 50% crystallized, the water content in the equilibrium silicic melt would be ~3–5 wt.%. This should cause the flux of H_2O from the underplating basalt into the silicic melt. Thus, if two adjacent convecting magma systems, basic and silicic, have been established, a transfer of water from the basaltic layer into the silicic one can be efficiently carried out by convective diffusion. The convection would also ensure effective transportation of H_2O from the bottom of the silicic magma chamber to its upper levels in a system which is far from being water saturated. Convective motion also promotes magma homogenization and removal of refractory restite.

It is probable that a similar redistribution mechanism may be also applied to alkalis, which have high diffusivities similar to H_2O. For potassium, such redistribution has actually been proved by experiment for adjacent silicic and mafic melts (Johnston and Wyllie, 1988; Koyaguchi, 1989; Watson, 1976, 1982). Watson (1984) showed that the distribution coefficient of potassium between coexisting granite and basaltic magmas is higher than 2.

The outlined mechanism of H_2O and alkalis transfer allows considerable volumes of silicic magma to be generated in the lower-

Table 4
Sr–Nd isotope data for Late Paleozoic and Triassic granitoids, gabbro and related volcanic rocks from Transbaikalia.

Sample #	Rock	Pluton	Age (Ma)	Rb	Sr	$^{87}Rb/^{86}Sr$	$^{87}Sr/^{86}Sr$	2 sm	$(^{87}Sr/^{86}Sr)_T$	Sm	Nd	$^{147}Sm/^{144}Nd$	$^{143}Nd/^{144}Nd$	2 sm	eNd (0)	f (Sm/Nd)	eNd (T)	T_{DM}-1 (Ma)	T_{DM}-2 (Ma)
Barguzin suite (Angara–Vitim batholith), high-K calc-alkaline granite, 330–310 Ma																			
Zg51/2-03	Gneis. granite	Zelenogriv.	325	107.3	172.9	1.797	0.715537	14	0.70723	1.444	7.003	0.1247	0.512093	6	−10.6	−0.37	−7.7	1805	1701
Zg64/3-04	Gneis. Granite	Zelenogriv.	325	143.3	150.2	2.762	0.715671	12	0.70289	0.855	4.295	0.1203	0.512148	7	−9.6	−0.39	−6.4	1632	1606
Gl-8/3-03	Granite	Goltsovy	313	61.5	289.3	0.615	0.709680	10	0.70694	2.406	13.17	0.1104	0.512152	8	−9.5	−0.44	−6.0	1471	1587
Gl-5/3-03	Granite	Goltsovy	313	176.4	279.7	1.826	0.714077	10	0.70594	3.754	22.79	0.0996	0.512149	7	-9.5	-0.49	-5.7	1335	1577
Te-44-02	Porph. granite	Temensky	318	12.67	439.1	0.083	0.707259	8	0.70688	1.425	7.713	0.1117	0.512090	8	−10.7	−0.43	−7.2	1581	1688
Chivyrkui suite, high-K calc alkaline Qtz monzonite, granodiorite, granite, gabbro (305–285 Ma)																			
Kh-62-02	Qtz monz.	Khangintui	302	77.16	447.4	0.499	0.711042	9	0.70890	4.219	24	0.1063	0.512223	6	−8.1	−0.46	−4.6	1315	1468
Kh-6-03	Qtz monz.	Khangintui	300	66.98	867	0.223	0.706903	12	0.70595	6.266	35.54	0.1066	0.512093	7	−10.6	−0.46	−7.2	1502	1676
Bu19/1-02	Gabbro	Burgasy	290	21.84	1136	0.056	0.706300	11	**0.70607**	4.674	24.45	0.1156	0.512322	6	−6.2	−0.41	**−3.2**	1285	
PR113-04	Qtz monz.	Burgasy	287	59.43	493.1	0.349	0.708272	10	0.70685	3.884	19.68	0.1193	0.511820	9	−16.0	−0.39	−13.1	2139	2129
Or-28-02	Gabbro	Orefyev	290	4.298	1455	0.009	0.706094	10	**0.70606**	2.173	10.02	0.1311	0.512239	7	−7.8	−0.33	**−5.4**	1678	
Or-28-03	Gabbro	Orefyev	290	17.63	1371	0.037	0.706171	8	**0.70602**	5.521	27.44	0.1216	0.512238	9	−7.8	−0.38	**−5.0**	1508	
Zaza suite, high-K CA to Alk granite, quartz syenite (305–285 Ma)																			
002/1-04	Granite	Angyr	303	81.19	90.41	2.601	0.718338	10	0.70712	1.956	11.78	0.1004	0.512163	7	−9.3	−0.49	−5.5	1326	1556
044/1-04	Granite	Angyr	303	134.5	27.52	***14.187***	0.741346	11	*0.68017*	2.098	12.01	0.1056	0.512178	6	−9.0	−0.46	−5.5	1369	1539
Sh-07-24	Gabbro	Shaluta	300	62.23	979.3	0.184	0.707023	10	**0.70624**	5.755	29.62	0.1175	0.512280	6	−7.0	−0.40	**−3.9**	1375	
Sh-07-25	Q-syenite	Shaluta	300	58.24	75.33	2.239	0.716818	10	0.70726	4.373	21.3	0.1241	0.512201	8	−8.5	−0.37	−5.7	1611	1527
Lower-Selenga suite, shoshonitic series (285–278 Ma)																			
B341	Syenite	Ust-Khilok	280	122	400	0.883	0.709423	13	0.70591	11.00	68.00	0.0978	0.512246	7	−7.6	−0.50	−4.1	1188	1419
B361-20	Syenite	Ust-Khilok	280	52.9	148	1.03	0.711615	9	0.70749	3.30	17.49	0.1141	0.512238	6	−7.8	−0.42	−4.9	1393	1454
B111	Monzonite	Ust-Khilok	280	48.9	1095	0.129	0.706773	10	0.70626	6.50	36.31	0.1082	0.512263	7	−7.3	−0.45	−4.2	1280	1406
B342	Alk. gabbro	Ust-Khilok	280	76	1500	0.147	0.706967	12	0.70638	11.00	57.00	0.1167	0.512263	5	−7.3	−0.41	**−4.5**	1391	
B517-3	Alk. Gabbro	Ust-Khilok	280	34.2	1489	0.066	0.706025	10	0.70576	7.19	38.33	0.1134	0.512275	6	−7.1	−0.42	**−4.1**	1328	
B144	syenite	Nadeino	270	51.3	221	0.672	0.709797	10	0.70722	6.62	35.95	0.1113	0.512297	7	−6.7	−0.43	−3.7	1269	1356
Early-Kunalei suite, AFS and PA syenite, granite, and related volcanic rocks (281–275 Ma)																			
B 626	AFS syenite	Bryansk	280	105	55.8	***5.48***	0.726765	7	*0.70494*	16.37	97.70	0.1013	0.512293	4	−6.7	−0.49	−3.3	1161	1349
B 626-1	AFS syenite	Bryansk	280	112	58.0	***5.62***	0.727423	8	*0.70502*	9.61	62.43	0.0931	0.512301	5	−6.6	−0.53	−2.9	1072	1325
B425	AFS granite	Bryansk	280	187	47.0	***11.6***	0.749261	7	*0.70323*	2.09	14.73	0.0858	0.512320	4	−6.2	−0.56	−2.2	989	1284
B627	PA syenite	Bryansk	280	142	45.5	***9.03***	0.739562	8	*0.70359*	18.74	113.46	0.0999	0.512317	4	−6.3	−0.49	−2.8	1115	1308
B388	PA granite	Bryansk	280	204	7.1	***86.0***	1.037942	10	*0.69543*	10.92	56.44	0.1170	0.512364	4	−5.3	−0.41	−2.5	1237	1256
A447-4	Comendite	Bryansk	285	265	39.0	***19.8***	0.785460	8	*0.70517*	21.81	116.14	0.1135	0.512356	4	−5.5	−0.42	−2.5	1207	1265
B382-2	Comendite	Bryansk	285	275	14.1	***57.8***	0.938820	10	*0.70443*	15.35	76.07	0.1220	0.512342	4	−5.8	−0.38	−3.1	1341	1299
B167-3	Trachybasalt	Bryansk	285	53.6	1241	0.125	0.705945	8	**0.70544**	7.60	39.12	0.1174	0.512436	4	−3.9	−0.40	**−1.1**	1130	
B385	Trachyandesite	Bryansk	285	112	620	0.524	0.708063	7	**0.70594**	5.93	34.36	0.1043	0.512295	5	−6.7	−0.47	**−3.3**	1191	

B386	Trachyandesite	Bryansk	285	125	639	0.565	0.707993	6	**0.70570**	5.77	33.04	0.1056	0.512290	5	−6.8	−0.46	−**3.5**	1211	
M-347	AFS syenite	Khorinsk	280	130	30.7	***12.3***	0.751267	10	*0.70226*	10.18	62.51	0.0985	0.512295	4	−6.7	−0.50	−3.2	1130	1342
3070	AFS granite	Khorinsk	280	215	37.0	***16.9***	0.768745	7	*0.70152*	7.98	44.69	0.1080	0.512311	5	−6.4	−0.45	−3.2	1209	1329
M-340	PA granite	Khorinsk	280	233	5.4	***130.9***	1.175625	19	*0.65401*	5.06	30.63	0.1000	0.512352	5	−5.6	−0.49	−2.1	1069	1253
479	PA granite	Khorinsk	280	219	7.5	***87.1***	1.018060	8	*0.67089*	6.07	35.98	0.1020	0.512253	4	−7.5	−0.48	−4.1	1223	1414
M-350	PA granite	Khorinsk	280	147	7.0	***62.6***	0.943791	12	*0.69441*	7.20	38.91	0.1119	0.512379	4	−5.1	−0.43	−2.0	1154	1226
M-487	Trachybasalt	Khorinsk	285	96.8	630	0.444	0.706933	7	**0.70513**	6.14	31.02	0.1197	0.512480	6	−3.1	−0.39	−**0.3**	1086	
M-342	Trachyandesite	Khorinsk	285	43.0	641	0.194	0.705841	7	**0.70505**	5.78	29.22	0.1196	0.512488	7	−2.9	−0.39	−**0.1**	1072	
M-492	AFS rhyolite	Khorinsk	285	260	10.3	***74.9***	0.978381	15	*0.67465*	6.74	31.91	0.1276	0.512327	6	−6.1	−0.35	−3.6	1455	1330
M-511	AFS rhyolite	Khorinsk	285	208	20.4	***29.8***	0.831608	12	*0.71057*	8.95	45.96	0.1177	0.512357	4	−5.5	−0.40	−2.6	1257	1269
M-501	Syenite (host)	Khorinsk	280	50.2	393	0.370	0.706927	6	0.70545	5.43	34.99	0.0938	0.512311	6	−6.4	−0.52	−2.7	1066	1310
Alaskite suite (280 ± 5 Ma)																			
M-351-S-Gr	Alaskite	Bolsh. Kool	280	88.8	26.7	***8.72***	0.799908	8	*0.76516*	1.302	9.884	0.0796	0.512310	6	−6.4	−0.60	−2.2	955	1292
M-493-S-Gr	Alaskite	Bolsh. Kool	280	230.8	87.3	***7.65***	0.733774	10	*0.70329*	1.189	7.675	0.0936	0.512318	5	−6.2	−0.52	−2.6	1056	1298
Early Mesozoic stage, Late-Kunalei suite of AFS and PA syenite and granites, related volcanics (230–210 Ma)																			
B440	Comendite	Tsagan-Khurtei	210	217	19.4	***32.6***	0.789440	8	*0.69204*	11.43	61.28	0.1128	0.512670	4	0.6	−0.43	2.9	725	761
B444	Comendite	Tsagan-Khurtei	210	135	18.2	***21.6***	0.763315	8	*0.69879*	18.74	100.50	0.1127	0.512676	4	0.7	−0.43	3.0	716	752
1/8[a]	Comendite	Tsagan-Khurtei	210	162	12.2	***38.8***	0.820440	23	*0.70444*	12.10	66.70	0.1097	0.512625	7	−0.3	−0.44	2.1	770	829
1/6[a]	Trachybasalt	Tsagan-Khurtei	210	12.7	988	0.037	0.704550	15	0.70444	6.09	30.09	0.1224	0.512632	7	−0.1	−0.38	**1.9**	865	
1/7[a]	Trachybasalt	Tsagan-Khurtei	210	10	1188	0.024	0.705060	12	0.70499	7.22	37.40	0.1167	0.512646	7	0.2	−0.41	**2.3**	792	
B446-1	Trachybasalt	Tsagan-Khurtei	210	16.9	1136	0.043	0.704340	8	0.70421	8.08	41.09	0.1189	0.512694	4	1.1	−0.40	**3.2**	734	
A13	PA granite	Atha	210	174	7	***73.8***	0.972651	24	*0.75231*	3.80	17.00	0.1351	0.512657	6	0.4	−0.31	2.0	957	813
A13-1	PA granite	Atha	210	174	19	***26.7***	0.795791	10	*0.71598*	17.00	82.00	0.1253	0.512664	7	0.5	−0.36	2.4	839	788
L716	PA granite	Atha	210	160	6	***78.6***	0.901733	33	*0.66695*	11.00	65.00	0.1023	0.512622	7	−0.3	−0.48	2.2	723	824
L722	PA granite	Atha	210	150	17	***25.7***	0.780302	13	*0.70352*	12.00	70.00	0.1036	0.512619	5	−0.4	−0.47	2.1	736	831
L725	PA granite	Atha	210	150	9	***48.9***	0.841547	26	*0.69565*	11.00	64.00	0.1039	0.512616	6	−0.4	−0.47	2.1	742	836
L726	PA syenite	Atha	210	70	24	***8.46***	0.729413	14	*0.70416*	10.00	58.00	0.1042	0.512620	7	−0.4	−0.47	2.1	739	830
L727	PA syenite	Atha	210	83	30	***8.02***	0.729600	13	*0.70564*	12.00	65.00	0.1116	0.512652	5	0.3	−0.43	2.6	744	789
L728	PA syenite	Atha	210	60	8	***21.8***	0.759577	18	*0.69444*	11.00	65.00	0.1023	0.512634	4	−0.1	−0.48	2.5	707	805
ERM-400	PA granite	Yermakovka	226									0.1450	0.512506				−1.0		1110
ERM-411	PA granite	Yermakovka	226									0.0616	0.512381				−1.1		1112
A519	PA syenite	Malo-Kunaley	220	43.3	22.1	***5.66***	0.724745	10	*0.70703*	5.33	28.23	0.1141	0.512689	7	1.0	−0.42	3.3	706	733
A516a	PA syenite	Malo-Kunaley	220	86	54	4.61	0.718594	11	0.70416	7.00	42.00	0.1008	0.512718	6	1.6	−0.49	4.3	584	668
KH14	Afs syenite	Kharitonovo	230	130	85	4.43	0.719194	10	0.70470	12.00	67.00	0.1083	0.512468	6	−3.3	−0.45	−0.7	986	1078
870	AFS syenite	Kharitonovo	230	65	89	2.11	0.714243	17	0.70733	14.00	77.00	0.1099	0.512513	5	−2.4	−0.44	0.1	936	1009
3008	AFS granite	Kharitonovo	230	272	30	***26.5***	0.795004	10	*0.70846*	4.80	31.00	0.0936	0.512336	8	−5.9	−0.52	−2.9	1033	1270
866	PA syenite	Kharitonovo	230	175	14	***36.6***	0.831658	12	*0.71191*	29.00	155.00	0.1131	0.512496	5	−2.8	−0.42	−0.3	991	1040

Data for Lower-Selenga, Early-Kunalei and Late-Kunalei suites are after Jahn et al. (2009). (1) Bold, ($^{87}Sr/^{86}Sr$)T values in gabbro and andesite. (2) Bold italics, enhanced values of $^{87}Rb/^{87}Sr$ suggesting disturbing of the Rb–Sr isotope system. (3) Italics, unrealistic values of ($^{87}Sr/^{86}Sr$)T.

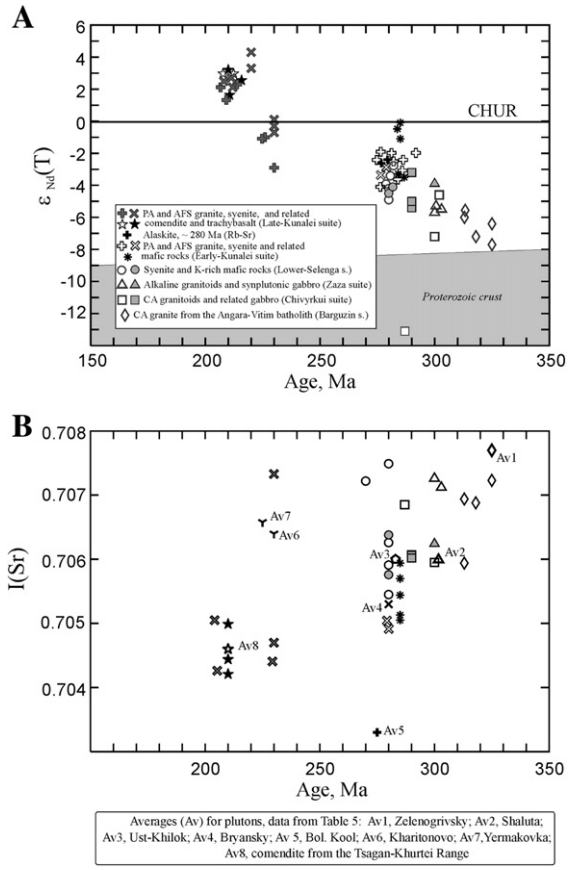

Fig. 10. εNd(T) vs. Intrusive age (A) and I(Sr) vs. Intrusive age (B) diagrams for the Late Palaeozoic and Early Mesozoic magmatic rocks from Transbaikalia (on a basis of data from Tables 4 and 5).

middle crust under conditions of fairly low water contents in the protolith and relatively low temperature of partial melting (<850 °C). Its likelihood in the case of the formation of the *Barguzin suite* in Transbaikalia is supported by the granitic composition of the batholith, chemical similarity of the granites throughout an area of about 150,000 km^2, and a high and stable K_2O content of 4.6±0.4 wt. % throughout the batholith (Litvinovsky et al., 1993). This mechanism also provides the realistic thickness of the metamorphic source layer, given the high melting degree (60–70%). Lastly, it explains the Sr–Nd and oxygen isotopic data pointing to prevalence of crust-derived component in the source region, although it is likely that measurable amounts of H_2O and alkalis were transported from the underplated mafic magma.

6.2.2. Coeval calc-alkaline and alkaline granitoids (Chivyrkui and Zaza suites)

Isotope ratios suggest that granite from the Zaza suite and low silica granitoids of the coeval Chivyrkui suite were crystallized from a hybrid magma formed by mixing of crustal- and mantle-derived melts. The significant role of magma mixing in the Chivyrkui granitoids is also indicated by abundant microgranular mafic enclaves and synplutonic mafic dykes (Table 1, Burgas and Nesterikha plutons). The overlap of REE patterns for mafic rocks and coeval granitoids both in the Chivyrkui and Zaza suites argues against fractional crystallization of mafic magmas as the dominant process in magma evolution (Fig. 12, A and B). Comparison of the REE patterns (Figs. 7C and 8C) shows clear distinctions between granitoids from these suites: in the Chivyrkui granitoids the Eu/Eu* is close to unity whereas in the Zaza suite pronounced negative Eu anomalies are exhibited. In addition, continuous trends of Sr (Fig. 6) and Ba decrease with SiO_2 increase are seen in silica variation plots. This suggests that the granitoids of the Chivyrkui suite were crystallized immediately from a magmatic mixture, whereas the silicic rocks of the coeval Zaza suite could be produced by fractional crystallization of the same or similar hybrid melts following magma mixing. Mass-balance calculation for the fractional crystallization process performed for average granitoids from the Chivyrkui suite as a parent and average granite of the Zaza suite as a daughter composition (Table 7) shows that the fractionated assemblage contained mostly plagioclase, amphibole and biotite. The residual granitic melt would constitute ca. 66 wt.%, so it could be easily separated from the crystal phase. Trace element testing demonstrates reasonable consistency between the observed and calculated compositions. However, the model of continuous evolution of the same hybrid magmatic batches by fractional crystallization looks debatable on closer inspection. Firstly, generation of quartz syenites with 10–11 wt.% alkalis that were emplaced at the onset of the Zaza suite formation and constitute approximately 10% of the total suite volume cannot be explained by this model (low Eu/Eu* value of 0.35–0.57 does not support the crystallization of quartz syenite from a cumulus-enriched granite magma). Secondly, areas occupied by the

Table 5
Selected Rb–Sr and U–Pb geochronological data for the Late Paleozoic and Triassic igneous suites from Transbaikalia.

	U–Pb		Rb–Sr		$(^{87}Sr/^{86}Sr)_T$
Suite, pluton, rock	Sample no.	Age, Ma	Rock type	Age, Ma	
Barguzin s., Zelenogrivsky, granite[1]	Zg-65/1	325±2.8	Gneissic granite	299±19 (n=6)	0.7077±0.0011
Zaza suite, Shaluta[2]		n.d.	Qtz syeite, granite	288±12 (n=6)	0.7060±0.0003
Low-Selenga s., Khasurta, monzonite[1]	Xc-59a	283.7±4.1	Monzonite	283±3 (n=8)	0.7063±0.001
Ust-Khilok pluton, syenite	B361-20	279.5±0.8	Monzonite, syenite	280±18 (n=9)	0.7060±0.0002
syenite	B343	278.7±3.0			
Early-Kunalei suite					
Bryansky complex, AFS syenite	B626-1	278.8±1.3	AFS syenite and granite	280±14 (n=6)	0.7050±0.0010
PA syenite	B627	277.3±1.1	PA granite and syenite	280±6 (n=20)	0.7053±0.0008
Khorinsk complex, AFS syenite	M347	278.4±1.2	AFS syenite and granite	268±12 (n=5)	0.7070±0.0002
Syenogranite suite, Bol. Kool		n.d.	syenogranite	282±5 (n=6)	0.7033±0.0007
Late-Kunalei suite					
Kharitonovo complex, AFS syenite	871	230.1±0.6			
PA syenite	A92	229.2±0.6	PA syenite and granite	221±1 (n=18)	0.7064±0.0004
Yermakovka		n.d.	PA granite	224±1.3 (n=10)	0.70658±0.0001
Tsagan-Khurtei volcanic suite		n.d.	Comendite, trachybasalt	212±5 (n=13)	0.7046±0.0006

[1]Tsygankov et al., 2007; [2]Litvinovsky et al., 1999a. All the rest references to the Rb–Sr geochronological data are in Jahn et al. (2009), Table 1.
n.d., no data.

Zaza and Chivyrkui suites overlap only partially, in the central and southern Transbaikalia (Fig. 1). The granitoids of the Zaza suite are mostly confined to the Mongolian–Transbaikalian Belt, whereas numerous plutons of the Chivyrkui suite are also abundant in the northern part of the region where they are closely spaced with the Angara–Vitim batholith (Fig. 1). Lastly, comparison of quartz monzonite from the Chivyrkui suite (60–69 wt.% SiO_2) and quartz syenite from the Zaza suite (64–69 wt.% SiO_2) shows total overlap of Nb, Zr (Fig. 6) and Rb (Fig. 3-SD, Online supplementary data) concentrations. This feature is inconsistent with the assumption of continuous transition from low-silica granitoids to alkaline granites in the course of fractional crystallization. Thus, we suggest that granitoid magmas that formed the Zaza suite could be produced from similar, but not the same, hybrid melts as the Chivyrkui granitoid magmas.

6.2.3. Coeval highly alkaline granitoids (Lower-Selenga and Early-Kunalei suites)

Radiogenic and oxygen isotope ratios indicate that mantle-derived components were dominant in the generation of magmas of the Early-Kunalei, Late-Kunalei and Lower-Selenga suites of Transbaikalia (Tables 4 and 6; Figs. 10 and 11). The origin of alkaline (alkali-feldspar) and peralkaline granitoids throughout the whole Central Asia Orogenic Belt and, in particular, the Mongolian–Transbaikalian belt was discussed recently in Jahn et al. (2009), so only the main arguments are outlined later. The following constraints to the origin of the rocks under consideration are recognized: (a) lack of petrographic, geological and isotope evidence for a significant contribution of crust-derived metamorphic components to the generation of the alkaline (alkali-feldspar) and peralkaline granitoid magmas; (b) the related volcanic suites are bimodal, commonly trachydolerite–rhyolite (comendite), and the plutonic suites are also bimodal, but the proportion of mafic rocks is very small; (c) study of melt microinclusions in subliquidus magmatic quartz and pyroxene revealed very high temperatures, about 1000–1100 °C, for the silicic magma generation.

The foregoing observations suggest that an alkali-rich mafic source could be considered as parental to the highly alkaline silicic magmas. Disposition of REE patterns of K-rich gabbro and granitoids in the Early-Kunalei suite (Fig. 12 D) also advocate genetic links between the mafic and felsic rocks. Of the two possible processes, fractional crystallization of the basalt magma and partial melting of gabbro/basalt, the former is less probable since fractionation processes cannot account for the absence or rare occurrence of rocks of intermediate composition in the highly alkaline, characteristically bimodal igneous suites. The production of highly alkaline granite magma by partial melting of alkali rich basalt was demonstrated in the melting experiments of Sisson et al. (2005). One of the three studied basalt samples (AD19-93) is fairly similar to the Early Permian mafic alkali-rich rocks from Transbaikalia; it is given in the last column of Table 3. Partial melting of this basalt to an extent of ~20% at 700 MPa and ~2 wt.% H_2O will produce a granite melt with 3.2 to 3.5 wt% Na_2O and 4.7 to 5.94 wt.% K_2O that is very similar to AFS and PA granites from Transbaikalia. Thus, the experimental results show that partial melting of alkali rich basalt/gabbro in the middle crust could produce significant amount of A-type granite magma that can be easily separated and emplaced at shallow levels. The melt inclusions data of 1000–1100 °C for the generation of silicic melts suggest that partial melting occurred at temperatures exceeding solidus temperature of basalt, but it is far less than its liquidus temperature in the middle–upper crust; therefore the assumption of 20% melting of K-rich mafic rocks in the lower crust looks reasonable. Thus, the most plausible 'mantle-like' source of the alkali-feldspar and peralkaline granitoids is alkali-rich basalt that repeatedly underplated the lower crust. We assume that soon after the solidification of the basaltic liquid (in granulite facies conditions) the newly formed mafic rock was subjected to partial melting by successive intrusion and underplating of similar magmas. The partial melting process in the lower crust explains the absence of igneous rocks of intermediate composition, as well as the very rare occurrence of co-genetic mafic rocks in plutonic suites. It also accounts for the pronounced negative Eu anomalies in alkaline granite because in the experiments of the Sisson et al. (2005) proportion of plagioclase in the residual phase in all runs was ≥50%. This likely caused the depletion of Eu in the partial melts.

Generation of the felsic (mostly syenitic) magmas of the Lower-Selenga suite is more likely consistent with the fractional crystallization model. Compositions of K-rich gabbro, monzonite and syenite from this suite form an almost continuous sequence in the classification diagrams (Fig. 5, A2, B2 and C2) and in other silica-variation diagrams (e.g., SiO_2 vs. Sr, Nb, Zr in Fig. 6). Although evidence of extensive magma mixing is clearly exhibited in some plutons (Litvinovsky et al., 1995a), it is highly improbable that mixing could play a main role in the generation of the dominantly syenitic magmas with 12–14 wt.% alkalis (Table 2). To the best of our knowledge, the only proven process that can result in production of almost quartz-free syenite magma is fractional crystallization of alkali-rich basalt magma (Brown and Becker, 1986; Thorpe and Tindle, 1992). Enrichment of syenite in Sr and Ba, in comparison to syenitic rocks from the coeval Early-Kunalei suite (Figs. 6 and 7E), could be caused by fractional crystallization of mafic minerals and minor plagioclase that produced a Sr and Ba-enriched evolved melt. Such phenomenon was studied in the younger alkaline monzodiorite–syenite Oshurkovo pluton in Transbaikalia (Litvinovsky et al., 2002b). Field observations suggest that fractional crystallization was accompanied by magma mixing as a secondary process. Mixing could occur between liquids at various stages of evolution, a process termed 'endo-hybridization' (Duchesne et al., 1998). In the chondrite-normalized REE diagram compiled for the best studied Ust-Khilok pluton (Fig. 12C) the disposition of REE patterns of the K-rich gabbro, monzonite and syenite is consistent with the fractional crystallization model, though correlation between REE patterns is not unambiguous due to effect of magma mixing in the course of monzonite formation. Less ambiguous is the primitive mantle-normalized spidergram for the main rock types making up this pluton (Fig. 12E). The spidergram shows the trace element contents of average monzonite and syenite, of one of the most representative syenite samples (B341) and of two samples of the least hybridized coeval K-rich trachydolerite (Table 3, samples B342 and B517-3). The patterns demonstrate a systematic decrease in Sr, P, Ti and increase in K, Ba, Zr and Nb from trachydolerite to syenite, suggesting progressive fractionation of plagioclase and mafic minerals.

Overall, petrogenetic analysis suggests that in the course of evolution of the Late Palaeozoic magmatism the proportion of crust- and mantle-derived components in the granitoids progressively changed, from dominant crustal source in the early stage (the Barguzin suite) through comparable proportions of both components in the Chivyrkui and Zaza suite to dominant mantle-derived source for granitoids from the Lower-Selenga and Early-Kunalei suites. Both in Late Carboniferous and Early Permian times, coeval intrusive suites originated from similar (although not the same) sources. It is likely that similar hybrid granitoid magmas formed the quartz monzonite–granodiorite association of the Chivyrkui suite and produced, after extensive fractional differentiation, the leucocratic granite of the Zaza suite. Also, formation of the monzonite–syenite Lower-Selenga suite resulted from fractional crystallization of K-rich basalt magmas, whereas the highly alkaline granitoids from the Early-Kunalei suite were possibly produced by partial melting of K-rich mafic rocks crystallized from the basalt magmas of similar age and composition.

6.3. Complex sequence and tectonic setting of Late Palaeozoic magmatic suites in Transbaikalia

Available geochronological data show that the Late Palaeozoic plutonic cycle in Transbaikalia was almost continuous (Fig. 4). Two

Table 6
$\delta^{18}O$ values (‰, SMOW) in whole-rock samples (WR) and minerals from plutonic rocks, Transbaikalia.

#	Pluton, locality	Sample	Rock	WR	Qtz	Afs	Pl	Ttn	$\Delta_{Qtz-Fsp}$
1	Upper Vitim Riv.	601	Granite	12	13.54	11.69			1.85
2	Upper Vitim Riv.	606-11	Granite	11.65				7.48	
3	Upper Vitim Riv.	607-2	Granite	11.5	13.18	10.96		7.6	2.22
4	Upper Vitim Riv.	606-4	granite	10.57					
5	Upper Vitim Riv.	607	Granite	11.31					
6	Upper Vitim Riv.	604	Gneiss[1]	12.23					
7	Barguzin Range	TB18	Granite	10.1	11.09	9.63		7.21	1.46
8	Barguzin Range	M42	Granite	10.79					
9	Barguzin Range	M40	Granite	10.7					
10	Temen	Te 2007*	Granite		10.33		7.94		
11	Zelenogrivsky	Z-07-63*	Granite		13.43	11.01			
12	Zelenogrivsky	Z-07-64*	Granite		14.21				
13	Zelenogrivsky	07/209-1*	Granite		10.86				
14	Nesteriha, Barg.	B126	Qtz monzonite	9.11					
15	Nesteriha, Barg.	B127	Qtz monzonite	8.71					
16	Nesteriha, Barg.	B127-2	Microgabbro	**8.85**					
17	Nesteriha, Barg.	B133-2	Microgabbro	**8.41**					
18	Nesteriha, Barg.	M105-6	Microgabbro	**8.31**					
19	Burgas	Bu-07-70*	Qtz monz		8.27		4.17		
20	Burgas	Bu-113a-07*	Qtz monz		8.51	6.58	6.68		
21	Burgas	Bu-113b-07*	Qtz monz				7.65		
22	Angyr	B73	granite	8.08				5.08	
23	Angyr	B736	granite	8.9				5.9	
24	Shaluta	TB3	Qtz syen	8	9.34	7.28			2.06
25	Shaluta	TB5	Qtz syen	8.6	9.49	8.23			1.26
26	Shaluta	ZZ-1	Qtz syen	7.71	8.88	6.72		4.71	2.16
27	Shaluta	ZZ-2	Qtz syen	7.3				4.3	
28	Shaluta	*ZZ-3*	granite	7.57				4.57	
29	Shaluta	22	Qtz syen	8.52				5.52	
30	Shaluta	SH1	Qtz syen	8.5	10.09	7.96			2.13
31	Shaluta	SH14	granite	8	9.81	7.1			2.71
32	Shaluta	SH15	Qtz syen	7.62	9.53	6.8		5.27	2.73
33	Shaluta	SH9a	Qtz syen	8.39				5.56	
34	Shaluta	136a	Qtz syen	8.14					
35	Shaluta	SH-07-25*	Qtz syen		8.92	6.57			
36	Shaluta	SH-07-21*	Qtz syen		9.7	7.6	7.7		
37	Shaluta	136	granite	7.84					
38	Shaluta	SH10	hyb monz	8.24		8.19		5.24	Amph 6.1
39	Shaluta	SH18C	Gabbro	**6.89**					Amph 6.9
40	Shaluta	SH-07-23*	Gabbro				8.52		
41	Shaluta	SH-07-24*	Gabbro				8.57		
42	Shaluta	SH21D	Gabbro	**6.93**			8.33		
43	Ulekchin	A302	Granite	7.37					
44	Bol. Amalat	599	Granite	7.41					
45	Bol. Amalat	600	Granite	7.74					
Low-Selenga suite (shoshonitic series), 285–278 Ma									
46	Ust-Khilok	B182-1	Syenite	6.38					
47	Ust-Khilok	B343	Syenite	7.2	7.42	7.11		4.99	0.31
48	Ust-Khilok	B341	Syenite	7.5		7.35		4.8	
49	Ust-Khilok	B337	Syenite	6.4	6.52	6.42		3.4	0.1
50	Ust-Khilok	B700-10	Syenite	7.39				4.39	
51	Ust-Khilok	B700	Syenite	7.74				4.74	
52	Ust-Khilok	B349	Syenite	6.5		6.48		3.44	
53	Ust-Khilok	884	Gabbro	7.17					
54	Ust-Khilok	A383-2	Syenite	6.76					
55	Ust-Khilok	M139	Syenite	6.3					
56	Ust-Khilok	M139-10	Gabbro	**6.23**					
Early-Kunalei suite, 280–276 Ma									
57	Khorinsk	496	Pa gran	5.69					
Syenogranite suite, ~280 Ma									
58	Bolshe-Kool	506	Granite	6.77					
59	Bolshe-Kool	M88	Granite	5.9	6.09	5.87			0.22
Late Kunalei suite, 230–210 Ma									
60	Kharitonovo	KH4	Afs granite	6.5	8.14	6.21		3.8	1.93
61	Kharitonovo	KH17	Afs syenite	6		6.33		3.66	
62	Kharitonovo	KH10	PA gran	5	7.6	4.63		2.8	2.97
63	Kharitonovo	A149	PA syen	6.18					
64	Kharitonovo	KH11	PA gran	5.1	7.78	4.82		3.2	2.96
65	Kharitonovo	KH1	PA gran	7.61	8.96	7.45			1.51
66	Kharitonovo	KH12	PA syen	7.2					
67	Kharitonovo	KHS	PA syen	6.36					
68	Kharitonovo	KH8	Microgabbro	**6.79**					

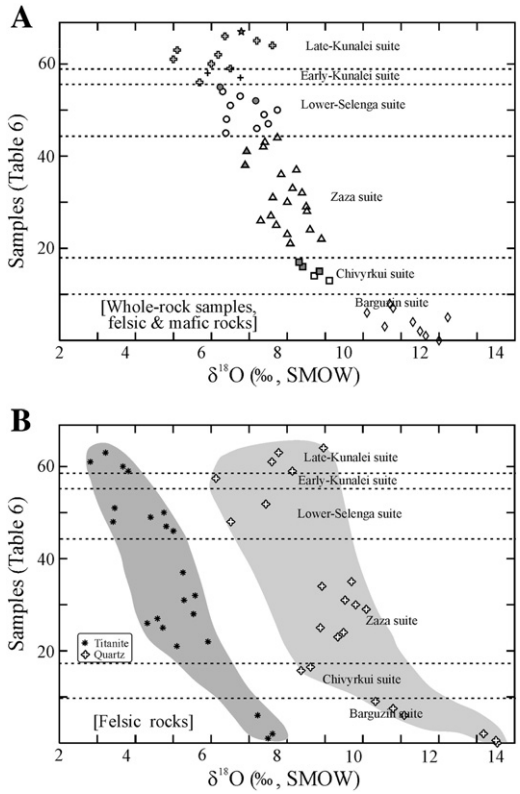

Fig. 11. Diagrams illustrating evolution of the $\delta^{18}O$ (‰, SMOW) values in the sequence of the Late Palaeozoic to Early Mesozoic magmatic suites from Transbaikalia (on a basis of data from Table 6). A, data from the whole-rock samples (symbols as in Fig. 10A). B, data from titanite and quartz from felsic rocks: granite, syenite, quartz syenite and quartz monzonite.

major observations concerning the evolution of the Late Palaeozoic granitoid magmatism can be made. First, a general trend of increase in alkalinity from older to younger magmatism is observed: high-K calc-alkaline igneous rocks (Barguzin and Chivyrkui suites) were followed by granites and quartz syenites that are transitional from high-K calc-alkaline to alkaline (Zaza suite) that in turn gave way to a shoshonitic series (Lower-Selenga suite) and, finally, to alkaline (alkali feldspar) and peralkaline syenite and granite (Early-Kunalei suite) (Figs. 5 and 6). The second observation concerns the complete or partial overlap in age of intrusive suites that are distinct in chemical and mineral compositions (Chivyrkui and Zaza suites, Lower-Selenga and Early-Kunalei suites, Figs. 7, C and E, and 8, C and E). It is important that variable intrusive suites of similar ages completely or partially overlap in space and are abundant throughout the same large region (Figs. 1–3). The close association in time and space of geochemically distinct igneous suites in Transbaikalia is not unique. Similar relations were first revealed in the Pan-African "stratoid granites" from Madagaskar (Nédélec et al., 1995) and later were described in many regions throughout the world:

1. In northern Mongolia the Early Mesozoic Khentei-Daurian calc-alkaline granitoid batholith and the closely spaced alkaline–peralkaline granite plutons were emplaced during the same time span of 227–207 Ma, (U–Pb ages; Yarmolyuk et al., 2002). Highly alkaline granite emplacement was confined to a ring-like rift zone surrounding the Khentei-Daurian batholith.
2. In the Ulungu River basin, NW China, calc-alkaline (I-type) and peralkaline granite plutons have similar Rb–Sr ages of 300–280 Ma (Chen and Jahn, 2004; Han et al., 1997). Immediately to the west of this area U–Pb zircon ages determined for six granite plutons (Wang et al., 2009) show a noticeable overlap of Carboniferous to Permian high-K calc-alkaline granitoids and alkaline granites, 294–280 Ma and 285–252 Ma, respectively.
3. In the Yangtze block of South China, Neoproterozoic I-type (high-K calc-alkaline) and A-type granites have similar SHRIMP zircon U–Pb ages of ~800 Ma (Zhao et al., 2008).
4. In western Newfoundland, Whalen et al. (2006) described almost concurrent, but extremely diverse Silurian post-collisional igneous suites that occurred immediately after formation of arc-like plutonic suites. During a period of ~8 m.y., from 435 to 427 Ma, large volumes of magmas with diverse compositions intruded in time intervals that are completely or partially overlapped. These magmas include calc-alkaline medium-K and low-K gabbro, diorite and granitoids, calc-alkaline medium- and high-K granite, monzogranite, both metaluminous and peraluminous, and typical A-type granites, including peralkaline arfvedsonite and riebekite bearing granite.
5. In the Sinai Peninsula (Egypt), formation of the Late Neoproterozoic post-collisional calc-alkaline batholithic suite and emplacement of alkaline and peralkaline granites occurred at 635–590 Ma and 608–580 Ma respectively with significant, ~20 m.y. overlap (Be'eri-Shlevin et al., 2009; Eyal et al., 2010).

These examples suggest that the emplacement of calc-alkaline and alkaline granitoids are not always sequential and may not represent the post-collisional and within-plate settings, respectively; they can partly or even completely overlap. This implies that formation of intracontinental rift zones conventionally considered to control alkaline magmatism could begin long before the completion of the post-collisional setting that is characterized by emplacement of voluminous high-K calc-alkaline granitoids and is likely caused by movement of terranes along trans-lithospheric shear zones (Liégeois, 1998). A geodynamic model of lithospheric delamination was suggested to account for the overlapping Neoproterozoic post-collisional and within-plate magmatism in the northern Arabian-Nubian Shield (Eyal et al., 2010). It is based on the model suggested by Liégeois and Black (1987) that was modified to describe association in space and time of various calc-alkaline and alkaline–peralkaline igneous suites. According to this model, at the end of the post-collisional period the regional structures could have been reactivated during transtention causing submergence of lithospheric blocks bordered by trans-lithospheric shear zones and upwelling of asthenospheric mantle (Liégeois et al., 2003, 2005). This would result in melting of sources with variable proportions of mantle and crustal components to form alkaline magmas. Calc-alkaline magmatism would occurr concurrently within the thicker lithospheric blocks that were not subjected to delamination processes. This model may also be applicable to the Transbaikalia magmatism, although restricted knowledge of tectonic structures in the region during the Late Palaeozoic, especially the late Carboniferous enables only speculative correlation of magmatic activity with tectonic evolution.

The Angara–Vitim batholith was emplaced in the upper-middle crust in the Barguzin Precambrian megablock, within and to the north

Notes to Table 6
Bold, the delta $\delta^{18}O$ values in the whole-rock gabbro samples.
Note: 1. The oxygen isotope data are given after Wickham et al., 1996, Table 2. Samples with evidence of only minimal modification of magmatic isotope equilibrium were chosen.
2. Gabbro samples in all suites were collected from synplutonic and composite dykes and sills.
[1]Gneiss from country rock xenolith in the 'in situ' granite.
*Unpublished authors' data.
Abbreviations: WR, whole-rock sample; Qtz, quartz; Afs, alkali feldspars; Pl, plagioclase; Ttn, titanite.

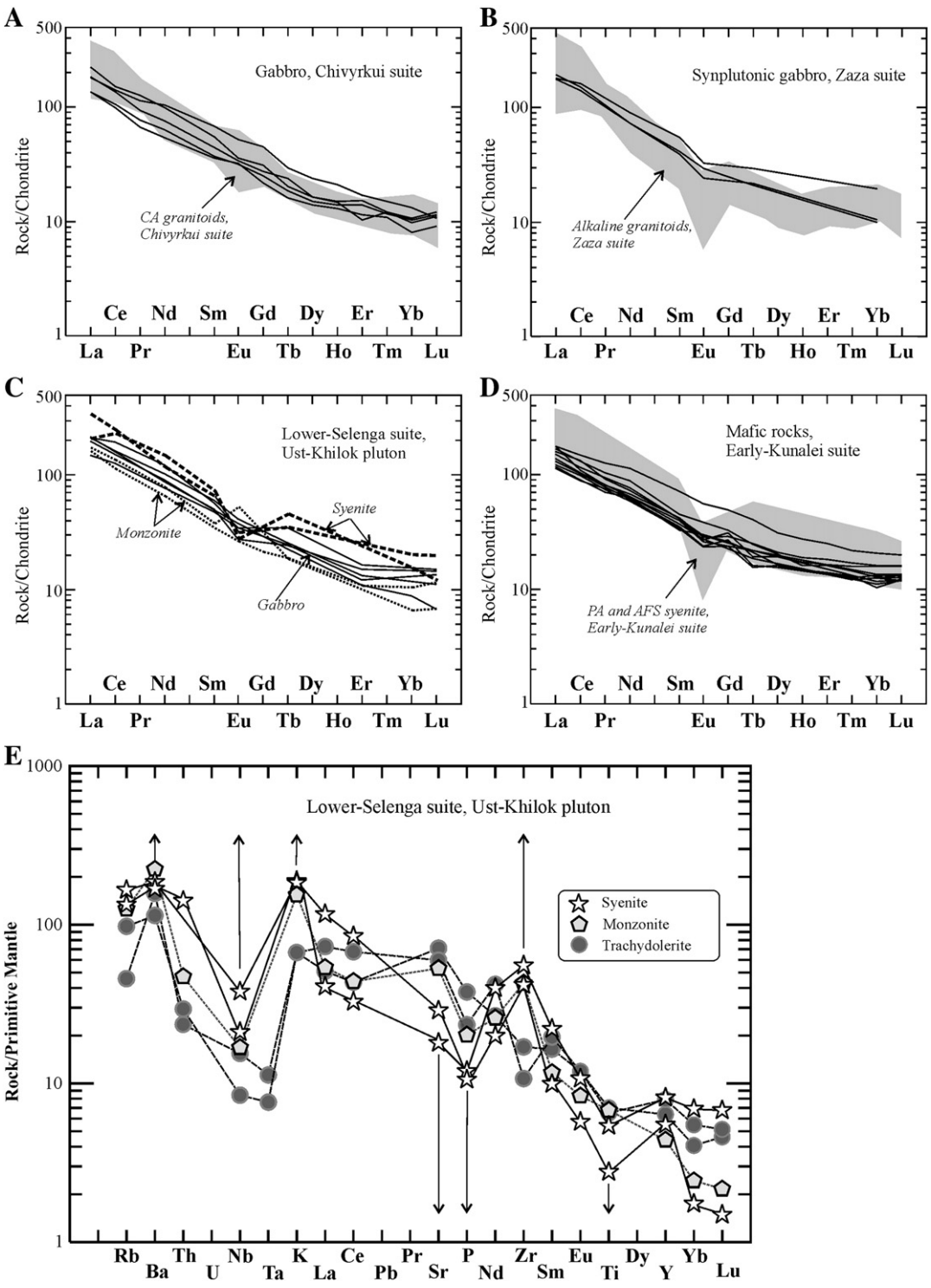

Fig. 12. A, B, and D, chondrite-normalized REE patterns of mafic rocks (lines) and granitoids (gray fields) of the Chivyrkui, Zaza and Early-Kunalei suites; C, the same for igneous rocks of the Ust-Khilok pluton, Lower-Selenga suite; E, primitive mantle-normalized multi-element spidergrams for main rock types of the Ust-Khilok pluton.

of the collision zone that is probably located along the Dzhida Suture (Inset in Fig. 1). The Barguzin megablock is confined to an angular space between the two cratons, Siberian and Aldano-Stanovoi, and was accreted and reworked significantly during the Caledonian orogenesis (Belichenko et al., 2006). The Early Carboniferous collision caused thickening of the crust and formation of a series of translithospheric shear zones that extended at an angle to the front of collision. The fact that large territories are occupied by granites, as well as the extremely extensive Mesozoic and Cenozoic rifting (completed by formation of contemporary Baikal rift) makes recognition of such shear zones problematic. We used geophysical data on linear zones with a length of more than a thousand kilometres and several tens of kilometres width. These are exhibited as extended belts of gravity anomalies, commonly accompanied with magnetic anomalies, and were interpreted as zones of structural and compositional heterogeneities in the upper-middle crust marking regional suture zones

Table 7
Results of least-square modeling of the Zaza granite generation by fractional crystallization of Qtz monzonite magma, with the trace element testing.

	Parent Qtz-monz & Qtz-sy (Chivyrkui)	Daughter, Zaza granite	
		Observed	Calculated
n	59	63	
wt.%			
SiO_2	65.57	73.8	73.69
TiO_2	0.57	0.19	0.02
Al_2O_3	16.73	13.7	13.61
FeO*	3.8	1.28	1.32
MnO	0.08	0.04	0.08
MgO	1.28	0.25	0.28
CaO	3.1	0.73	0.72
Na_2O	4.45	3.7	4.14
K_2O	4.22	5.4	5.47
P_2O_5	0.21	0.05	0.07
Fractionating minerals, wt.%			
	Pl_{40}		24.1
	Amph		2.4
	Bt		5.2
	Fe–Ti		1.8
	Ap		0.4
Residual melt		66 wt.%	
Sum residuals squared, R	0.24		

Trace element testing

ppm	Parent	Daughter	
		Observed	Calculated
Rb	136	215	181
Sr	778	188	212
Ba	1223	423	722
Nb	14	22	15
Y	18	16	16
Zr	222	163	263
La	47	56	53
Ce	95	117	107
Sm	6.04	5.07	7.01
Eu	1.46	0.65	1.02
Yb	1.78	2.33	2.29

(1) Sources of partition coefficient values: Arth, 1976; Nash and Crecraft, 1985; Rollinson, 1993.

(Alakshin and Pismenny, 1988; Litvinovsky et al., 1993). Four zones are shown in Fig. 1, Inset. Three northeast-trending zones are parallel to the southeast contour of the Siberian craton; the longest western zone coincides with the western contour of the Angara–Vitim batholith. It is likely that in the final stages of collision and/or in the beginning of the post-collisional stage voluminous silicic magma generation occurred in the thickened crust formed in the process of collision. A transpression setting in the shear zones would have caused squeezing out of ascending magmatic batches laterally from the shear zones within the subhorizontal structures (thrusts?) in the brittle middle-upper crust (Acef et al., 2003) leading to the plate shape of the forming batholith. It is likely that the location of the Barguzin megablock with normal or even thinned lithosphere between two cratons with thick lithosphere defined focussing of mantle energy flows beneath the megablock and caused production of a very large volume of granite magma.

During the late post-collisional stage (305–285 Ma) the extensional regime dominated throughout the whole region. For the Barguzin megablock, transpression ended and was replaced by transtention. Low-silica hybrid granitoids and coeval K-rich gabbro (the Chivyrkui sute) were emplaced in a transtensional and extensional setting. Judging from the close spatial association of the newly formed plutons with the Angara–Vitim batholith (Fig. 1), granitoid magmas could be produced by mixing of underplated K-rich basalt magma and remelted granite of the Angara–Vitim batholith. In the southern part, spreading occurred along the Mongolian–Transbaikalian Belt that controlled emplacement of K-rich calc-alkaline and alkaline granites and quartz syenites of the Zaza suite. Reactivation of the long-lived Dzhida suture zone was probably caused by the onset of the delamination process. Leucocratic granites were emplaced from much deeper magma chambers after extensive fractional crystallization of magmas generated from the mixed mantle-derived and crustal source.

In the Early Permian, magmatic activity was localized in the within-plate Mongolian–Transbaikalian Rift Zone (Jahn et al., 2009) formed along the boundary between the cratons and the southern Palaeozoic terrane. Delamination processes during the final post-collisional stage caused upwelling of the lithospere mantle and generation of voluminous highly alkaline granitoid magmas mostly from K-rich basaltic mantle-derived sources. A similar case was described in the Anti-Atlas in Morocco (Ennih and Liégeois, 2008). Although liquidus temperatures for the silicic magmas could be very high, up to 1000–1100 °C (Jahn et al., 2009; Litvinovsky et al., 2002a, 2002b), the gentle slopes of the REE patterns and pronounced negative Eu anomalies characteristic of the highly alkaline granitoids (Fig. 8) suggest that silicic magmas were produced above the garnet stability zone in the lithospheric mantle or, more likely, in the lower crust.

One more special feature of the Transbaikalian magmatism is the occurrence of two highly alkaline granitoid suites, the Early Permian Early-Kunalei and Late Triassic Late-Kunalei suites (Fig. 4). Both suites include two groups of syenites and granites: peralkaline with Na-amphibole and pyroxene and alkaline (alkali feldspar) granitoids with Fe-rich biotite and Ca-Na amphibole. Rocks of the two suites cannot be distinguished on the basis of conventional geological, mineralogical and chemical characteristics (Fig. 3B, Bryansky and Kharitonovo complexes). However, the εNd(T) values in the Early Permian granitoids range from −5 to −1, whereas in the Late Triassic suite positive values (up to +4) dominate (Table 4; Fig. 10). These data suggest different sources for the highly alkaline granitoid magmas in Early Permian and Late Triassic times, but the problem of discerning the two suites remains unsolved. The spatial association of the two similar highly alkaline granitoid suites was interpreted to be the result of superposition of the northern border of the Late Triassic, 207–227 Ma, North-Mongolian large igneous province (1500 by 800 km) on the central and northeastern part of the Mongolian–Transbaikalian Belt (Jahn et al., 2009; Yarmolyuk et al., 2002). According to Yarmolyuk et al. (2002), the North-Mongolian LIP formed immediately to the southeast of the MTB after closure of the younger Mongol-Okhotian oceanic trough in Triassic times. The outer contours of the oval-shaped province are rift systems that controlled the location of alkaline volcanics, AFS and PA granitoids. If this model is correct, the Early Permian and Late Triassic highly alkaline granitoids in the MTB are not related, although they formed in similar geodynamic setting.

7. Main conclusions

1. Late Palaeozoic intrusive rocks are widespread in Transbaikalia and occupy a total of more than 200,000 km^2. U–Pb zircon dating show that the Late Palaeozoic magmatic cycle lasted almost continuously for ~55 m.y., from ~330 Ma to ~275 Ma.
2. The granitoids display a general trend of increase in alkalinity, from high-K calc-alkaline through alkaline and shoshonitic series to peralkaline quartz syenite and granite. Yet temporal overlap, complete or partial, between various suites of variable alkalinity disturbs this trend. In particular, within the interval of 305–285 Ma two magmatic suites were emplaced concurrently: the Chivyrkui suite of calc-alkaline quartz monzonite and granodiorite and the Zaza suite which is transitional from calc-alkaline to alkaline granite and quartz syenite. During the next stage

formation of the Lower-Selenga suite (285–278 Ma) of syenite, monzonite and alkali-rich gabbro is partially overlapped in time by the Early-Kunalei suite of peralkaline and alkali feldspar syenite and granite (281–276 Ma). Clear geochemical distinctions between coeval granitoid suites are established.

3. Notwithstanding the overlap in age noted earlier, two stages of emplacement of peralkaline and alkali feldspar granitoids, 281–276 Ma and 230–210 Ma, are recognized in the region (Early-Kunalei and Late-Kunalei suites, respectively). Despite the significant time span separating the two suites, geochemical and mineralogical distinctions between the same rock types of different ages were not found. The only detected distinction is the negative εNd(T) of the older rocks compared to the dominance of positive εNd(T) values in the younger suite (Jahn et al., 2009). Two opposite tendencies thus characterize the evolution of post-collisional and within-plate magmatism in Trabsbaikalia: on the one hand, overlap in the ages of distinct granitoid suites and, on the other hand, a significant time interval (several tens of million years) between emplacement of voluminous granitoid suites of similar composition.
4. The Late Palaeozoic magmatic cycle incorporates post-collisional and within-plate settings, with a transitional period that lasted about 20 m.y. During this period both calc-alkaline and alkaline granitoids were emplaced concurrently. Similar temporal and spatial overlaps were described for calc-alkaline and alkaline granitoid suites in a number of regions around the world. These data indicate that the sequence of magmatic events following continental collision can be more complex than the order implicit from the conventional conceptions.
5. Contribution of crustal and mantle components to the generation of silicic magmas at successive stages of magmatic activity is estimated on the basis of Sr–Nd and oxygen isotope ratios and elemental geochemichal data. (i) The high-K calc-alkaline granite magmas that formed the Angara–Vitim batholith were generated by high degree of melting of metamorphosed supracrustal rocks, with likely minor contribution of H_2O and K from underplated mafic intrusions (a convective diffusion model). (ii) The coeval calc-alkaline low-silica granitoids of the Chivyrkui suite and transitional to alkaline granite and quartz syenite of the Zaza suite formed as a result of mixing of silicic crust and mafic mantle-derived materials in comparable proportions. Whereas the low-silica granitoids formed by crystallization of hybrid magma, the leucocratic rocks of the Zaza suite crystallized from magmas formed by fractional crystallization of the hybrid melts following magma mixing. (iii) The gabbro–monzonite–syenite Lower-Selenga suite and the highly alkaline AFS and PA quartz syenite–granite of the Early-Kunalei suite, which overlap in time and space, formed from a similar K-rich mantle-derived source. In the Lower-Selenga suite magmas evolved by fractional crystallization of pristine K-rich basaltic melt with subordinate magma mixing, whereas the highly alkaline granitoids were produced by partial melting (~20%) of K-rich mafic rocks in the lower crust.

Supplementary materials related to this article can be found online at doi:10.1016/j.lithos.2011.04.007.

Acknowledgements

This paper could not have been written without the contribution of late Ada Zanvilevich, our permanent co-worker and co-author.

We highly appreciate the thoughtful reviews by B. Bonin and J.P. Liégeois and the valuable notes of Editor-in-Chief N. Eby, which caused us to carry out a serious revision of the manuscript and improve it dramatically. The study was supported by an International grant #06-05-72007 of the Russian Foundation of Basic Researches (RFBR) and the Ministry of Science and Technology, Israel, grant RFBR-Siberia08-05-98017, Integration Project #37 of the Siberian Division of the Russian Academy of Sciences. BMJ acknowledges the support of National Scientific Council (NSC) of Taiwan through grants NSC97-2752-M-002-003-PAE, NSC97-2116-M-001-011, and NSC98-2116-M-001-009.

References

Abramovich, G.Ya., buldygerov, V.V., Sryvtsev, N.A., Taskin, A.P., 1989. Magmatic Formations in Southern Siberia and Northern Mongolia (explanatory note to a map of magmatic formations in Southern Siberia and Northern Mongolia, Scale 1:1,500,000) [in Russian]. VostSibNIIGGiMS, Irkutsk.

Acef, K., Liégeois, J.P., Ouabadi, A., Latouche, L., 2003. The Anfeg post-collisional Pan-African high-K calc-alkaline batholith (Central Hoggar, Algeria), result of the Latea microcontinent metacratonisation. Journal of African Earth Sciences 37, 295–311.

Alakshin, A.M., Pismenny, B.M., 1988. Structure of the Earth crust in the join of the Siberian platform and its southern folded frame. Russian Geology and Geophysics 11, 24–31.

Antipin, V.S., Makrygina, B.A., Petrova, Z.I., 2006. Comparative geochemical characteristics of the granitoids and metamorphic country rocks in the western part of the Angara–Vitim batholith (Pribaikalia). International Geochemistry 3, 293–308.

Arth, J.G., 1976. Behavior of trace elements during magmatic processes — a summary of theoretical models and their applications. Journal of Research of the U.S. Geological Survey 4, 41–47.

Be'eri-Shlevin, Y., Katzir, Y., Whitehouse, M., 2009. Post-collisional tectono-magmatic evolution in the northern Arabian-Nubian Shield (ANS): time constraints from ion-probe U–Pb dating of zircon. Journal of the Geological Society, London 166, 71–85.

Belichenko, V.G., Gelety, N.K., Barash, I.G., 2006. The Barguzin microcontinent (Baikal mountain region): the recognizing problem. Russian Geology and Geophysics 47, 1049–1059.

Bonin, B., 1998. Orogenic to non-orogenic magmatic events: overview of the Late Variscan magmatic evolution of the Alpine Belt.. Turkish Journal of Earth Sciences 7, 133–143.

Bonin, B., 2004. Do coeval mafic and felsic magmas in post-collisional to within-plate regimes necessarily imply two contrasting, mantle and crustal, sources? A review. Lithos 78, 1–24.

Bonin, B., 2007. A-type granites and related rocks: evolution of a concept, problems and prospects. Lithos 97, 1–29.

Bonin, B., Azzoini-Sekkal, A., Bussy, F., Ferrag, S., 1998. Alkali-calsic and alkaline post-orogenic (PO) granite magmatism: petrological constraints and geodynamic settings. Lithos 45, 45–70.

Brown, P.E., Becker, S.M., 1986. Fractionation, hybridization and magma mixing in the Kialineq center East Greenland. Contributions to Mineralogy and Petrology 92, 57–70.

Budnikov, S.V., Kovalenko, V.I., Yarmolyuk, V.V., Antipin, V.S., Goreglyad, A.V., Sal'nikova, E.B., Kotov, A.B., Kovach, V.P., Kozakov, I.K., Yakovleva, S.Z., Berezhnaya, N.G., 1995. New data on the age of the Barguzin granitoid complex in the Angara–Vitim batholith. Doklady of the Russian Academy of Sciences 344 (3), 377–380.

Bukharov, A.A., Khalilov, V.A., Strakhova, T.M., Chernikov, V.V., 1992. Geology of the Baikal-Patom Upland according to new data of U–Pb dating of the accessory zircon. Russian Geology and Geophysics 33, 29–39.

Chen, B., Jahn, B.M., 2004. Genesis of post-collisional granitoids and basement nature of the Junggar Terrane, NW China: Nd–Sr isotope and trace element evidence. Journal of Asian Earth Sciences 23, 691–704.

DePaolo, D.J., Linn, A.M., Schubert, G., 1991. The continental crustal age distribution: methods of determining mantle separation ages from Sm–Nd isotopic data and application to the southwestern United States. Journal of Geophysical Research 96, 2071–2088.

Duchesne, J.-C., Berza, T., Liégeois, J.-P., Auwera, J.V., 1998. Shoshonitic liquid line of descent from diorite to granite: the Late Precambrian post-collisional Tismana pluton South Carpathians, Romania. Lithos 45, 281–303.

Dvorkin-Samarsky, B.A., 1965. Granitoids of the Sayano-Baikal mountain region. Buryatian Publisher, Ulan-Ude. 287 pp. (in Russian).

Ennih, N., Liégeois, J.P., 2008. The boundaries of the West African craton, with a special reference to the basement of the Moroccan metacratonic Anti-Atlas belt. In: Ennih, Liégeois (Eds.), The boundaries of the West African craton: Geological Society, London, Special Publication, 297, pp. 1–17.

Eyal, M., Litvinovsky, B.A., Jahn, B.M., Zanvilevich, A., Katzir, Y., 2010. Origin and evolution of post-collisional magmatism: coeval Neoproterozoic calc-alkaline and alkaline suites of the Sinai Peninsula. Chemical Geology 269, 153–179.

Frost, B.R., Barnes, C.G., Collins, W.J., Arculus, R.J., Ellis, D.J., Frost, C.D., 2001. A geochemical classification for granitic rocks. Journal of Petrology 42, 2035–2048.

Gordienko, I.V., 1987. The Paleozoic Magmatism and Geodynamics of the Central Asian Mobile Belt. Nauka, Moscow. 289 pp. (in Russian).

Han, B.F., Wang, S.G., Jahn, B.M., Hong, D.W., Kagami, H., Sun, Y.L., 1997. Depleted-mantle magma source for the Ulungur River A-type granites from north Xinjiang, China: geochemistry and Nd–Sr isotopic evidence, and implication for Phanerozoic crustal growth. Chemical Geology 138, 135–159.

Huppert, H.E., Sparks, R.S.J., 1988. The generation of granite magmas by intrusion of basalt into continental crust. Journal of Petrology 29, 596–624.

Jahn, B.M., 2004. The Central Asian Orogenic Belt and growth of the continental crust in the Phanerozoic. Geological Society of London, Special Publication 226, 73–100.

Jahn, B.M., Litvinovsky, B.A., Zanvilevich, A.N., Reichow, M.K., 2009. Peralkaline granitoid magmatism in the Mongolian–Transbaikalian Belt: evolution, petrogenesis and tectonic significance. Lithos 113, 521–539.

Johannes, W., Holtz, F., 1996. Petrogenesis and experimental petrology of granitic rocks. Springer-Verlag, Berlin. 330 pp.
Johnston, A.D., Wyllie, P.J., 1988. Interaction of granite and basic magmas: experimental observations on contamination processes at 10 kbar with H_2O. Contributions to Mineralogy and Petrology 98, 352–362.
Keto, L.S., Jecobsen, S.B., 1987. Nd and Sm isotope variations of Early Paleozoic oceans. Earth and Planetary Science Letters 84, 27–41.
Kovalenko, V.I., Yarmolyuk, V.V., Kovach, V.P., Kotov, A.B., Kozlovsky, A.M., Salnikova, E.B., Larin, A.M., 2004. Isotope provinces, mechanisms of generation and sources of the continental crust in the Central Asian Mobile Belt: geological and isotopic evidence. Journal of Asian Earth Sciences 23, 605–627.
Koyaguchi, T., 1989. Chemical gradient at diffusive interfaces in magma chambers. Contributions to Mineralogy and Petrology 103, 143–152.
Kozubova, L.A., Mirkina, S.L., Rublev, A.G., Chukhonin, A.P., 1980. The radiologic age and composition of the Chivyrkui pluton (Baikal mountainous area). Doklady Akademii Nauk SSSR 251 (4), 948–951.
Le Maitre, R.W. (Ed.), 1989. A Classification of Igneous Rocks and Glossary of Terms. Blackwell Scientific Publ., Oxford. 193 pp.
Leontyev, A.N., Litvinovsky, B.A., Gavrilova, S.P., Zakharov, A.A., 1981. Paleozoic Granitoid Magmatism in the Central Asian Fold Belt. Nauka, Novosibirsk. 331 pp. (in Russian).
Liégeois, J.P., 1998. Preface — some words on the post-collisional magmatism. Lithos 45, 15–17.
Liégeois, J.P., Black, R., 1987. Alkaline magmatism subsequent to collision in the Pan-African belt of the Adrar des Iforas. In: Fitton, J.G., Upton, B.G.J. (Eds.), Alkaline IgneousRocks: Geological Society London, Special Publication, 30, pp. 381–401.
Liégeois, J.P., Navez, J., Hertogen, J., Black, R., 1998. Contrasting origin of post-collisional high-K calc-alkaline and shoshonitic versus alkaline and peralkaline granitoids. The use of sliding normalization. Lithos 45, 1–28.
Liégeois, J.P., Latouche, L., Boughrara, M., Navez, J., Guiraud, M., 2003. The LATEA metacraton (Central Hoggar, Tuareg shield, Algeria): behaviour of an old passive margin during the Pan-African orogeny. Journal of African Earth Sciences 37, 161–190.
Liégeois, J.P., Benhallou, A., Azzouni-Sekkal, A., Yahiaoui, R., Bonin, B., 2005. The Hoggar swell and volcanism: reactivation of the Precambrian Tuareg shield during Alpine convergence and West African Cenozoic volcanism. In: Foulger, G.R., Natland, J.H., Presnall, D.C., Anderson, D.L. (Eds.), Plates, Plumes and Paradigms, Geological Society of America Special Paper, 388, pp. 379–400.
Litvinovsky, B.A., Podladchikov, Yu.Yu., 1993. Crustal anatexis during the influx of mantlevolatiles. Lithos 30, 93–107.
Litvinovsky, B.A., Zanvilevich, A.N., 1976. Paleozoic Granitoid Magmatism in Western Transbaikalia. Nauka, Novosibirsk. 225 pp. (in Russian).
Litvinovsky, B.A., Zanvilevich, A.N., 1998. Compositional trends of silicic and mafic magmas formed in the course of evolution of the Mongolian–Transbaikalian mobile belt. Russian Geology and Geophysics 2, 155–180.
Litvinovsky, B.A., Zanvilevich, A.N., Alakshin, A.M., Podladchikov, Yu.Yu., 1993. The Angara–Vitim Batholith, the Largest Granitoid Pluton. Izdatelstvo OIGGM SO RAN, Novosibirsk. 143 pp. (in Russian).
Litvinovsky, B.A., Zanvilevich, A.N., Wickham, S.M., 1994. Angara–Vitim batholith, Transbaikalia: structure, petrology, and petrogenesis. Russian Geology and Geophysics 35, 190–203.
Litvinovsky, B.A., Zanvilevich, A.N., Kalmanovich, M.A., 1995a. Repeated mixing of coexisting syenitic and basic magmas and its petrological significance, Ust'-Khilok massif, Transbaikalia. Petrologiya 3 (2), 133–157.
Litvinovsky, B.A., Zanvilevich, A.N., Lyapunov, S.M., Bindeman, I.N., Davis, A.M., Kalmanovich, M.A., 1995b. Model of composite basite-granitoid dyke generation (Shaluta Pluton, Transbaikalia). Russian Geology and Geophysics 7, 1–19.
Litvinovsky, B.A., Posokhov, V.F., Zanvilevich, A.N., 1995c. Unusual Rb–Sr data on the age of two standard alkaline-granitoid massifs of Transbaikal. Russian Geology and Geophysics 36, 61–68.
Litvinovsky, B.A., Posokhov, V.F., Zanvilevich, A.N., 1999a. New Rb–Sr data on the age of Late Palaeozoic granitoids in Western Transbaikalia. Russian Geology and Geophysics 5, 677–685.
Litvinovsky, B.A., Zanvilevich, A.N., Wickham, S.M., Steele, I.M., 1999b. Origin of syenite magmas in A-type granitoid series: syenite-granite series from Transbaikalia. Petrology 7, 483–508.
Litvinovsky, B.A., Yarmolyuk, V.V., Vorontsov, A.A., Zhuravlev, D.Z., Posokhov, V.F., Sandimirova, G.P., Kuz'min, D.V., 2001. Late Triassic stage of formation of the Mongolo-Transbaikalian alkaline-granitoid province: data of isotope-geochemical studies. Russian Geology and Geophysics 3, 433–444.
Litvinovsky, B.A., Jahn, B.-M., Zanvilevich, A.N., Saunders, A., Poulain, S., 2002a. Petrogenesis of syenite-granite suites from the Bryansky Complex (Transbaikalia, Russia): implications for the origin of A-type granitoid magmas. Chemical Geology 189, 105–133.
Litvinovsky, B.A., Jahn, B.-M., Zanvilevich, A.N., Shadaev, M.G., 2002b. Crystal fractionation in the petrogenesis of an alkali monzodiorite-syenite series: Oshurkovo plutonic sheeted complex, Transbaikalia, Russia. Lithos 64, 97–130.
Nash, W.P., Crecraft, H.R., 1985. Partition coefficients for trace elements in silicic magmas. Geochemica et Cosmochemica Acta 49, 2309–2322.
Nédélec, A., Stephens, W.E., Fallick, A.E., 1995. The Pan- African stratoid granites of Madagaskar: alkaline magmatism in a post-collisional extensional setting. Journal of Petrology 36, 1367–1391.
Pismenny, B.M., Alakshin, A.M., 1984. Structure of the Earth crust in the Middle Vitim Mountain Land. Russian Geology and Geophysics 4, 14–27.
Polyakov, G.V. (Ed), 1989. Map of Magmatic Formations in Southern Siberia and Northern Mongolia. Scale 1 : 1,500,000. Publisher MinGeo, Moscow (in Russian).
Posokhov, V.F., Shadaev, M.G., Litvinovsky, B.A., Zanvilevich, A.N., Khubanov, V.N., 2005. Rb–Sr age and sequence of formation of granitoids of the Khorinka volcanoplutonic structure in the Mongolo-Transbaikalian belt. Russian Geology and Geophysics 6, 625–632.
Reichow, M.K., Litvinovsky, B.A., Parrish, R.R., Saunders, A.D., 2010. Multi-stage emplacement of alkaline and peralkaline syenite–granite suites in the Mongolian–Transbaikalian Belt, Russia: evidence from U–Pb geochronology and whole rock geochemistry. Chemical Geology 273, 120–135.
Reyf, F.G., 1976. The Physicochemical Conditions of Formation of Large Granitoid Masses in Eastern Baikal region. Nauka, Novosibirsk. 152 pp. (in Russian).
Rickwood, P.C., 1989. Boundary lines within petrologic diagrams which use oxides of major and minor elements. Lithos 22, 247–263.
Rollinson, H., 1993. Using Geochemical Data: Evaluation, Presentation, Interpretation. Longman, New York. 352 pp.
Rudnick, R.L., Gao, S., 2003. Composition of the continental crust. Treatise on Geochemistry, vol. 3. Elsevier Ltd, pp. 1–64.
Rytsk, E.Yu., Makeev, A.F., Shalaev, V.S., 2002. Granitoids in the east of the Angara–Vitim batholith: U–Pb isotope data. Geology, Geochemistry, and Geophysics at the Boundary of the 20th and 21st Centuries. Proc. Conf. Russian Foundation for Basic Research in Asian Russia. Irkutsk, pp. 400–401 (in Russian).
Shkodzinsky, V.S., 1985. Evolution of phase composition and genesis of granitic magma. Geochemistry International 18, 25–42.
Sisson, T.W., Ratajevski, K., Hankins, W.B., Glazner, A.F., 2005. Voluminous granitic magmas from common basaltic source. Contributions to Mineralogy and Petrology 148, 635–661.
Sun, S.S., McDonough, W.F., 1989. Chemical and isotopic systematics of oceanic basalts: implications for mantle composition and processes/magmatism in the oceanic basins. In: Saunders, A.D., Norry, M.J. (Eds.), Geological Society Special Publications, 42, pp. 313–345.
Thorpe, R.S., Tindle, A.G., 1992. Petrology and petrogenesis of a Tertiary diorite/peralkaline–subalkaline trachyte-rhyolite dike association from Lundy, Bristol Channel. Geological Journal 27, 101–117.
Tsygankov, A.A., Matukov, D.I., Berezhnaya, N.G., Larionov, A.N., Posokhov, V.F., Tsyrenov, B.Ts., Khromov, A.A., Sergeev, S.A., 2007. Late Paleozoic granitoids of western Transbaikalia: magma sources and stages of formation. Russian Geology and Geophysics 1, 156–180.
Tsygankov, A.A., Litvinovsky, B.A., Jahn, B.M., Reichow, M.K., Liu, D.Y., Larionov, A.N., Presnyakov, S.L., Lepekhina, Ye, Sergeev, S.A., 2010. Complex sequence of magmatic events in the Late Palaeozoic of Transbaikalia, Russia (U–Pb isotope data). Russian Geology and Geophysics 51, 901–922.
Vielzeuf, D., Holloway, J.R., 1988. Experimental determination of the fluid-absent melting relation in the pelithic system. Contributions to Mineralogy and Petrology 98, 257–276.
Wang, Bo, Cluzel, D., Shu, L., Faure, M., Charvet, J., Yan, Chen, Meffre, S., de Jong, K., 2009. Evolution of calc-alkaline to alkaline magmatism through Carboniferous convergence to Permian transcurrent tectonics, western Chinese Tianshan. International Journal of Earth Sciences (Geol Rundsch) 98, 1275–1298. doi:10.1007/s00531-008-0408-y.
Watson, E.B., 1976. Two-liquid partition coefficients: Experimental data and geochemical implications. Contribution to Mineralogy and Petrology 56, 119–134.
Watson, E.B., 1982. Basalt contamination by continental crust: some experiments and models. Contributions to Mineralogy and Petrology 80, 73–87.
Watson, E.B., 1984. Behavior of alkalis during diffusive interaction of granitic xenoliths with basaltic magmas. Journal of Petrology 92, 121–131.
Whalen, J.B., McNicoll, V.J., van Staal, C.R., Lissenberg, C.J., Longstaffe, F.J., Genner, G.A., van Breeman, O., 2006. Spatial, temporal and geochemical characteristics of Silurian collision-zone magmatism, Newfoundland Appalachians: an example of a rapidly evolving magmatic system related to slab break-off. Lithos 89, 377–404.
Wickham, S.M., 1987. The segregation and emplacement of granitic magmas. Journal of the Geological Society, London, 44, pp. 281–297.
Wickham, S.M., Litvinovsky, B.A., Zanvilevich, A.N., Bindeman, I.N., Schauble, E.A., 1995. Geochemical evolution of Phanerozoic magmatism in Transbaikalia, East Asia: a key constraint on the origin of K-rich silicic magmas and the process of cratonization. Journal of Geophysical Research 100, 15641–15654.
Wickham, S.M., Albertz, A.D., Zanvilevich, A.N., Litvinovsky, B.A., Bindeman, I.N., Schauble, A., 1996. A stable isotope study of anorogenic magmatism in East Central Asia. Journal of Petrology 37, 1063–1095.
Windley, B.F., Alexeiev, D., Xiao, W.J., Kroner, A., Badarch, G., 2007. Tectonic models for accreton of the Central Asian Orogenic Belt. Bicentennial review. Journal of the Geological Society, London 164, 31–47.
Wu, F.Y., Sun, D.Y., Li, H.M., Jahn, B.M., Wilde, S.A., 2002. A-type granites in Northeastern China: age and geochemical constraints on their petrogenesis. Chemical Geology 187, 143–171.
Yang, J.H., Chung, S.L., Wilde, S.A., Wu, F.Y., Chu, M.F., Lo, C.H., Fan, H.R., 2005. Petrogenesis of post-orogenic syenites in the Sulu Orogenic Belt, East China: geochronological, geochemical and Nd–Sr isotopic evidence. Chemical Geology 214, 99–125.
Yarmolyuk, V.V., Budnikov, S.V., Kovalenko, V.I., Antipin, V.S., Goreglyad, A.V., Sal'nikova, E.B., Kotov, A.B., Kozakov, I.A., Kovach, V.P., Yakovleva, Z.S., Berezhnaya, N.G., 1997a. Geochronology and geodynamic setting of the Angara–Vitim batholith. Petrologiya 5 (5), 451–466.
Yarmolyuk, V.V., Kovalenko, V.I., Kotov, A.B., Salnikova, E.B., 1997b. The Angara–Vitim Batholith: on the problem of batholiths formation in the Central Asia Fold Belt. Geotectonics 5, 18–32.
Yarmolyuk, V.V., Ivanov, V.G., Kovalenko, V.I., 1998. Sources of the intraplate magmatism of Western Transbaikakia in the late Mesozoic–Cenozoic: trace element and isotope data. Petrology 6, 101–124.

Yarmolyuk, V.V., Litvinovsky, B.A., Kovalenko, V.I., Jahn, Bor- Ming, Zanvilevich, A.N., Vorontsov, A.A., Zhuravlev, D.Z., Posokhov, V.F., Kuz'min, D.V., Sandimirova, G.P., 2001. Formation Stages and Sources of the Peralkaline Granitoid Magmatism of the Northern Mongolia–Transbaikalia Rift Belt during the Permian and Triassic. Petrologiya 9 (4), 351–380.

Yarmolyuk, V.V., Kovalenko, V.I., Salnikova, E.B., Budnikov, S.V., Kovach, V.P., Kotov, A.B., Ponomarchuk, V.A., 2002. Tectono-magmatic zoning, magma sources, and geodynamic of the Early Mesozoic Mongolo-Transbaikalian magmatic area. Geotectonics 36 (4), 293–311.

Yarmolyuk, V.V., Kovalenko, V.I., Kozlovsky, A.M., Vorontsov, A.A., Savatenkov, V.M., 2005. Late Palaeozoic–Early Mesozoic Rift System of Central Asia: composition of magmatic rocks, sources, order of formation and geodynamics. In: Kovalenko, V.I. (Ed.), Tectonic Problems of Central Asia. World of Science Publisher, Moscow, pp. 197–226.

Zanvilevich, A.N., Litvinovsky, B.A., Andreev, G.V., 1985. The Mongolian–Transbaikalian Peralkaline Granitoid Province (in Russian). Nauka, Moscow. 231 pp.

Zanvilevich, A.N., Litvinovsky, B.A., Wickham, S.M., Bea, F., 1995. Genesis of alkaline and peralkaline syenite-granite series: the Kharitonovo pluton (Transbaikalia, Russia). Journal of Geology 103, 127–145.

Zhao, X.-F., Zhou, M.L., Li, J.-W., Wu, F.-Y., 2008. Association of Neoproterozoic A-type and I-type granites in South China: implications for generation of A-type granites in a subduction-related environment. Chemical Geology 257, 1–15.